CZECH TECHNICAL UNIVERSITY
IN PRAGUE

Faculty of Nuclear Sciences and Physical
Engineering

Department of Physics

Diploma thesis

Applications of Event Shape Sorting

Renata Kopečná

Supervisor: doc. Dr. Boris Tomášik

Prague, 2016

ČESKÉ VYSOKÉ UČENÍ TECHNICKÉ
V PRAZE
Fakulta jaderná a fyzikálně inženýrská
Katedra fyziky

Diplomová práce

Aplikace třídení událostí podle tvaru

Renata Kopečná

Školitel: doc. Dr. Boris Tomášik

Praha, 2016

Prohlášení:

Prohlašuji, že jsem svou diplomovou práci vypracovala samostatně a použila jsem pouze podklady (literaturu, projekty, software, atd.) uvedené v přiloženém seznamu.

Nemám závažný důvod proti užití tohoto školního díla ve smyslu § 60 Zákona č. 121/2000 Sb., o právu autorském, o právech souvisejících s právem autorským a o změně některých zákonů (autorský zákon).

V Praze dne

Renata Kopečná

Title:

Applications of Event Shape Sorting

Author: Renata Kopečná

Specialization: Experimental nuclear and particle physics

Sort of project: Master thesis

Supervisor: doc. Dr. Boris Tomášik

Abstract:
We present a novel method for sorting events according to their *shape*. In ultrarelativistic collisions, a small drop of quark-gluon plasma, called *fireball*, is produced. The shape of the fireball is determined by the different initial conditions of the collisions, there are hotter and colder places in the fireball. Anisotropies present in the fireball evolve up to the freeze-out and are reflected by anisotropies in azimuthal angle particle distributions. Our goal is to sort events according to their *history* using the *whole* particle distribution rather than one variable.

We implemented the code ESSTER that uses iterative algorithm to automatically sort the events. The algorithm is based on Bayesian concept of probability. We present results of this method on data simulated by AMPT motivated by PbPb $\sqrt{s_{NN}} = 2.76\,\mathrm{TeV}$ collisions at the LHC.

We propose several practical application of this method. It can be used for more exclusive experimental studies of flow anisotropies that can then be compared more easily to theoretical calculations. It may also be useful in the construction of mixed-events background for correlation studies or in the determination of initial orientation of ions in collisions of asymmetric nuclei such as UU collisions at RHIC.

Key words: Quark-gluon plasma, heavy-ion collisions, transverse flow anisotropies, elliptic flow, Event Shape Engineering, ESSTER, AMPT, particle fluctuations, distribution theory

Název diplomové práce:

Aplikace třídění událostí podle tvaru

Author: Renata Kopečná

Obor: Experimentální jaderná a částicová fyzika

Školitel: doc. Dr. Boris Tomášik

Abstrakt:

V této práci popisujeme novou metodu pro třídění eventů podle jejich *tvaru*. V ultrarelativistických jaderných srážkách se produkuje kapička kvark-gluonového plazmatu, které se říká *fireball*. Tvar fireballu se liší podle různých počátečních podmínek, ve fireballu jsou teplejší a studenější místa. Anizotropie fireballu se vyvíjejí až po vymrz-nutí a projevují se ve formě azimutálních anizotropií v distribuci částic. Našim cílem je třídit srážky na základě jejich *historie* za použití *celé distribuce* azimutálního úhlu částic.

Naimplementovali jsme program ESSTER, který používá iterativní algoritmus k automatickéu setřídění srážek. Tento algoritmus je založen an Bayesovské teorii pravděpodobnosti. Předkládáme výsledky získané za pomoci AMPT modelu, motivované srážkami PbPb na LHC při $\sqrt{s_{NN}} = 2.76\,\mathrm{TeV}$.

Dále navrhujeme několik praktických aplikací této metody. Může být použita pro detailnější studie anizotropií toku a tedy i pro lepší srovnání s teoretickými výsledky. Dále ji lze použít při konstrukci mixovaných pozadí, nutných pro různé korelační studie, nebo při určování orientace jader při srážkách asymetrických jader, jako jsou například srážky UU na RHIC.

Klíčová slova: Kvark-gluonové plazma, těžko-iontové srážky, anizotropie příčného toku, eliptický tok, Event Shape Engineering, ESSTER, AMPT, fluktuace částic, distribuční teorie

Acknowledgement

First and foremost my sincere thanks goes to my supervisor doc. Tomášik for his patience and for unflaggingly explaining the same things to me all over again. Without his attention to detail, encouragement and questions on my statements this project would not have been possible. He gave me a lot of freedom in my work while constantly pushing me towards new experiences and knowledge. I could not have imagined having a better advisor for my master studies.

I am grateful too for the support and advise of the whole academic staff at the department of physics for their enthusiasm and willingness to help anytime.

Besides the academic staff, I must also acknowledge my friends all around the world for stimulating discussions, endless encouragement on both professional and personal level, for their immense inspiration and occasional language help. In particular, my sincere thanks goes to my friend Ester for letting me name my code after her.

My special thanks goes to music groups Daft Punk and The Prodigy for providing me with hours of perfect music for coding and writing.

Contents

List of Figures

List of Tables

Introduction

Since the beginning of history, humans have wondered how the Universe began. One method of how to investigate the conditions just a fraction of a second after the Big Bang is to collide heavy ions at high energies. For that purpose, powerful facilities such as the Large Hadron Collider at CERN or the Relativistic Heavy Ion Collider at Brookhaven were built. At those facilities, heavy ions are being collided at very high energies. Those collisions are called *ultrarelativistic*, because the velocity at which researchers collide the heavy ions is very close to the speed of light in vacuum c.

These collisions produce the *Quark Gluon Plasma* (QGP), a state of matter being present a few microseconds after the Big Bang. This matter is very hot and very dense. The name comes from the similarity with regular plasma, but instead of ions and electrons being freed out of an atom, QGP consists of almost free quarks and gluons. This drop of hot and dense medium, the *fireball*, cools down, quarks and gluons are recombined into hadrons, which are later being registered by a detector.

In this thesis, we investigate this state of matter via the anisotropy of the azimuthal angle distribution of those particles. We present a novel method that automatically sorts events according to the whole azimuthal angle distribution.

First chapter briefly describes QGP and explains the origin of azimuthal angle anisotropies.

In the second chapter we introduce basic terms and explain the motivation of our study. Differential flows are defined. Furthermore, we suggest several cases where this method is applicable. A short subsection is dedicated to a study of rapidity distribution.

The third part describes our program ESSTER, explains its properties and its usage. The structure of the algorithm is described in detail. Moreover, we propose several possible extensions of the algorithm.

The AMPT model is described in the fourth chapter. Its structure, basic properties and parameters are presented. The choice of AMPT parameters is explained.

Last part is dedicated to the results we obtained via AMPT. We present results for three different centrality classes, thoroughly studying collisions corresponding to the centrality class of 0 - 20%. We analyzed sorted events using principal component analysis method a present the results of this method at the end of this chapter.

In the appendix, we include ESSTER documentation. We attach a complete list of parameters used in AMPT. Moreover, we add published and soon-to-be-published publications done while working on this thesis.

1 Quark gluon plasma

Recent results from experiments at facilities such as Relativistic Heavy Ion-Collider (RHIC) or the Large Hadron Collider (LHC) suggest the existence of an ultra-dense state of matter, the *quark-gluon plasma* (QGP). This state of matter may provide us information about the early stages of the Universe, the behavior of compact stars and much more. We are not able to study QGP directly, but via analyzing produced hadrons at experiments at RHIC and the LHC, using computer simulations or using mathematical models and simplifications. Then we investigate its properties, namely in this work we focus on azimuthal angle anisotropies.

Quark-gluon plasma was present just a few microseconds after the Big Bang. It is present in the hypothetical quark stars and possibly neutron stars [1]. In terrestrial conditions, it is present during the first fm/c of high-energy heavy-ion collisions. Small drop of QGP, called *fireball* can be created during these collisions. Due to the analogy with the expansion of the hot universe, these collisions are called *Little Bangs*.

In classic plasma, neutral atoms are dissolved into ions and free electrons. In QGP, hadrons are dissolved into quarks and gluons which are free to move over distances larger than size of a hadron (we say they are *deconfined*).

First theoretical predictions of QGP appeared in the 1970's. Few years later, the idea of studying it via heavy-ion collisions emerged. Promising results, such as strangeness enhancement, were obtained in the 1990's at the SPS (CERN) [2], supported later by RHIC results in 2000's. Today, all the big LHC experiments, this year also including LHCb, are also measuring PbPb collisions, proving the importance of QGP studies.

Despite the early predictions, QGP seems to be behaving as an almost perfect fluid. The lower limit for its shear viscosity, using natural units ($\hbar = 1$, $k_B = 1$), η/s is $1/4\pi$. This limit was established using AdS/CFT theory [3]. We focus at the ratio of viscosity and entropy density because in the case of natural units η/s is a dimensionless quantity.

The conditions needed to create QGP are rather extreme. Hadrons need to be very close to each other, requiring high energy density or high baryon chemical potential μ_B. Temperature which is required for the phase transition from hadrons to QGP at $\mu_B = 0$, denoted T_c, the *critical temperature*, is estimated at 140 - 175 MeV [4]. One of the theoretical predictions of the dependence of the critical temperature on the baryon chemical potential is shown in Fig. 1. As can be seen in the figure, baryon chemical potential much smaller than the proton mass m_p corresponds to the conditions created at LHC or RHIC, while in neutron stars we expect the baryon potential to be more than the m_p. The transition from confined hadrons to QGP for small μ_B appears to be smooth: looking at the energy density expressed as a function of temperature $\epsilon = \epsilon(T)$, all the derivatives are continuous. We speak about *cross-over transition*.

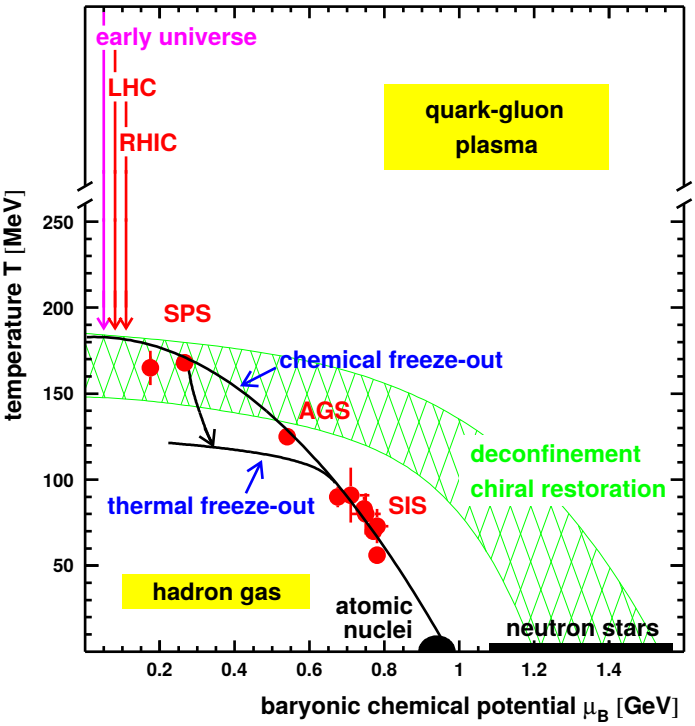

Fig. 1: QGP phase diagram. Dependence of the critical temperature T on baryon chemical potential μ_B. Taken from [5].

1.1 Studying quark-gluon plasma

It is impossible to study QGP directly due to its properties as well as its very short presence in the collision point. The only way to examine QGP is studying the hadrons originating from the fireball. Transverse momentum distribution or hadron yields and their correlations are usually studied.

We focus on the anisotropic expansion of the fireball. The fireball is produced in vacuum, so there is a big pressure gradient. The distribution of these gradients is anisotropic due to the presence of hotter and colder places. Those initial anisotropies lead to flow anisotropies, because the system tends to flow in the direction towards the lowest pressure. The non-zero viscosity of QGP comes into importance now. Since the viscosity is small, only small dissipative effects are present and initial fluctuations are not erased during the freeze-out stage. They survive in the form of anisotropic flow. Anisotropic flow can be measured and is strongly connected to the initial conditions *and* the evolution of the system.

Moreover, one has to take into account the fact that the fireball travels towards the detector: *blue shift* is present. Blue shift influences the final hadron distribution: it is responsible for higher multiplicities and higher mean p_T in the stronger flow direction.

Our goal is to separate events according to their azimuthal angle distribution. As mentioned above, azimuthal angle distribution is strongly connected to the initial conditions and the event evolution. Events with similar shape have similar initial conditions and evolution. Our approach is to sort events according to their overall shape rather than one variable. Simply said, we are sorting out events according to their similar history.

2 Motivation

First in this section, we mention our first motivation: verifying if *Event Shape Engineering* provides the best possible observable that can be used for selecting events with similar shape. Besides the general idea of sorting events with similar azimuthal angle distribution, there exist several purely practical applications of our method. We describe why and how it is useful to apply our method in the construction of mixed-events background for correlation studies or in the determination of mutual orientation of asymmetric nuclei in UU collisions. Lastly, we shortly mention the possible application of studying rapidity distributions using our method.

2.1 Event Shape Engineering

Event Shape Engineering is one of the existing methods how to select events with similar initial conditions. It was proposed in 2012 by J. Schukraft, A. Timmins and S. A. Voloshin in [6]. It studies azimuthal angle anisotropies. The usual treatment is to expand the distribution into the Fourier series:

$$\frac{dN}{dyd^2p_T} = \frac{dN}{2\pi p_T dydp_T}\left[1 + \sum_{n=1}^{\infty} 2v_n \cos(n(\Phi - \Phi_n))\right]. \tag{1}$$

The notation follows usual convention; N is the number of particles, p_T transverse momentum, y rapidity, Φ azimuthal angle, Φ_n is the n$^{\text{th}}$ reaction plane azimuthal angle, v_n's are n$^{\text{th}}$ differential flows. The flow coefficients v_n are the parameters we are going to focus on. An example of their role in the azimuthal angle distribution is depicted in Fig. 2.

Event Shape Engineering works in the following way: first, one divides events into two subevents. One (subevent a) is used for event selection. Second one, denoted subevent b, is used for the physical analysis. These two subevents are selected in a given momentum region or randomly. This helps to reduce nonphysical biases due to nonflow effects [6]. More about the biases caused by nonflow effects can be found for example in [7].

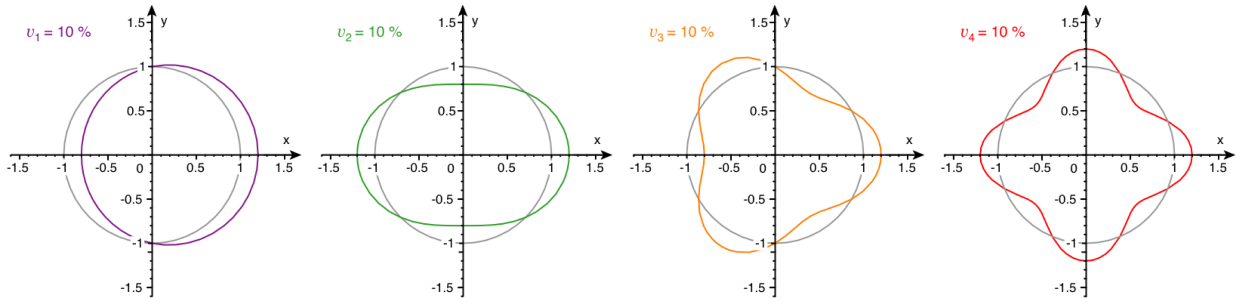

Fig. 2: Radial distributions with n$^{\text{th}}$ differential flow v_n behaviour illustration.

The measure used for distinguishing events in this approach is usually the *magnitude of the reduced flow vector* q_n. Usually, second order flow vectors are used. The reason for this is that flow vectors determine the direction where most of the particles are emitted. Hence, there is a strong connection to flow. Well known fact is that elliptic flow v_2 dominates in the most heavy-ion collisions (besides the very central collisions where triangular flow v_3 is comparable). Therefore, the analysis is done via q_2.

First, *flow vectors* are defined via the following equation:

$$\vec{Q}_n = \left(\sum_{i=1}^{M} \cos(n\phi_i) \, , \sum_{i=1}^{M} \sin(n\phi_i) \right) \, . \tag{2}$$

M denotes multiplicity of the subevent, ϕ_i is i$^{\text{th}}$ particle azimuthal angle. Second, one calculates the reduced magnitude as

$$q_n = Q_n / \sqrt{M} \, . \tag{3}$$

The multiplicity normalization is necessary since $\vec{Q}_n$ clearly scales with multiplicity. The analysis is usually done over a broad range of multiplicity.

In this analysis, two particle correlation can be also used. The magnitude of flow vector q_n can be also obtained as follows

$$q_n^2 = 1 + (M-1) \left\langle \cos[n(\phi_i - \phi_j)] \right\rangle_{i<j} \, .$$

The angular brackets denote average over all particles in the given subevent. The condition $i < j$ eliminates self-correlations and double counting of correlations (correlating particle i with particle j is the same as correlating particle j with particle i).

As stated in [6], the performance of this method is rather good. Our motivation was to verify that statement and investigate what happens if we take into account the whole shape of the azimuthal angle distribution rather than one variable, in this case q_2.

2.2 Femtoscopy

One of the possible future applications of our method are femtoscopy studies. Following the laws of quantum mechanics, the amplitude of production of a pair of bosons contains two symmetrical terms, as illustrated in Fig. 3. Simply speaking, the total amplitude of production of two particles produced at points x_1 and x_2 with momenta k_1 and k_2 consists of two amplitudes: probability of particle being produced at x_1 with momentum k_1 and particle being produced at x_2 with momentum k_2 and probability of particle being produced at x_1 with momentum k_2 and particle being produced at x_2 with momentum k_1.

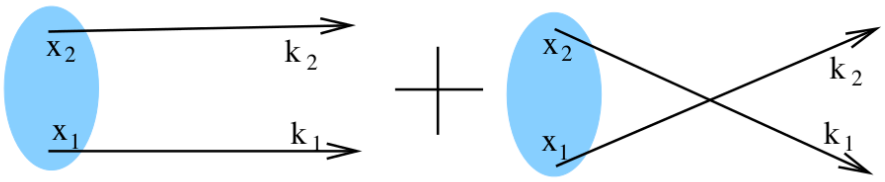

Fig. 3: Symmetrization of the two-boson amplitude.

Schematically, the amplitude of such a process consists of a sum of two symmetric amplitudes:

$$A(p_1, p_2) = \frac{1}{\sqrt{2}} \left(A(x_1 \to k_1, x_2 \to k_2) + A(x_1 \to k_2, x_2 \to k_1) \right) .$$

The probability A^*A contains mixed element of the two processes in Fig. 3. Since we want to obtain plain two-boson spectra, we need to get rid of the interference term in the amplitude

and preserve the symmetrization effect. We simply factorize the interference out using single-boson probabilities $P_1(k_1), P_1(k_2)$:

$$C(k_1,k_2) \stackrel{def}{=} \frac{E_1E_2d^6N/dk_1^3dk_2^3}{(E_1d^3N/dk_1^3)(\,E_2d^3N/dk_2^3)} = \frac{P_2(k_1,k_2)}{P_1(k_1)P_1(k_2)}\,. \tag{4}$$

Notation is usual, k is particle momentum, E energy and N particle yield. $P_2(k_1,k_2)$ is the two-boson probability, $P_1(k)$ is one-boson probability.

Rewriting k_1 and k_2 in terms of $q = k_1 - k_2$ and $K = (k_1 + k_2)/2$ significantly simplifies further manipulation. With these variables we can use the relation

$$q^\mu K_\mu = 0\,.$$

This immediately implies that only three components of q are independent. Since $q^0 = \vec{q}\cdot\vec{\beta}$ and $\vec{\beta} = \vec{K}/K$, only the spatial components of q become relevant. We denote those components in a suitable coordinate system q_{out}, q_{side} and q_{long}, there q_{out} is the component in the direction of transverse component of $\vec{K}$, q_{long} is in the beam axis direction and the orthogonal complement is q_{side}. For further simplification, we assume the reference frame is moving longitudinally with velocity β_l.

We presume the fireball is azimuthally symmetric with respect to the longitudinal axis as well as the region producing particles with some transverse momentum is symmetric in the sideward direction. Then, one can obtain the famous *Bersch-Pratt parametrization*:

$$C(q,K) - 1 = \exp\left(-q_{out}^2R_{out}^2\,(K) - q_{side}^2R_{side}^2\,(K) - q_{long}^2R_{long}^2\,(K)\right)\,.$$

This leaves us with information about the size of the system R_{out},R_{side} and R_{long}.

Experimentally, the product $P_1(k_1)P_1(k_2)$ in eq. (4) is not used. Instead, background function $B(k_1,k_2)$ is constructed. It is obtained using pairs, where each particle of a pair is taken from a different event. This procedure is called *event mixing*. This guarantees that particles are not correlated due to symmetrization of the wave function. However, for proper

establishment of the background function, one should use different but still somewhat similar events. It is nonsense to mix different events with different single-particle distributions. As we will describe later, our method might distinguish similar events that can be later used for such an analysis. Possibly, it could lead to even single event femtoscopy which is unreachable using customary methods.

This method is often referred to as Hanbury Brown-Twiss (HBT) method. It was proposed in [8], where they used similar approach for measurement of the angular size of the star Sirius, using *the correlation between photons in coherent beams of radiation* [8].

2.3 Two-particle correlations in relative angle

Another nice example of using our method are two-particle correlation studies in relative angle. Correlations of produced hadrons in pseudorapidity $\Delta\eta$ and azimuthal angle $\Delta\phi$ can be investigated. This study is a valuable probe of collective effects in collisions. Originally, this study was done in heavy-ion collisions, since the collective effects are expected to play a crucial role in QGP. However, recent measurements evince unexpected long-range correlations also in high-multiplicity pp collisions. Long range correlations are such correlations where $\Delta\eta \gtrsim 2$ [9].

Similar to previous case, the final distribution is calculated as a ratio of signal over background. Background is obtained using event-mixing. Again, we state that our method can be used for better event selection in the event-mixing procedure.

We briefly describe the method mostly used by experimentalists [9].

The signal distribution $S(\Delta\eta, \Delta\phi)$ is defined as:

$$S(\Delta\eta, \Delta\phi) = \frac{1}{N_{trig}} \frac{d^2 N_{same}}{d\Delta\eta d\Delta\phi}. \tag{5}$$

The number of *trigger particles* N_{trig} denotes the number of all particles in the given p_T and multiplicity bin. N_{same} means the correlation between tracks from the same event.

The background distribution $B(\Delta\eta, \Delta\phi)$ is evaluated, similar to the eq. (5), as

$$B(\Delta\eta, \Delta\phi) = \frac{1}{N_{trig}} \frac{d^2 N_{mix}}{d\Delta\eta d\Delta\phi}. \tag{6}$$

This time, N_{mix} stands for the number of particle pairs obtained by combining a trigger particle from one event with all the tracks from similar events. In order to normalize this distribution, $B(\Delta\eta, \Delta\phi)$ is divided by the zeroth bin $B(0,0)$. Given this normalization, background distribution can be understood as a pair-acceptance efficiency.

Finally, the correlation function itself is obtained as a ratio of signal distribution and background distribution:

$$\frac{1}{N_{trig}} \frac{d^2 N_{pair}}{d\Delta\eta d\Delta\phi} = B(0,0) \times \frac{S(\Delta\eta, \Delta\phi)}{B(\Delta\eta, \Delta\phi)}. \tag{7}$$

2.4 UU collisions

Let us move from PbPb collision to collisions of asymmetric nuclei. The RHIC facility has been studying uranium-uranium collisions. ^{238}U is very asymmetric nucleus [10]. Hence, there are many different possibilities of the overlap geometry during the collision. Three basic examples of the collision geometry are in Fig. 4. There were many attempts how to establish initial orientations of the nuclei from the data. Simulations suggest that there are differences in pseudorapidity, p_T and elliptic flow distributions for different nuclei orientations [10]. Another

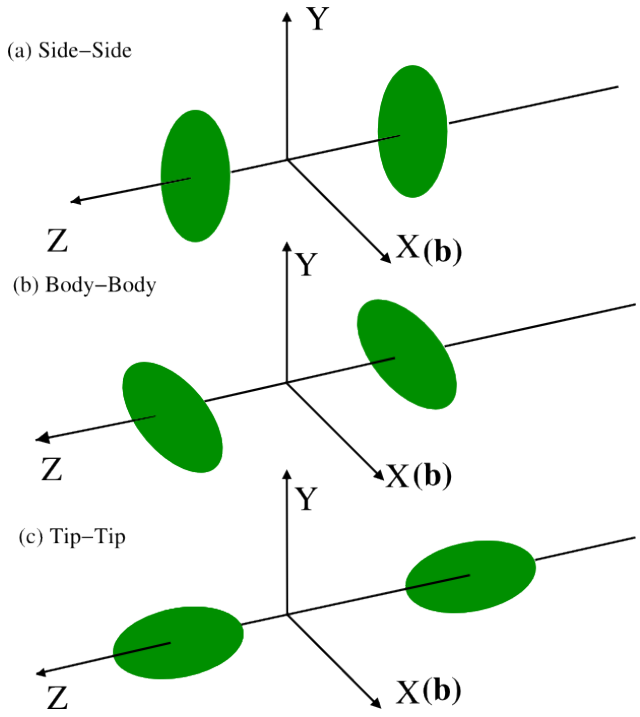

Fig. 4: Different UU collisions geometries. Taken from [10].

example is a method that uses the signal from ZDC to investigate the number of spectators in the most central collisions [11].

Our method could potentially distinguish tip-tip collisions from the body-body ones within a *wide centrality range* and/or distinguish small differences in the initial geometry of the collision, for instance differentiating between non-central body-body collisions and central tip-tip collisions.

2.5 Rapidity distribution

In [12], we were interested in the influence of fireball fragmentation on rapidity distribution. This may happen in heavy-ion collisions studied at future NICA facility. NICA (**N**uclotron-based **I**on **C**ollider f**A**cility) is a future accelerator facility located in Dubna, Russia, designed for studying QGP. NICA operates at lower energies (4-11 GeV [13]). Fireball created there may find itself in the region of the phase diagram, where it can undergo a first-order phase transition. Moreover, the fireball is rapidly expanding. This results in supercooling and spinodal decomposition. The final hadron distribution consists of hadrons produced from the fragments and those produced from the matter present between the fragments. The presence of fragments should be reflected in the rapidity distribution. However, the task to disentangle the events with similar fragment structure is rather complicated: rapidity distributions fluctuate from event to event. Our approach could help to identify the first-order phase transition and distinguish events with similar fragment structure.

3 ESSTER

For the purpose of testing the algorithm, we implemented a simple program called ESSTER: **E**vent-**S**hape **S**or**TER**. The documentation of this program is in Appendix A. Here, we will shortly introduce main functions of the program. ESSTER consists of two main parts: Toy Model Monte Carlo generator and Event Shape Sorter. We used a simple Monte Carlo model for the purpose of initial testing of the algorithm and for obtaining several promising results. This motivated further the use of more advanced Monte Carlo models such as AMPT.

3.1 Toy Model

The azimuthal angle distribution can be expressed using Fourier decomposition (see eq. (1)). Hence, we generated particles with azimuthal angle ϕ according to

$$\frac{dN}{d\phi} \propto 1 + \sum_{n=1}^{\infty} 2v_n \cos(n(\phi - \Psi_n)) \,. \tag{8}$$

The v_n parameters for each event depend quadratically on multiplicity M:

$$v_n = aM^2 + bM + c \,,$$

where a, b and c are coefficients obtained from the fits to PbPb LHC data [14, 15], actual values are in Appendix A. Then, they are smeared according to Gaussian distribution. Furthermore, the event plane angle Ψ_n is set randomly for every event and is independent for every n.

3.2 Event Sorting

The sorting method applied here is based on Bayesian probability. Short description of the algorithm can be found in [16]. For our purposes, two main relations are applied. First one is the *Bayes' theorem*. It makes it possible to rewrite conditional probability of event A given event B, denoted as $P(A|B)$, using the probability of event B given event A, $P(B|A)$.

Mathematically, denoting probabilities of events A and B as $P(A)$ and $P(B)$

$$P(A|B) = \frac{P(B|A)P(A)}{P(B)}\,. \tag{9}$$

The second important relation is expanding probability of event B using a set of different independent events $\{\mathrm{A}_1, \ldots, \mathrm{A}_n\}$ which fulfills the condition $\sum_{i=1}^{n} P(A_i) = 1$:

$$P(B) = \sum_{i=1}^{n} P(B|A_i)P(A_i)\,. \tag{10}$$

3.2.1 Algorithm

The algorithm was inspired by [17] and [18]. The authors used this algorithm for distinguishing between good a bad scientists. They took their citation record, made a histogram out of the distribution of citation counts and compared the *shapes* of those distributions. They also tried to find a good variable for the determination of a good scientist[1].

Since our algorithm compares whole distributions, first, one needs to draw histograms of the desired distribution. Hence, we make azimuthal angle histogram. Let us denote the number of bins in this histogram k. We will refer to these bins using Roman letters, meaning we have k bins denoted as $1, \ldots, i, \ldots, k$. An example of such an event can be seen in figure 5. This event is described the azimuthal angle distribution of charged particles {208, 163, 177, 146, 162, 158, 171, 146, 181, 226, 240, 216, 182, 196, 127, 160, 160, 187, 209, 238}. The total charged multiplicity of this event is 3653.

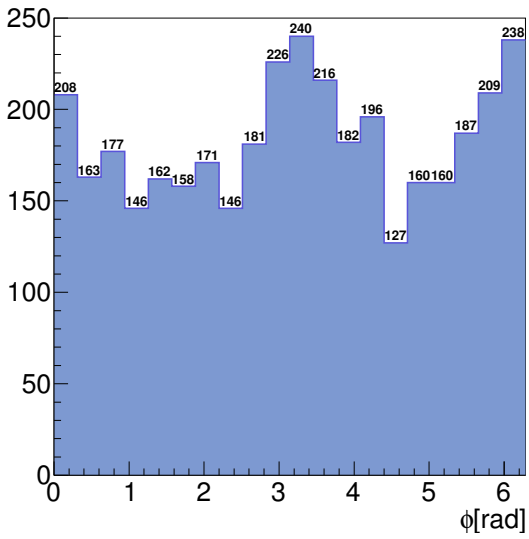

Fig. 5: Azimuthal angle histogram example.

[1]Interesting result is that the correlation of scientific quality and Hirsch index is comparable to the correlation of scientific quality and number of papers per year.

Next step is to organize events according to some good measure. The advantage of this algorithm is the fact that it is an iterative process, as is shown later. Hence, even if one organizes the events randomly, the algorithm eventually sorts them. This means that the initial sorting does not bring any bias to our study. Moreover it allows us to study different measures and separate the good ones from the bad ones. In our case, we started with events organized according to q_2 or a random number.

Then, we make event bins from the organized events. In order to distinguish the event bins from the azimuthal angle bins, event bins are denoted using Greek letters: we have ω event bins $1, \ldots, \mu, \ldots, \omega$. For simplicity, we will use quantiles as bins (meaning we have ω-quantiles).

Now, we want to obtain the probability that the event with record $\{n_i\}$ belongs to an event bin μ, shortly denoted as $P(\mu|\{n_i\})$. Using Bayes' theorem (9) and eq. (10), we can rewrite $P(\mu|\{n_i\})$ using the probability $P(\{n_i\}|\mu)$ that an event in the bin μ has an angle record $\{n_i\}$:

$$P(\mu|\{n_i\}) = \frac{P(\{n_i\}|\mu)P(\mu)}{P(\{n_i\})} = \frac{P(\{n_i\}|\mu)P(\mu)}{\sum_{\mu'} P(\{n_i\}|\mu')P(\mu')} \,. \tag{11}$$

The probability $P(\{n_i\}|\mu)$ can be calculated using the probability $P(i|\mu)$ that particle is in the i^{th} bin given the event is in the event bin μ:

$$P(\{n_i\}|\mu) = N! \prod_i \frac{P(i|\mu)^{n_i}}{n_i!} \,, \tag{12}$$

N denotes total number of particles (multiplicity). This formula takes into account all the possible permutations of particles among their angle bins. We will address the case of weighted events later in this section. Substituting for $P(\{n_i\}|\mu)$ in eq. (11) leads to canceling all factorials. This significantly simplifies the computation.

The probability $P(i|\mu)$ is the number of particles in ith bin for all events in μ divided by the number of all particles in all events in μ:

$$P(i|\mu) = \frac{\#\text{ of particles in i}^{th}\text{ bin for all events in } \mu}{\#\text{ of all particles in all events in } \mu} \,. \tag{13}$$

3.2 Event Sorting

Now we can rewrite eq. (11) in the terms of $P(i|\mu)$:

$$P(\mu|\{n_i\}) = \frac{\prod_i P(i|\mu)^{n_i} P(\mu)}{\sum_{\mu'} \prod_i P(i|\mu')^{n_i} P(\mu')} \,. \tag{14}$$

$P(\mu)$ (as well as $P(\mu')$) denotes the *prior*. Now it is clear why we used quantiles: the prior is always 1/(number of quantiles). Worth noticing is also the fact, that this formula uses *all* the available data. Hence, if there are any exceptional or rare events, their statistical influence is highly suppressed.

Since we know how to obtain the probability $P(\mu|\{n_i\})$ that an event with the record $\{n_i\}$ belongs to the event bin μ, one can easily obtain the *mean event bin number*

$$\bar{\mu} = \sum_{\mu} \mu P(\mu|\{n_i\}) \,. \tag{15}$$

Once we calculate the mean bin number for every event, we sort the events according to $\bar{\mu}$. This means we obtain new μ bins, we do the bayesian analysis again, obtain new $\bar{\mu}$. We repeat this until the events assigned into event bins μ remain unchanged.

For readers comfort, we add simple bullet overview of the algorithm with Fig. 6 depicting the structure of the algorithm.

1. For every event make azimuthal angle $\frac{dN}{d\phi}$ histogram.

2. Order events and divide them into ω event bins.

3. For each angle bin i and event bin μ calculate the probability that particle is in the i^{th} bin given the event is in the event-bin μ according to eq. (13):

$$P(i|\mu) = \frac{\text{\# of particles in i}^{th} \text{ bin for all events in } \mu}{\text{\# of all particles in all events in } \mu} \,.$$

4. Calculate the probability that an event in bin μ is described by a set of numbers $\{n_i\}$ denoting n_i particles belong to i^{th} bin, reducing the factorials in eq. (12), (14)

$$P(\{n_i\}|\mu) \propto \prod_i P(i|\mu)^{n_i} \,.$$

5. For each event with record $\{n_i\}$ calculate the probability that it belongs to the bin μ according to eq. (11):

$$P(\mu|\{n_i\}) = \frac{P(\{n_i\}|\mu)\, p(\mu)}{P(\{n_i\})} = \frac{P(\{n_i\}|\mu)\, p(\mu)}{\sum_{\mu'} P(\{n_i\}|\mu')\, p(\mu')}\,.$$

6. For every event calculate mean bin number (eq. (15)):

$$\bar{\mu} = \sum_{\mu} \mu P(\mu|\{n_i\})\,.$$

7. Sort according to $\bar{\mu}$.

8. Repeat from the third step until the content of μ bins remains unchanged.

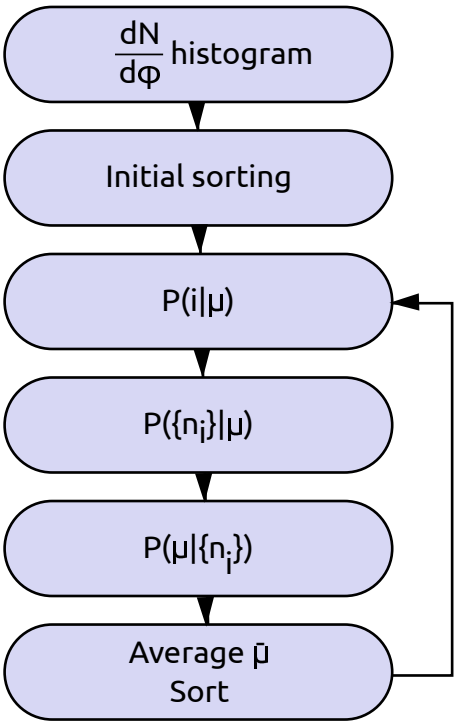

Fig. 6: Algorithm flowchart.

3.2.2 Initial assignment error

We are not only interested in sorting the events, we also want to find the variable that would be good for sorting itself. If such a variable exists, one could directly sort events according to it and not use this rather long iterative algorithm. To verify if a variable is good, one can obtain the error of original bin assignment. Keeping the previous approach, we want to calculate the probability $P(\alpha|\beta)$ that an event originally assigned to bin β ('*before*') ends up in bin α ('*after*') after applying the sorting algorithm. We will calculate this probability as an average of the probability $P(\alpha|\{n_i\})$ for all events $\{n_i\}$ in bin β:

$$P(\alpha|\beta) = \frac{1}{N_\beta} \sum_{\{n_i\}\in\beta} P(\alpha|\{n_i\}) \tag{16}$$

If the original sorting variable was good, we expect the values of $P(\alpha|\beta)$ to be approximately one around diagonal, and approximately zero elsewhere. We do not expect a clear diagonal tough, there are fluctuations and we have only limited sample of events and limited size of bins. This is also reflected by the fact that the probability that an event $\{n_i\}$ belongs to some event-bin is normalized as

$$\sum_{\mu=1}^{N} P\left(\mu|\{n_i\}\right) = 1\,,$$

but the probability that an event in any of the event-bins has an angle record $\{n_i\}$ is not necessarily one:

$$\sum_{\mu=1}^{N} P\left(\{n_i\}|\mu\right) \neq 1\,.$$

3.2.3 Events rotation

Since we are studying an azimuthal *angle* distribution, we can rotate all events along the beam axis arbitrarily. As is shown later, different initial rotation yields slightly different results. Considering the fact that v_2 is apparently dominant constituent in eq. (1), our first

choice of rotation is in the way that the second-order event plane $\Psi_2 = 0$. As shown later, this introduces a bias in our algorithm, since it leads to smearing of other flow coefficients. The sorting is then clearly dominated by v_2.

Since the second biggest coefficient is v_3, it is reasonable to study such a rotation where $\Psi_3 = 0$. Results obtained by toy model [16, 19] suggests that sorting is then clearly dominated by v_3. Furthermore, this makes another problem visible: parity symmetry. We have a free choice of choosing a mirror image of the event or not. This was not visible in the previous case since $|\Psi_2| < \pi/2$. Our solution to the problem of eliminating the parity symmetry was to perform the sorting first. Once the events are sorted, we made a mirror image of the second half of the *sorted* events. Then, we sorted the events again. This reduces the effects of the parity symmetry to a minimum since the algorithm initially sorts the events in a way that mirror images are in the *opposite* bins (meaning bins 1-10, 2-9, ...).

One way how to reduce such effects is to take into account both Ψ_2 and Ψ_3 while putting a constraint on the parity. For this purpose, we introduce the angle Ψ_{2-3}. This angle is the bisector between Ψ_2 and Ψ_3, while Ψ_2 is less than $\pi/2$ away *counterclockwise* from Ψ_{2-3}.

Second way how to remove such a bias is to look at two-particle correlations. This eliminates the trouble with initial rotations as well as parity. The toll for that is a loss of information, since we look at correlations in one event, meaning we convolute an event with itself.

3.2.4 Normalized histograms

The histograms described so far were normalized to the number of particles. In this case, events with higher multiplicity influence the sorting more than the ones with smaller multiplicity. To prevent that, some kind of normalization is necessary. A probability density function $f(x)$ is normalized as

$$\int_{-\infty}^{+\infty} f(x)dx = 1\,.$$

In our case, we want the content of the histograms to be normalized in a way it is as close as possible to the probability density. Considering we have an angle distribution and

denoting the width of a bin Δ

$$\int_0^{2\pi} f(x)dx \approx \sum_{i=1}^{\omega} n_i \cdot \Delta = N \cdot \Delta \stackrel{!}{=} 1\,.$$

This means we have to divide the number of particles in each bin by $(N \cdot \Delta)$, resulting in having a record for an event $\{n_i/N\}$. First, we again calculate the probability $P(i|\mu)_{norm}$ as [2]

$$P(i|\mu)_{norm} = \frac{\sum_{\{n_i\}\in\mu} n_i/N}{\sum_i \sum_{\{n_i\}\in\mu} n_i/N} = \sum_{\{n_i\}\in\mu} n_i/N\,.$$

We can happily ignore the weight Δ describing the width of a bin. It is the same for every event, and it will be factorized out similarly as in (11). However, the next step requires a power to the number of particles in bins without the normalization. Since our probability $P(\{n_i\}|\mu)$ still describes that an event in bin μ is characterized by a set of numbers $\{n_i\}$, one needs to calculate it as

$$P(\{n_i\}|\mu)_{norm} = N! \prod_i \frac{P(i|\mu)^{n_i}_{norm}}{n_i!}\,.$$

The latter steps are performed as in the Sec. 3.2.1. Again, the factorials are not an issue since they are factorized out.

3.2.5 Weighted events

In experiments, one has to deal with several detector effects. Main corrections applied are acceptance correction, efficiency correction and reconstruction software corrections. This leads to non-integer values in histograms. We will denote a weight for every event $\{n_i\}$ as $w_{\{n_i\}}$. The modification of the algorithm is straight-forward.

First, we simply obtain $P(i|\mu)$:

$$P(i|\mu) = \frac{\sum_{\{n_i\}\in\mu} n_i w_{\{n_i\}}}{\sum_i \sum_{\{n_i\}\in\mu} n_i w_{\{n_i\}}}\,.$$

[2] Note that $P(i|\mu)_{norm} \neq P(i|\mu)$.

Now, one has to deal with the fact that there are non-integer numbers of particles in each bin. Considering simple assumption that given the probability of rolling six twice on a dice is 1/36, the probability of rolling six once is $\sqrt{1/36}$ and thrice $(1/36)^{3/2}$, we expand eq. (11) as follows:

$$P(\{n_i\}|\mu) = (Nw_{\{n_i\}})! \prod_i \frac{P(i|\mu)^{n_i w_{\{n_i\}}}}{(n_i w_{\{n_i\}})!} \,.$$

The problem of non-integer factorials can be solved with a help of a Γ-function:

$$z! = \Gamma(z+1), \qquad z \in \mathbb{R} \,.$$

This formal requirement for factorials is, however, still factorized out as in eqs. (12, 14). Hence, rather complicated calculation of Γ-functions is not necessary. The rest of the calculations is the same as in the Sec. 3.2.1.

As mentioned in the beginning of this section, we have tested this algorithm using a toy model (see Appendix A). The results obtained from this were very promising. However, a simple toy model does not provide a sufficient physics insight. Therefore, we have used AMPT. AMPT is a Monte Carlo model used for simulating relativistic heavy-ion collisions, providing us more realistic data and a better insight in the underlying physics.

4 AMPT

As mentioned in the previous section, AMPT is a Monte Carlo model widely used for simulating relativistic heavy-ion collisions. It was released for public use in 2004. The name stands for **A** **M**ulti-**P**hase **T**ransport Model. It includes both initial and final hadronic interactions as well as the transition between confined and deconfined phase of matter [20]. AMPT is a model used for generating pA and AA collisions with CMS energy roughly from 5 GeV to 5500 GeV. In this region, initial interactions are dominated by strings and minijets. Final interactions are, however, also important. AMPT starts with HIJING (Heavy Ion Jet Interaction Generator), used for modeling initial conditions. It is followed by ZPC (Zhang's Parton Cascade) used for modeling partonic scatterings. Next step is hadronization: Lund string fragmentation model or quark coalescence is used. Since we used quark coalescence for our study, from now on we will consider only the later. Finally, hadron scattering is treated by ART (A Relativistic Transport model). The final results are obtained at so-called *cutoff time* t_{cut}. At this time, hadron interactions do not significantly change the observables.

We used the version 2.26t5 (released on April, 2015) accessible at [21]. The model is written in Fortran 77 language. The main advantage of this code language is its fast performance, which is crucial for such a complicated Monte Carlo Model.

As mentioned before, AMPT consists of four parts: the initial conditions, parton cascade, the hadronization, and hadronic interactions. Now we briefly describe each part [20]. A flowchart of the AMPT structure is in Fig. 7.

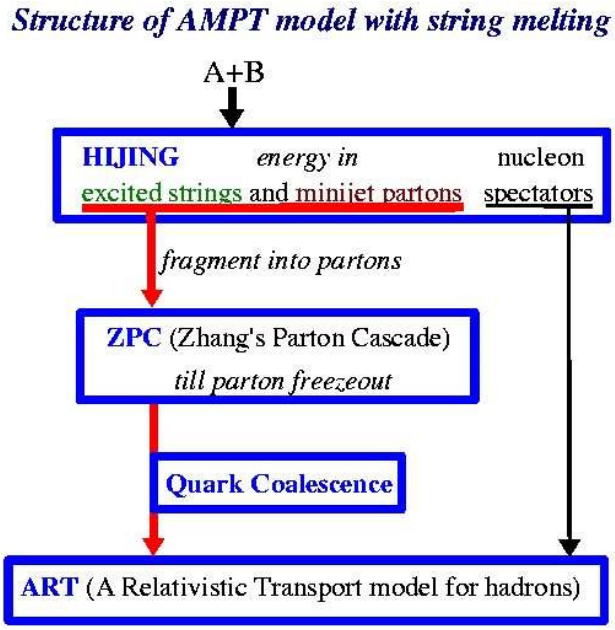

Fig. 7: AMPT Flowchart with string melting included. Taken from [20].

4.1 Initial conditions

As mentioned, this part is based on the HIJING model. For the colliding nuclei density, Wood-Saxon shape is used. Multiple scatterings among nucleons are described by the eikonal formalism. The hard and soft components of particle production processes are treated separately. Hard component is calculated using perturbative QCD, soft component using the formation of strings. The cutoff momentum p_0 used for distinguishing between soft and hard process is equal to 2 GeV.

Since the energy density in very central collisions is really high even at RHIC energies, not including the string melting mechanism would underestimate the partonic effects: using string fragmentation only, partons would coalescence back to the original hadron since they would pair-up with the closest partner at the same freeze-out time. The position of partons originating from string melting is obtained using straight-line trajectories from their parent hadrons. The formation time t_f is introduced. It represents the time needed for production of the partons from strong color fields. This ensures all the partons coming from the same parent hadron have the same formation time. It is defined as $t_f = E_H/m_{T,H}^2$, where E_H denotes the energy of the parent hadron and $m_{T,H}$ is transverse mass of the parent hadron. The advantage of this approach is that those initial conditions can be directly obtained from HIJING with partonic and hadronic interactions turned-off.

4.2 Partonic interactions

The interaction is treated as equations of motions for partons' Wigner distribution functions. They can be approximated by Boltzmann equations, resulting (for two-body interaction) in

$$p^\mu \partial_\mu f\left(\mathbf{x}, \mathbf{p}, t\right) \propto \int \sigma f\left(\mathbf{x_1}, \mathbf{p_1}, t\right) f\left(\mathbf{x_2}, \mathbf{p_2}, t\right) \mathrm{d}\mathbf{p_1} \mathrm{d}\mathbf{p_2}\,,$$

where the integral is evaluated over the momenta of other three partons. σ is the cross section for partonic two-body scattering, $f\left(\mathbf{x}, \mathbf{p}, t\right)$ is the partonic distribution function dependent on the time t and phase space $\mathbf{x}, \mathbf{p}$.

These equations are solved by Zhang's parton cascade (ZPC). In this approach, two partons are scattered anytime they get closer to each other than $\sqrt{\sigma/\pi}$. ZPC can solve only two-body scatterings such as $gg \to gg$, cross sections obtained from pQCD. One crucial parameter is needed here: the Debye screening mass μ. It characterizes the lowest momentum exchange with the medium [22].

Worth mentioning is the fact that jet-quenching in AMPT is effectively replaced by ZPC. However, only two-body interactions are implemented, higher-order contributions are absent in AMPT.

4.3 Hadronization

There are strings remaining from the initial conditions. String systems are gluons connected with their partner quarks or diquarks. Those strings are converted to soft partons. Later, soft partons are turned into hadrons using quark coalescence model. This model is similar to the ALCOR (Algebraic Coalescence Rehadronization) model [23]. The hadronization is simply done by combining two or three nearest quarks or antiquarks. Since the invariant mass of combined partons is discrete, 4-momentum is not conserved during coalescence. This problem is solved using 3-momentum conservation and determination of hadron species using the invariant parton mass and flavor. In case of pseudo-scalar vector mesons with the same flavor, the meson with invariant mass closest to coalescing $q\bar{q}$ pair is formed. The baryons are treated accordingly. In case of flavor-diagonal mesons (e.g. π^0 and η with ρ^0 and ω in SU(2) flavor space), AMPT calculates probability P_{π^0} of π^0 formation via the average numbers of π^- and π^+ and total number of $u\bar{u}$, $d\bar{d}$ pairs. Similarly, P_{ρ^0} is obtained. After that, the $u\bar{u}$ and $d\bar{d}$ pairs are sorted according to their mass and the lightest one are assigned as π^0. The rest of the pairs forms ρ^0 with the probability $P_{\pi^0}/\left(1 - P_{\pi^0}\right)$ and is equally divided between ω and η mesons.

Since hadronization is spread over time in the parton cascade, there are hadrons and partons coexisting at the same time during hadronization.

Several states are excluded: $\eta', \Sigma^*, \Xi^*, K_L^0$ and K_S^0.

4.4 Hadronic interactions

AMPT includes $\pi, \rho, \omega, \eta, K, K^*, \phi, N, \Delta, N^*(1440), N^*(1535), \Lambda, \Sigma, \Xi$ and Ω with all possible charges or antiparticles. Several other resonances are implicitly implemented as intermediate states in scattering among the previously listed particles.

ART Model (A Relativistic Transport model) was implemented for the simulation of heavy-ion collisions at AGS energies [24]. It includes baryon-baryon, meson-baryon and meson-meson scatterings, both elastic and inelastic. It was successfully used for studying isospin effects since it treats explicitly the isospin degrees of freedom.

Explicit inclusion of $\mathbf{K^*}$ mesons is added to AMPT, even tough K^* is implicitly implemented in ART (in the πK scattering). It is done by adding several scattering channels. This is due the fact that K^* becomes significant for the strange particle production.

Baryon-antibaryon annihilation and production needs to be added to AMPT. Initially, only $N\bar{N}$ annihilation was included. Now, also $(N\Delta N^*)(\bar{N}\bar{\Delta}\bar{N}^*)$ is included. Moreover, baryon-antibaryon production from mesons is included.

Multistrange baryon production from strangeness-exchange reactions is implicitly included. Multistrange baryons are produced via the strangeness-exchange reactions (such as $(\bar{K})\Xi \leftrightarrow \pi\Omega$). Since there are no experimental data about the cross section of these reactions, an approximation using N and Σ instead of Ξ and Ω is applied. These cross sections are similar to those obtained by the coupled-channel calculations based on the SU(3) invariant hadronic Lagrangian. However, the strange baryons only interact with mesons, the implementation of their baryon annihilation is missing.

ϕ meson production and scattering is built in AMPT. Inelastic scattering includes baryon-baryon and meson-baryon channels. The elastic scattering of ϕ and meson (5 mb) or N (8 mb) is estimated from quark counting and ϕ photoproduction.

Other interactions are explicitly added. This includes $\bar{\Delta}, \bar{N}^*$ with their creations, decays and scatterings, several inelastic meson-meson interactions (such as $\pi\pi \leftrightarrow \rho\rho$), elastic scattering of π and ρ, ω, η inelastic scattering. Moreover, more recent versions include deuteron interactions [25].

5 Results

Results from our Toy Model generator can be found in [16, 19]. Briefly summarized, we proved that the final sorting does not depend on initial sorting as well it does not depend on multiplicity. Furthermore, we found that the sorting of events is neither determined solely by q_2, v_2 or v_3. Higher harmonics are however negligible. The sorting depends also on the mutual position of the second and third event plane Ψ_2 and Ψ_3. Moreover, in simple cases where we neglected all harmonics but v_1 and v_2, it turned out that v_2 is better sorting variable than q_2.

Here we preset data from AMPT simulation. We set the AMPT parameters to reflect the LHC data [26]. We were interested in PbPb collisions at $\sqrt{s_{NN}} = 2.76\,\mathrm{TeV}$. The parameters we used are listed in Appendix B. For easier result analysis, we set the reaction plane not to be random.

We simulated three sets, each consisting of 5000 events. Each set was generated with a different impact parameter range, $0\,\mathrm{fm} < b < 7\,\mathrm{fm}$, $7\,\mathrm{fm} < b < 10\,\mathrm{fm}$, $10\,\mathrm{fm} < b < 12\,\mathrm{fm}$, corresponding to 0-20%, 20-40% and 40-60% centrality classes [27]. We will refer to these sets as *central*, *mid-central* and *peripheral*, respectively.

5.1 Analysis methods

Azimuthal angle distributions of all charged particles were studied. We were interested in various rapidity regions. Rapidity is calculated as

$$y = \frac{1}{2} \ln \left(\frac{E + p_z}{E - p_z} \right) ,$$

where E is the energy of a particle, p_z is the momentum component parallel to the beam direction. We made three rapidity cuts: $|y| < 1.5$, $|y| < 1$ and $|y| < 0.5$. However, there was no significant change in the algorithm results. Hence, we present the cut $|y| < 1$ unless it is specified differently.

To see the relation of initial shape of the fireball and the final distribution of sorted events, we also analyzed the initial parton distribution generated by AMPT. It was done calculating spatial eccentricity moments ε_n. The eccentricities ε_n in initial energy densities describe inhomogeneities in the fireball in a similar way as v_2 describes the anisotropies in the final hadron distributions and eventually lead to flow anisotropies. It was done as follows:

First, we made a $|y| < 1$ cut for all the partons. Then, we calculated the integrated area energy densities ϵ in the transverse plane. One of examples of such a fireball is in Fig. 8. From that, we calculated spatial eccentricity moments ε_n as

$$\varepsilon_n = \frac{\sqrt{\langle r^n \cos(n\phi)\rangle^2 + \langle r^n \sin(n\phi)\rangle^2}}{\langle r^n \rangle},$$

where $\langle\cdot\rangle$ denotes energy-density weighted average, r and ϕ are polar coordinates in the transverse plane [28].

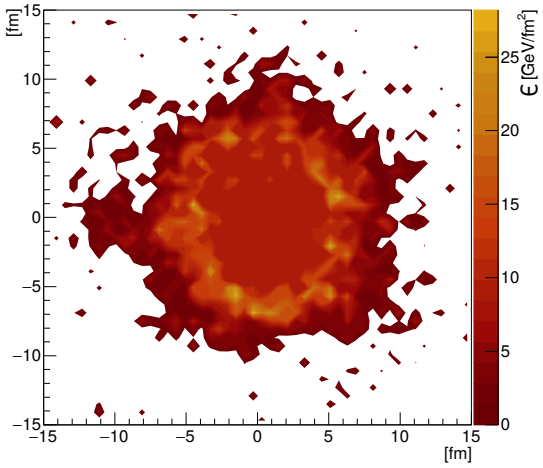

Fig. 8: Integrated area energy density ϵ of the fireball in the transverse plane for a central event.

We used two methods for the flow analysis of hadron azimuthal angle distributions: event plane method and cumulant method.

Event plane method [7] uses estimation of the reaction plane - *event plane*. It is defined as the direction of maximum final-state particle density. This is done using *event flow vector* $\vec{Q}_n = (Q_{n,x}, Q_{n,y})$, being defined as

$$Q_{n,x} = \sum_j p_T \cos(n\Phi_j) = |\vec{Q}_n| \cos(n\Psi_n),$$
$$Q_{n,y} = \sum_j p_T \sin(n\Phi_j) = |\vec{Q}_n| \sin(n\Psi_n).$$

The sum goes over all particles, Φ_j denotes azimuthal angle of j$^{\text{th}}$ particle. We can use p_T as a weight in the low p_T region since $v_n \sim p_T$.

5.1 Analysis methods

The event plane angle Ψ_n is defined as the azimuthal angle of $\vec{Q}_n$ in the polar coordinate system:

$$\Psi_n = \frac{\arctan(Q_{n,x}, Q_{n,y})}{n}\,.$$

The n$^{\text{th}}$ differential flow is then calculated as

$$v_n = \langle \cos(\Phi_j - \Psi_n) \rangle\,,$$

where the brackets $\langle\cdot\rangle$ represent average over all particles in one event.

Cumulant method [7] estimates the n$^{\text{th}}$ differential flow directly using particle correlations. Two-particle studies are done as

$$v_n\{2\}^2 = \langle \cos\left[n(\phi_i - \phi_j)\right] \rangle = \langle u_{n,i}, u^*_{n,j} \rangle\,. \tag{17}$$

Pair-brackets $\langle\cdot\rangle$ this time denotes an average over all particle pairs ($i \neq j$). $u_{n,j}$ is j$^{\text{th}}$ particle's *unit flow vector*[3];

$$u_n = e^{in\phi}\,. \tag{18}$$

Four-particle cumulant method is done in a similar fashion:

$$v_n^4\{4\} = -\langle\langle u_{n,i} u_{n,j} u^*_{n,k} u^*_{n,l} \rangle\rangle \equiv 2\langle u_{n,i}, u^*_{n,j} \rangle - \langle u_{n,i} u_{n,j} u^*_{n,k} u^*_{n,l} \rangle\,. \tag{19}$$

This time, $\langle\langle\cdot\rangle\rangle$ denotes cumulants, while $\langle\cdot\rangle$ is again average over all pairs or quartets of particles. The cumulant method can be also p_T wighted as in the case of event plane method.

There are advantages and disadvantages of both of these methods. Nonflow effects are mainly due to low multiplicities. Therefore, four-particle cumulant method reduces those effects stronger than two-particle cumulants. However, statistical errors of four-particle cumulants are bigger than those of event plane method [7].

We wanted to see the difference of those methods once we applied our sorting. In

[3] Asterisk denotes complex conjugate.

Fig. 9 we see correlations of average bin number $\bar{\mu}$ defined in eq. (15) with v_2 obtained using four-particle cumulant method, two-particle cumulant method, event plane method with p_T weighting and without p_T weighting. Each point represents one event. For better illustration of the event distribution among bins we assign different color to every event-bin. There are several *lines* around integers. Those lines are caused by a big difference between bins (it will be explained in detail later).

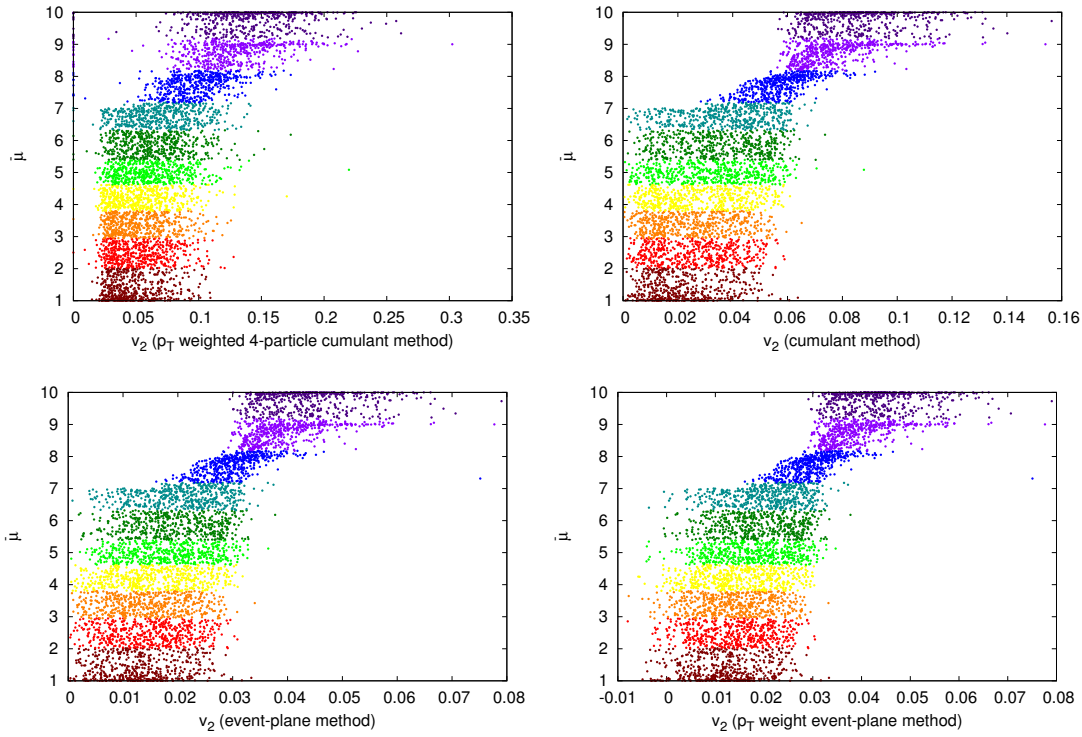

Fig. 9: Flow analysis method comparison. Central events, rotated according to Ψ_2.

There are differences between the used methods. However, this does not reflect on the final shape of the $\bar{\mu} = \bar{\mu}(v_2)$ dependence. Hence, from now on, v_2 from the event plane method *with* p_T weighting only will be shown. This is due to fact that we also obtained Ψ_n using this method.

For the event analysis, we also applied Event Shape Engineering, as described in Sec. 2.1. We calculated the magnitudes of reduced flow-vectors up to $n = 5$.

5.2 Central collisions

Since the energy density is highest in the most central collisions, we started our analysis there. As mentioned in Sec. 3.2.3, rotation of events along the beam axis can be arbitrary. Therefore we had to take care of initial rotation of events. This was usually done by estimating n^{th} event-plane Ψ_n and rotating the events in a way that Ψ_n was zero. Since v_2 is dominant in central collisions, the first step was rotating the events according to Ψ_2.

We applied the sorting on the events and the algorithm naturally ordered the events from events with smaller v_2 to those with higher v_2. This can be seen in Fig. 10 (bottom). In this figures, each histogram represents an average event bin: it is a sum of 500 histograms (since we have 5000 events and deciles) divided by 500. The y-axis captions are removed for readers comfort, it depicts number of particles in each bin, there was no weight or any normalization applied. For illustrating the power of the algorithm, we add the average azimuthal angle histograms *before* the sorting was applied in Fig. 10 (top). Since the initial sorting was random and events were rotated according to Ψ_2, the fluctuations in individual events are smeared and v_2 is the only flow coefficient clearly visible.

We study possible correlations of $\bar{\mu}$ with several variables. The correlation coefficient of $\bar{\mu}$ and v_2 after the sorting is 0.77. However, there is a visible influence of higher harmonics. This is shown in Fig. 11. Again, each point represents one event and each color represents one event bin. Worth noticing is the strong correlation of v_2 and q_2 with $\bar{\mu}$, which is expected. However the q_2 dependence is broader than the v_2 one, the correlation of $\bar{\mu}$ and q_2 is 0.75. Apparently, v_3 is not a good variable for sorting events, neither is impact parameter b, number of participants N_{part} or multiplicity of charged particles. Moreover, in the region of $\bar{\mu} < 7$, v_2 fails to satisfactory describe the shape. There is no apparent correlation of any studied variable with $\bar{\mu}$. This suggest that event shape is indeed a complex problem.

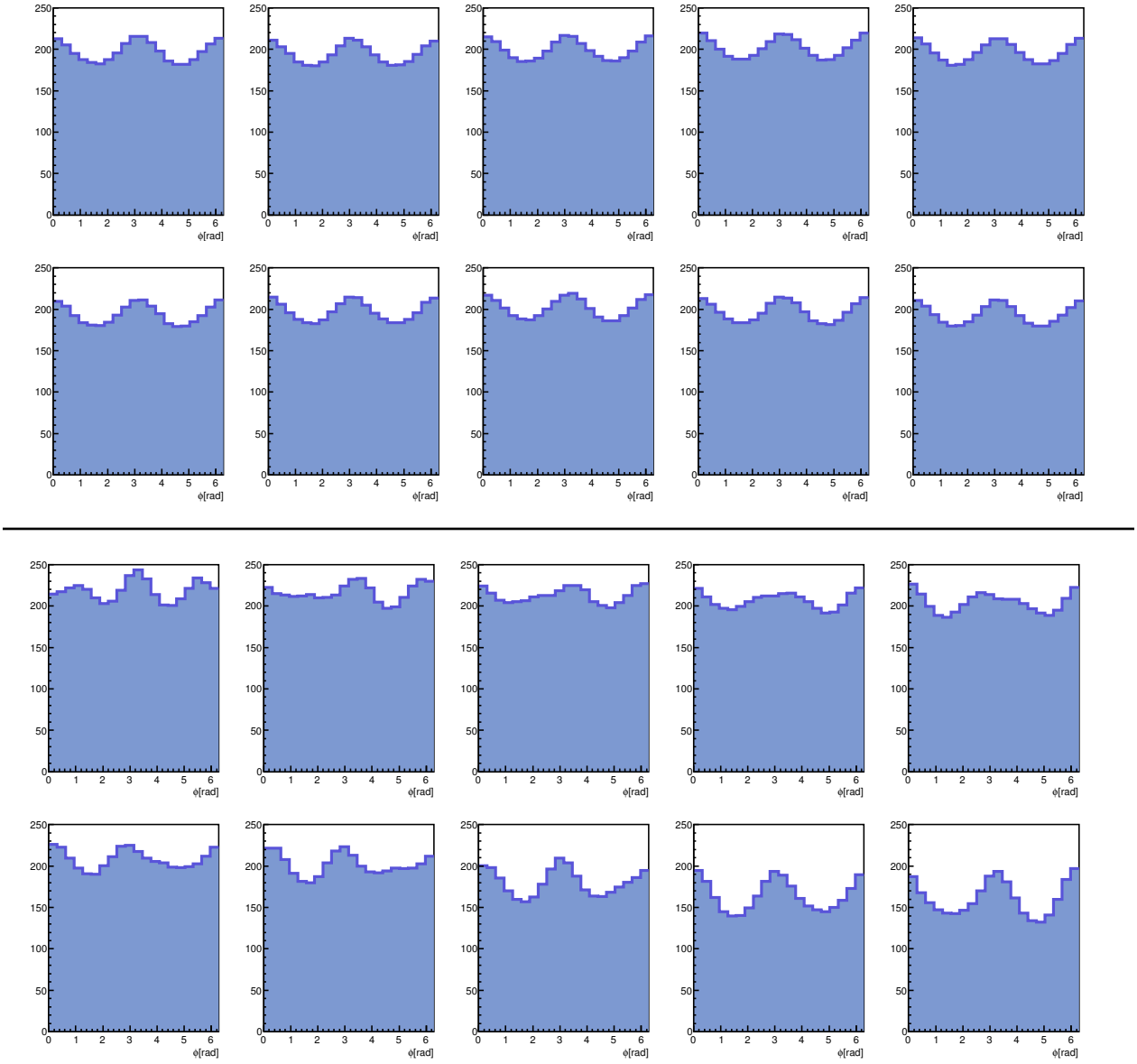

Fig. 10: Average azimuthal angle histograms of central collisions. Top figure: average azimuthal angle histograms *before* sorting was used. Lower figure: average azimuthal angle histograms *after* sorting was used. Events were rotated according to Ψ_2.

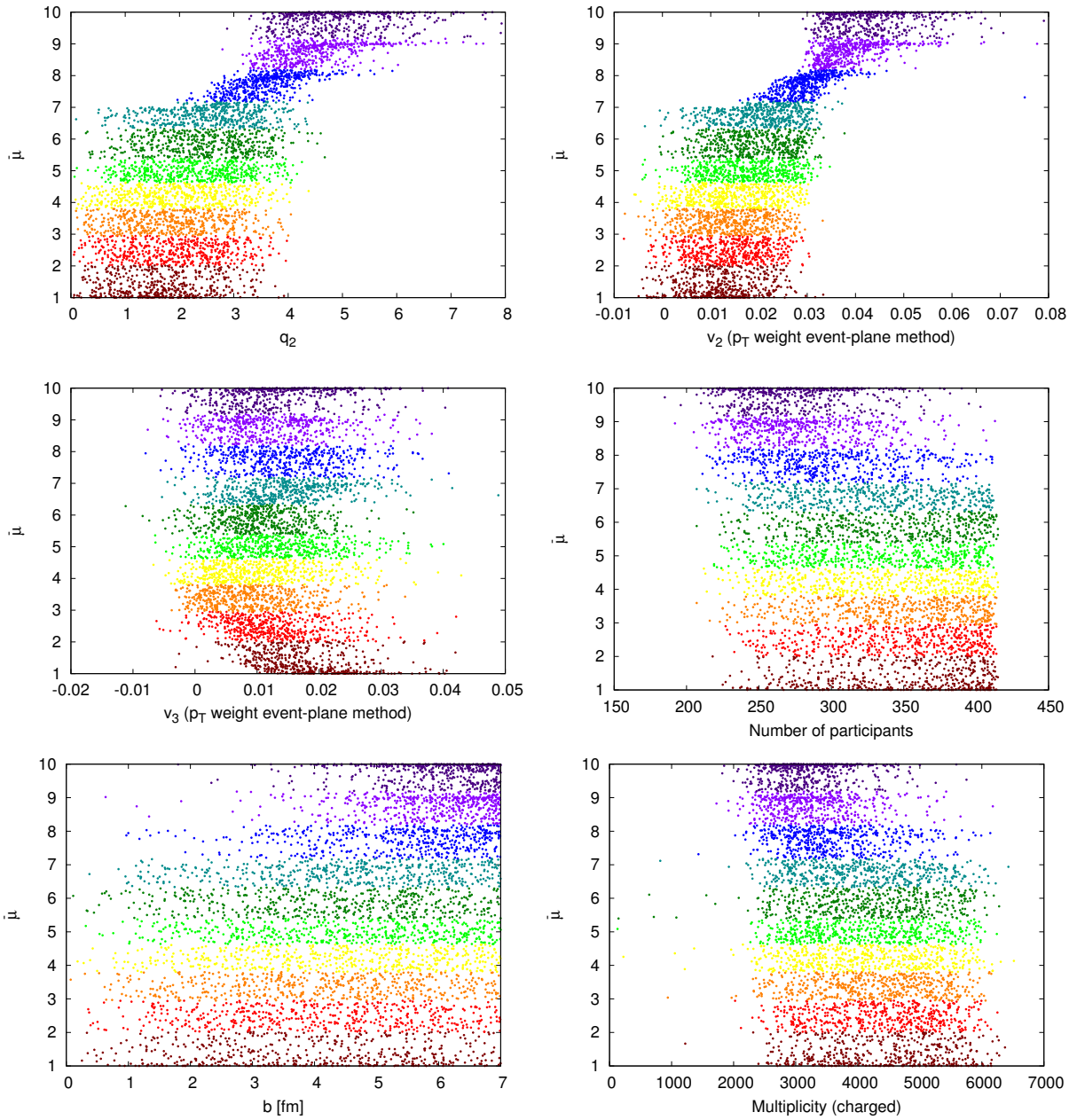

Fig. 11: Correlation of $\bar{\mu}$ with q_2 (top left), v_2 (top right), v_3 (middle left), N_{part} (middle right), b (bottom left) and M (bottom right) for central collisions. Events were initially rotated according to Ψ_2.

Next step was rotating events according to Ψ_3. The situation in the case of Ψ_2 is not very clear, especially in the region of $\bar{\mu} < 7$ (Fig.11), where no apparent correlation of $\bar{\mu}$ with any variable is visible. In the ultra-central collisions, triangular flow v_3 becomes more significant than v_2 in the very central collisions, therefore the dominant axis in the event is Ψ_3. It is clear from Fig. 12 that the linear shape of $\bar{\mu} = \bar{\mu}(v_2)$ is lost. However, we can see a W - shape structure there, suggesting v_2 is still significant. Moreover, even v_3 is clearly not a good sorting variable neither in this case.

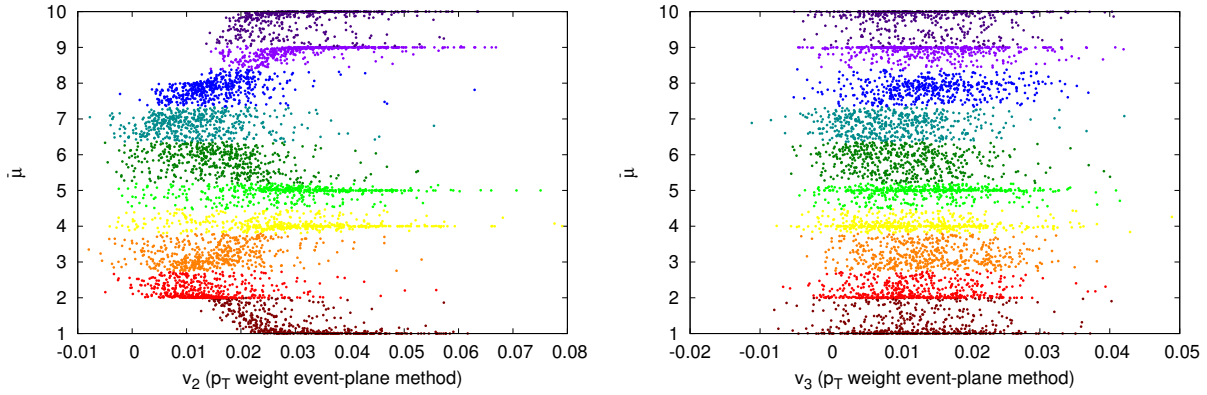

Fig. 12: Correlation of $\bar{\mu}$ with v_2 (left) and v_3 (right) for central collisions. Events were initially rotated according to Ψ_3.

Since in the case of roatiton according to Ψ_3 the parity symmetry becomes important, we tried to flip the events, as described in Sec. 3.2.3. Now it is obvious from Fig. 13 that v_2 plays a crucial role in the shape sorting. However, events with $v_2 \sim 0.35$ ended up either in the first two or last two bins. This suggests that one indeed needs to take into account *both* v_2 and v_3 *as well as* mutual orientation of Ψ_2 and Ψ_3.

5.2 Central collisions

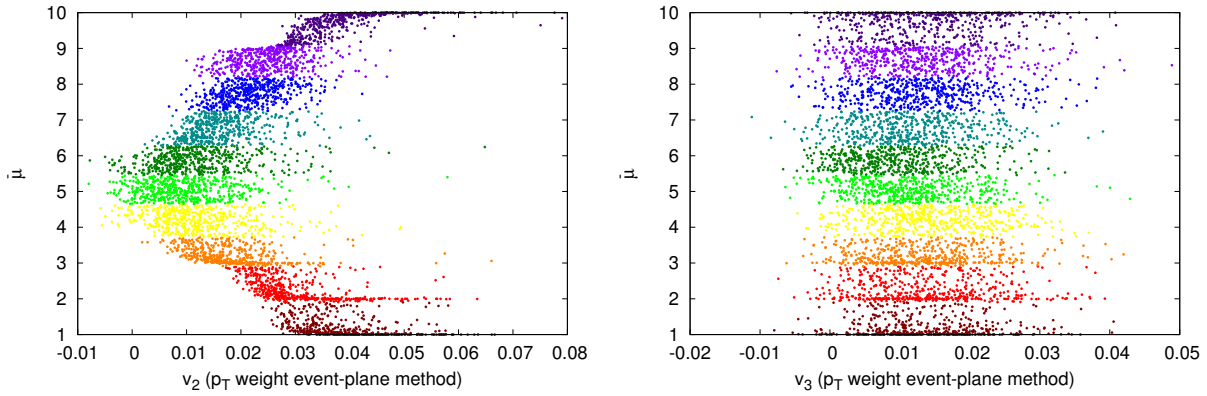

Fig. 13: Correlation of $\bar{\mu}$ with v_2 (left) and v_3 (right) for central collisions. Events were initially rotated according to Ψ_3. Events were flipped after first convergence.

Therefore, we rotated events according to Ψ_{2-3}, defined in Sec. 3.2.3. The correlations of $\bar{\mu}$ with v_2 and v_3 are shown in Fig. 14. v_2 is still dominant as well as the sorting does not depend on v_3. Even in this case the correlation of $\bar{\mu}$ and v_2 is better than correlation of $\bar{\mu}$ and q_2, -0.689 compared to -0.669. This time the correlation is negative. Since we started with randomly sorted events, the algorithm arranges them in *some* way. Sometimes, events are sorted from the one with biggest v_2 to the smallest v_2, sometimes from the smallest to the biggest v_2. The final arrangement in those two cases is just an inverse image of each other.

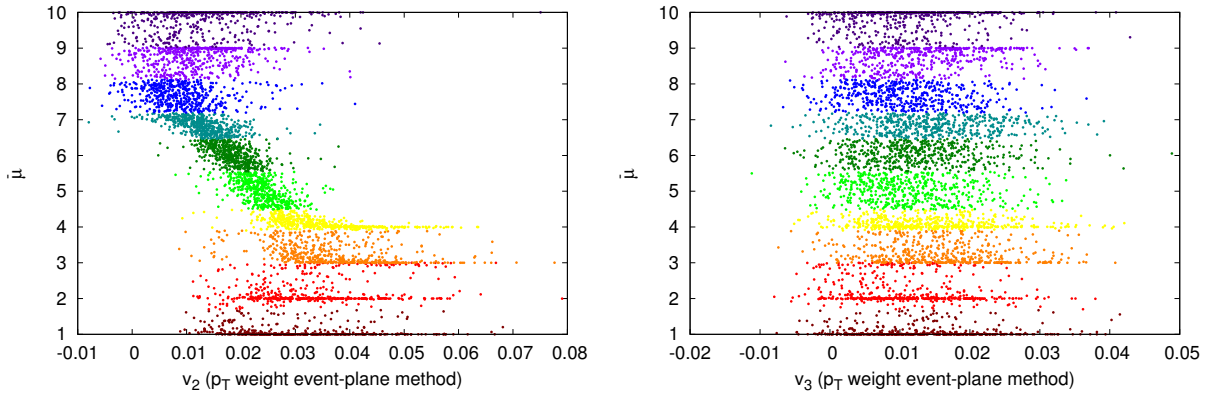

Fig. 14: Correlation of $\bar{\mu}$ with v_3 (left) and v_2 (right) for central collisions. Events were initially rotated according to Ψ_{2-3}. Events were flipped after first convergence.

More interesting were the results for particle correlation histograms. The algorithm struggled to converge even after 10000 steps. The overall shapes of the pair distributions are in Fig. 15. For better visual comparison, the bins are divided by the number of pairs in each event bin μ. Events were initially sorted according to q_2. This is reflected in the figure by decreasing number of pairs present. However, after sorting the events, multiplicity dependence is lost, as seen from Fig. 16. It seems that the sorting strongly depends on v_2 only and any other variable dependence is smeared, since two-particle correlations are a convolution of an event with itself, hence we lose some information about the events. It seems that events can be sorted using v_2 or q_2. The correlation between $\bar{\mu}$ and v_2 is 0.932, $\bar{\mu}$ and q_2 is 0.922.

The lines around integers are very pronounced now, meaning the bins are distinctly given. If $\bar{\mu}$ is an integer, there is a big probability that it indeed belongs to this bin, while values such as $\bar{\mu} = 2.5$ indicate the bin belongs to bin 2 *or* 3 or even anywhere else, assuming the $\bar{\mu}$ is uniformly distributed. This is not a necessarily true assumption: we sort events according to $\bar{\mu}$. In case of all events having $\bar{\mu} \in (5, 6)$, the algorithm *can* converge. However, this would require rather identical events and the events would fluctuate from bin to bin. Hence, this is very unlikely to happen.

If we have a look at the initial assignment error matrix (Fig. 16, bottom right), defined by eq. (16), we see that the probability that an event from bin β ends up in bin α is almost uniformly ~ 0.1 with tiny fluctuations. Within the computational precision those fluctuations are negligible. This is caused by the multiplicity independence of the algorithm, while q_2 depends also on multiplicity, the shape does not.

Nonetheless one phenomenon is obvious: if he have a closer look at, for example, $\bar{\mu} = \bar{\mu}(v_2)$ dependence, we see that several events from the 10^{th} bin have $\bar{\mu}$ around 9, leading to problems with convergence. This is caused by the fact that we use *quantiles*. The bins are rather distinct and it seems that last two bins should be in the same bin, while the other bins division might be even finer. Hence, we tried to make finer division of the azimuthal angle histograms. We increased the number of ϕ bins[4] from 20 to 40. The results are in Fig. 17.

[4]Do not confuse azimuthal angle bins with event bins!

5.2 Central collisions

The problem with error matrix has not disappeared and the results have not changed much compared to Fig. 16. This suggest the events in the last two bins are very similar and they indeed belong to one event bin.

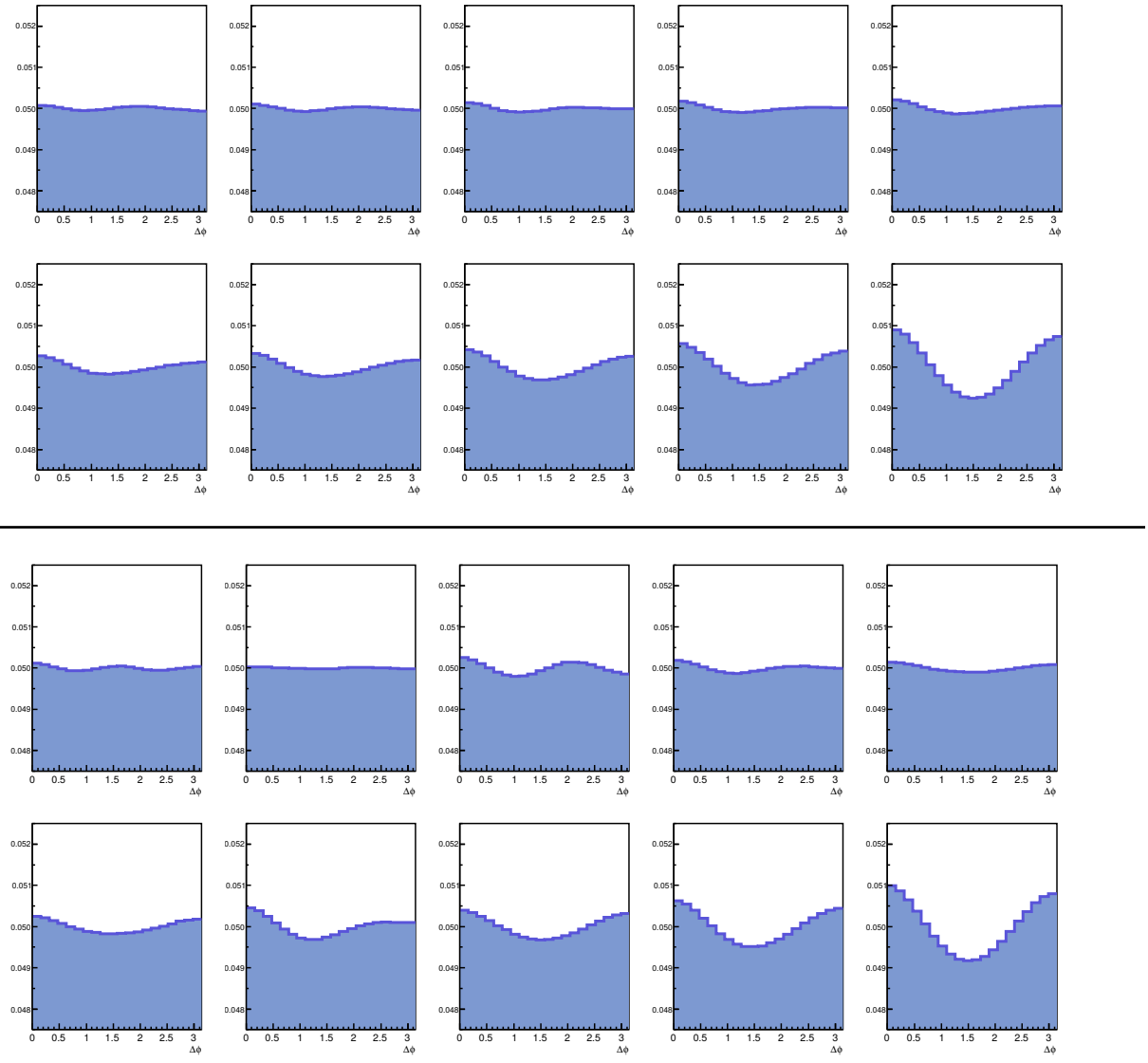

Fig. 15: Average azimuthal angle histograms of central collisions *before* sorting was used (sorted according to q_2) (top) and *after* sorting was used (bottom).

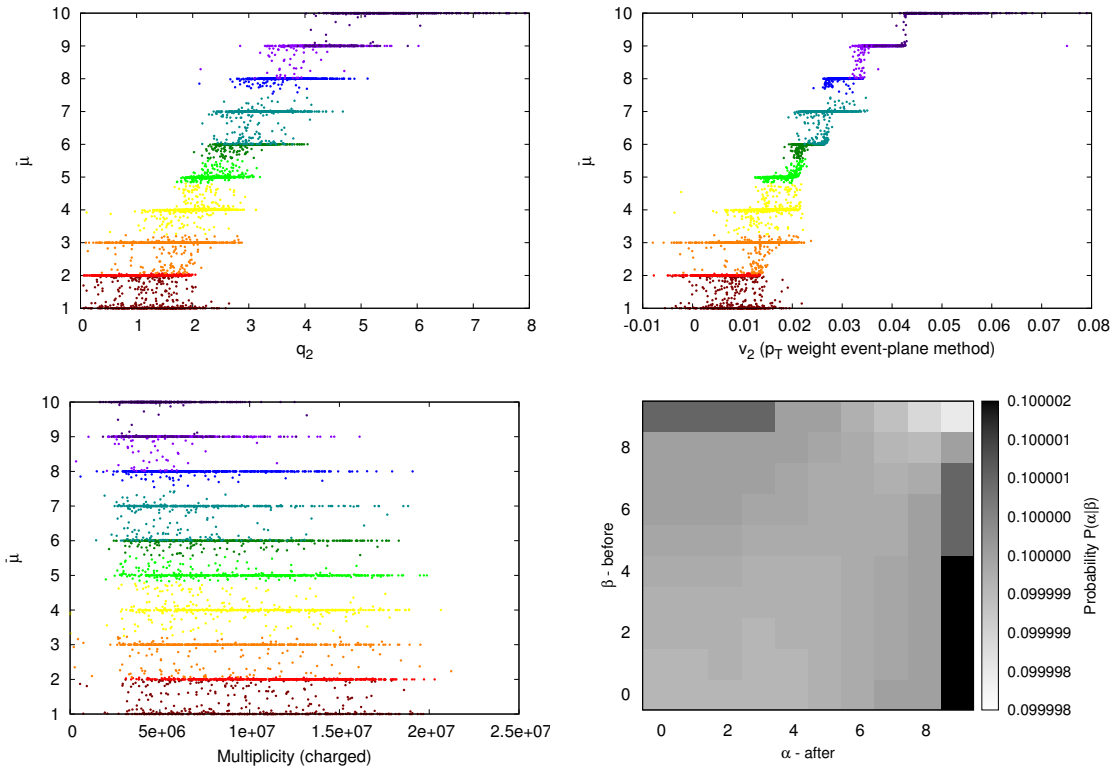

Fig. 16: Correlation of $\bar{\mu}$ with on q_2 (top left), v_2 (top right) and number of pairs M (bottom left) and error assignment matrix (bottom right) for pair distribution in central collisions.

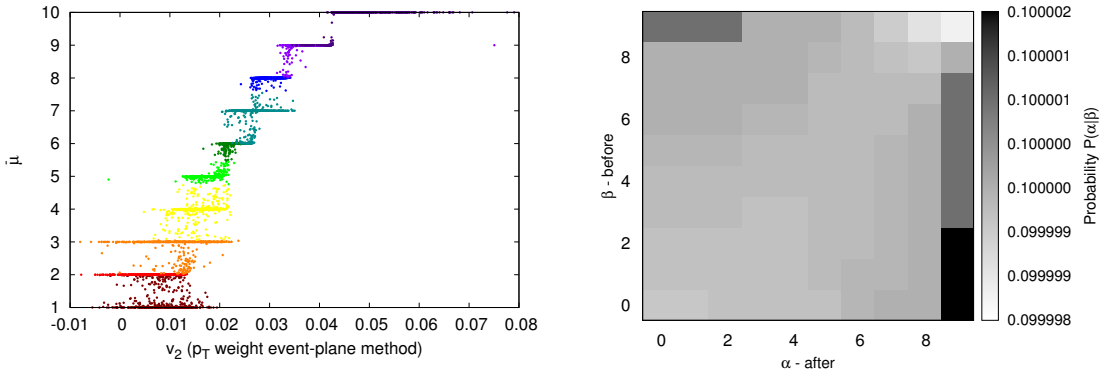

Fig. 17: Correlation of $\bar{\mu}$ with v_2 (left) and error assignment matrix (right) for pair distribution in central collisions with *fine* azimuthal angle binning.

5.3 Comparison of central, mid-central and peripheral collisions

Now, we study the differences between event-bins for different centralities.

First, we studied events oriented according to Ψ_2. Average histograms can be seen in Figs. 18, 19 and 20. Notice the differences in the number of particles. There are also differences in v_3 influence on the events. In Fig. 18, there is v_3 visible in all the event bins including the last two bins - they appear to be a symmetric image of each other. Per contra, in Fig. 19 the third *bumb* is clearly visible in the last bin only as well as in Fig. 20. This reflects the fact that v_3 is bigger than v_2 in the most central collisions as well as the fact that for small v_2, v_3 becomes visible in all the centrality classes.

The dependencies of $\bar{\mu}$ on v_2 and v_3 are in Figs. 21, 22 and 23. It is clear that v_2 is dominant in peripheral collisions and its dominance decreases with centrality. For peripheral collision, the correlation between $\bar{\mu}$ and v_2 is -0.891 (with q_2 it is -0.836). However, v_3 is still not significant.

The role of both v_2 and v_3 is even more visible in the results for Ψ_3 rotation (Figs. 24, 25 and 26). Once again, events were flipped after the first convergence of algorithm. It is clear that rotating the events smeared the influence of v_2 in the mid-central and peripheral collisions. Since the influence of v_2 is still visible for central collisions, this rotation appears as arbitrary and it is not a good choice. This agrees with our expectations since v_3 is most significant in ultra-central collisions while v_2 being the biggest in central collisions.

Similar behavior can be seen in Figs. 27, 28 and 29, reflecting the results for Ψ_{2-3} rotation. v_3 is not a significant variable in all three cases, the v_2 dependence is enhanced in the peripheral collisions, suggesting the importance of Ψ_3. In the case of central and mid-central collisions, the dependence of $\bar{\mu}$ on v_2 is more clear than in the case of Ψ_2 rotation (Figs. 21, 22 and 23). This is due to the fact that this rotation eliminates the parity symmetry and pronounces the influence of v_3, which is small in mid-central and peripheral collisions.

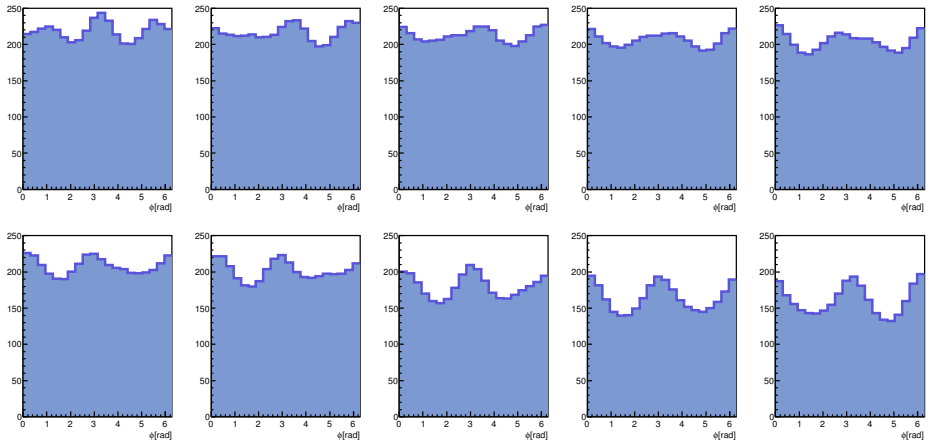

Fig. 18: Average azimuthal angle histograms of *central* collisions after sorting was used.

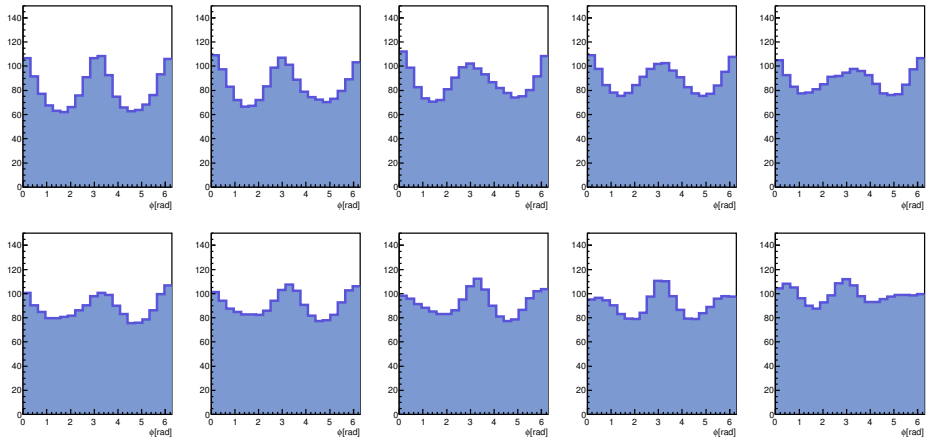

Fig. 19: Average azimuthal angle histograms of *mid-central* collisions after sorting was used.

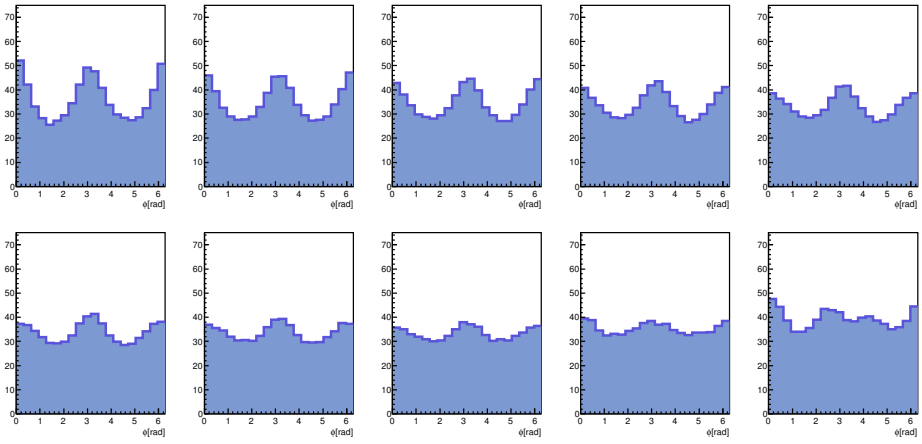

Fig. 20: Average azimuthal angle histograms of *peripheral* collisions after sorting was used.

5.3 Comparison of central, mid-central and peripheral collisions

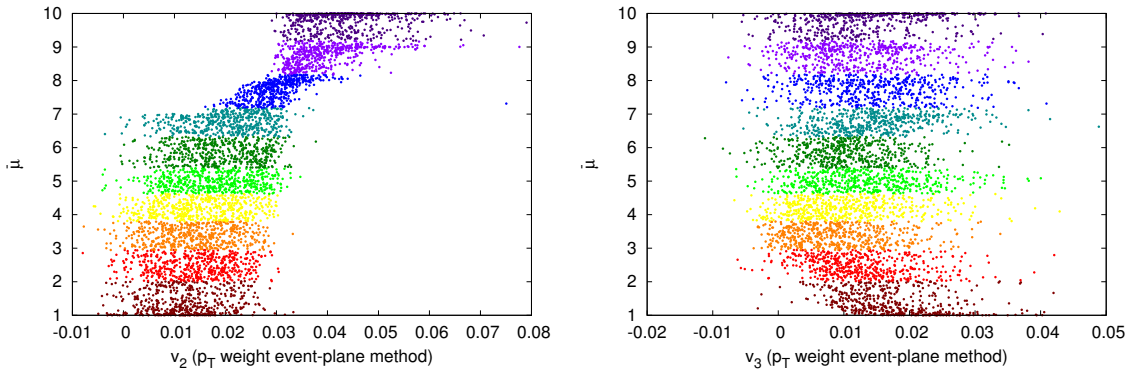

Fig. 21: Correlation of $\bar{\mu}$ with v_2 (left) and v_3 (right) for central collisions. Events were initially rotated according to Ψ_2.

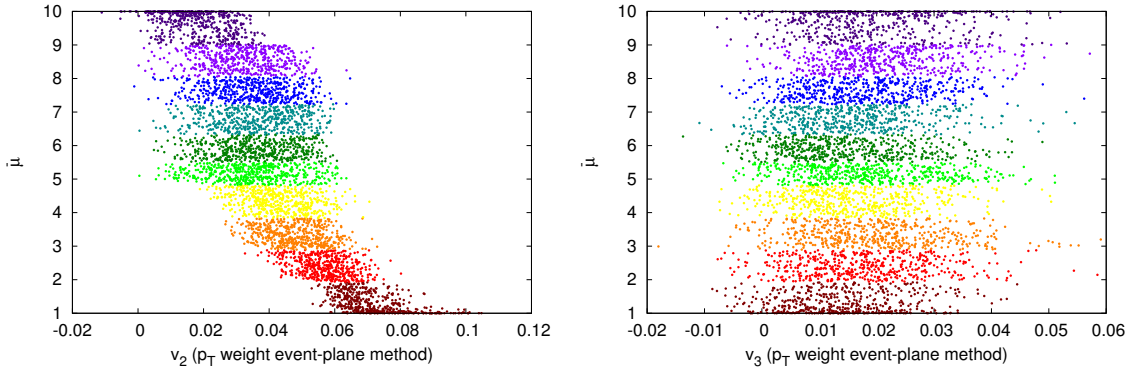

Fig. 22: Correlation of $\bar{\mu}$ with v_2 (left) and v_3 (right) for mid-central collisions. Events were initially rotated according to Ψ_2.

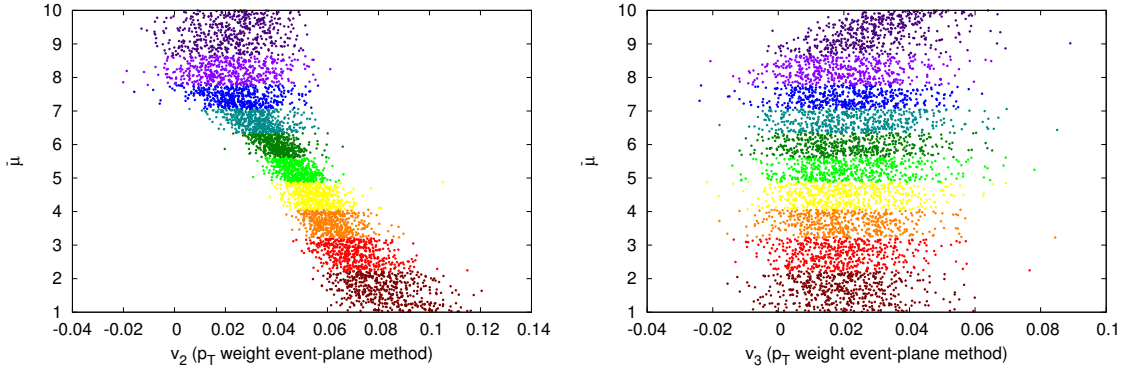

Fig. 23: Correlation of $\bar{\mu}$ with v_2 (left) and v_3 (right) for peripheral collisions. Events were initially rotated according to Ψ_2.

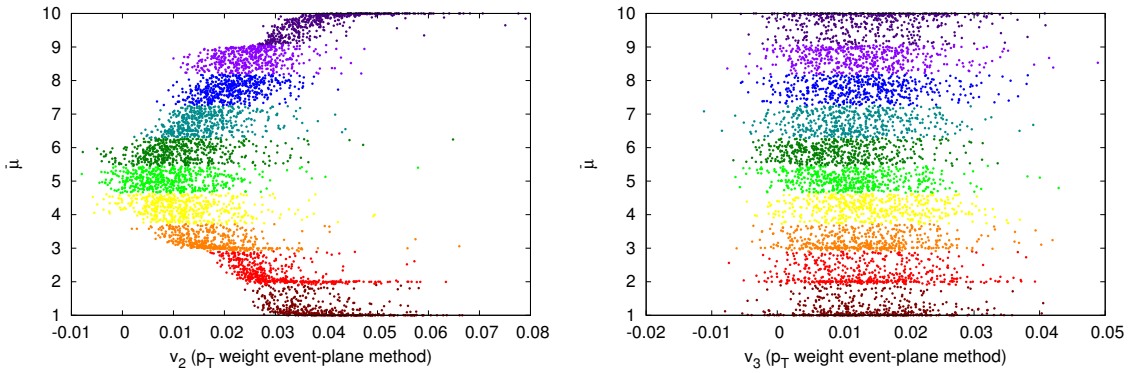

Fig. 24: Correlation of $\bar{\mu}$ with v_2 (left) and v_3 (right) for central collisions. Events were initially rotated according to Ψ_3 and flipped.

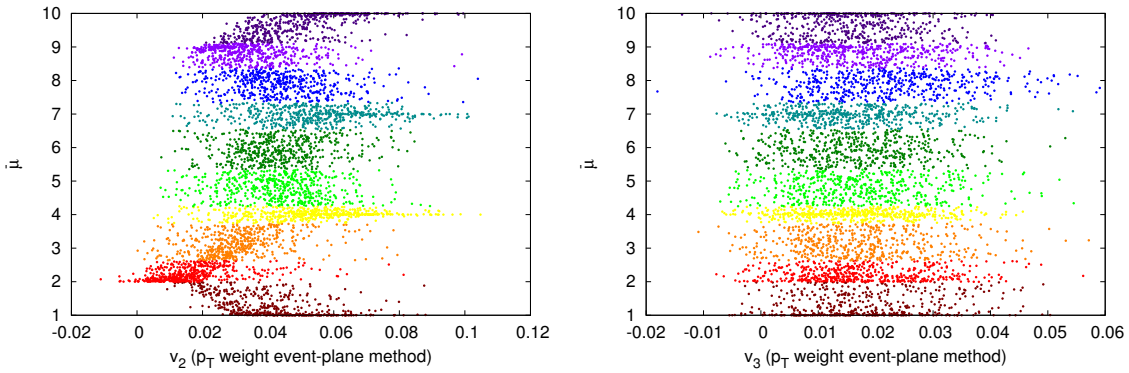

Fig. 25: Correlation of $\bar{\mu}$ with v_2 (left) and v_3 (right) for mid-central collisions. Events were initially rotated according to Ψ_3 and flipped.

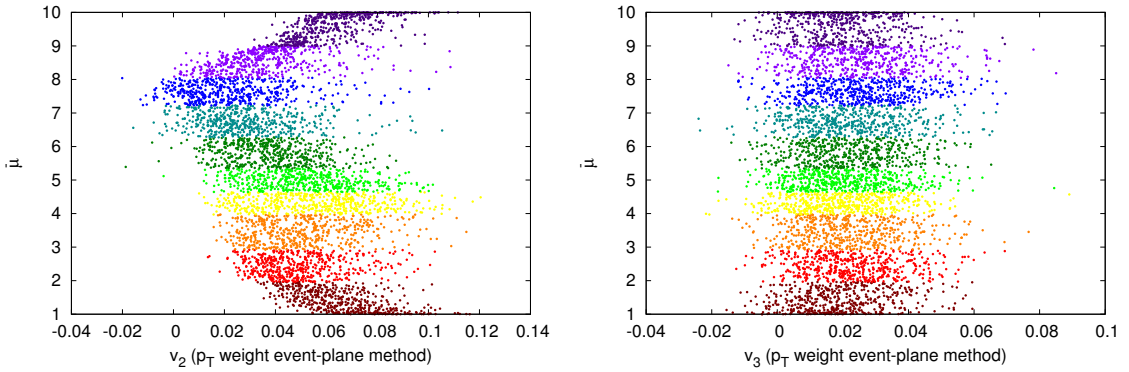

Fig. 26: Correlation of $\bar{\mu}$ with v_2 (left) and v_3 (right) for peripheral collisions. Events were initially rotated according to Ψ_3 and flipped.

5.3 Comparison of central, mid-central and peripheral collisions

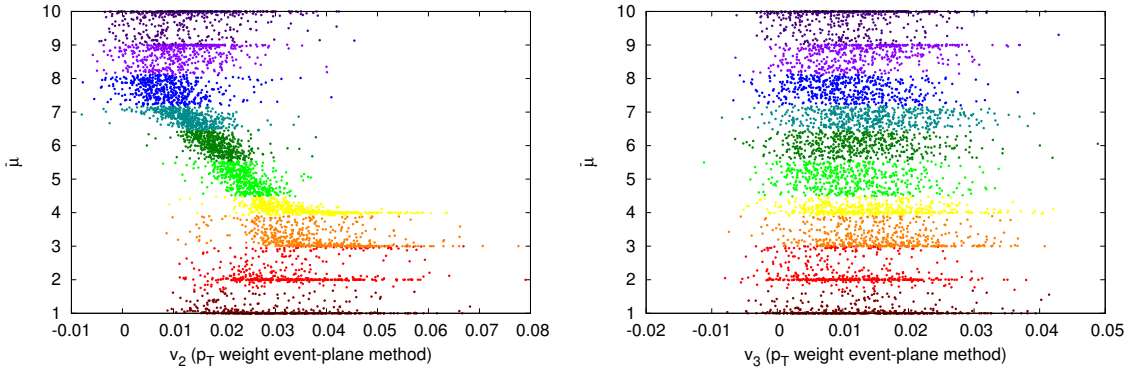

Fig. 27: Correlation of $\bar{\mu}$ with v_2 (left) and v_3 (right) for central collisions. Events were initially rotated according to Ψ_{2-3}.

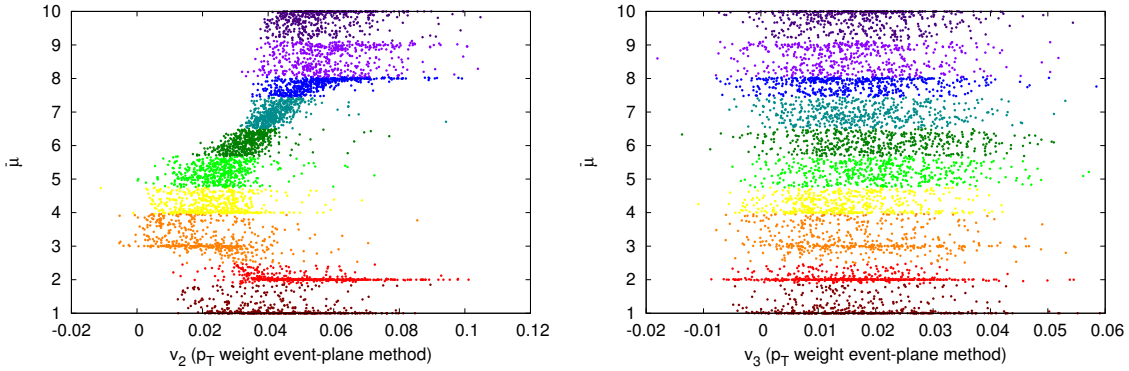

Fig. 28: Correlation of $\bar{\mu}$ with v_2 (left) and v_3 (right) for mid-central collisions. Events were initially rotated according to Ψ_{2-3}.

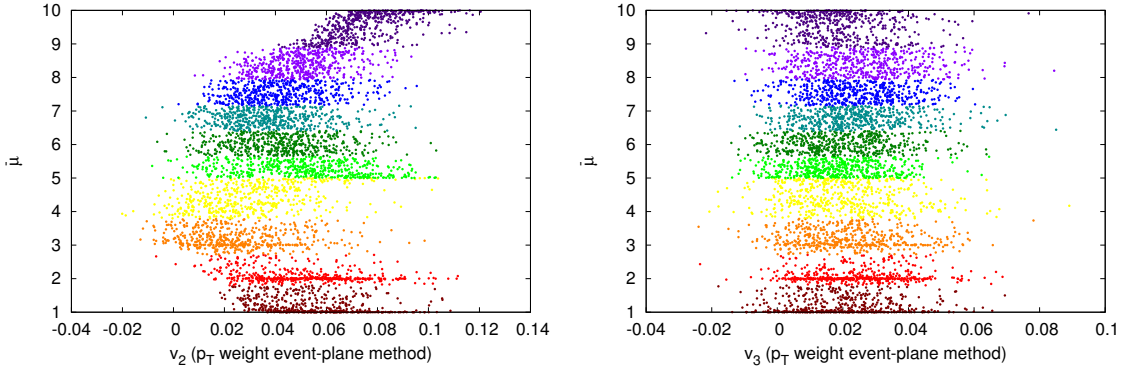

Fig. 29: Correlation of $\bar{\mu}$ with v_2 (left) and v_3 (right) for peripheral collisions. Events were initially rotated according to Ψ_{2-3}.

5.4 Study of rapidity cuts

We also looked at narrow mid-rapidity region $|y| < 0.5$ and in the wider region of rapidity $|y| < 1.5$. We present results from central collisions. The results are fairly similar, however, the correlation of $\bar{\mu}$ with v_2 is even less pronounced for $|y| < 0.5$, the correlation coefficient of $\bar{\mu}$ and v_2 is 0.724. On the other hand, the correlation of $\bar{\mu}$ and v_2 for $|y| < 1.5$ is 0.771 (for $|y| < 1$ it is 0.770). The average histograms *after* sorting in Fig. 30 suggest also a non-negligible influence of v_3 in the region $|y| < 0.5$. In comparison with Fig. 31 and Fig. 32, where the v_3 is smeared, there is a visible presence of three *bumps*. Thus, v_3 appears as a more local effect.

This is confirmed by the $\bar{\mu} = \bar{\mu}(v_3)$ dependence. In Figs. 33, 34 and 35 we present dependence of $\bar{\mu}$ on v_2 and v_3. In the $|y| < 0.5$ region, there is a hint of weak linear dependence of $\bar{\mu}$ on v_2 in the first two bins. This corresponds to the fact that in the most central collisions, v_3 starts to dominate. This comparison also tells us a lot about the algorithm behaviour: it is apparent that in the case of $|y| < 1.5$, the events are fairly different while in the case of $|y| < 0.5$ the difference between event bins is small. Hence, for our needs, regardless of any physical motivation, the condition $|y| < 1$ may be an ideal choice, considering the case of $|y| < 0.5$ being very unclear for $\bar{\mu} < 8$ and events being very disting in the case of $|y| < 1.5$, leading to similar trouble as in the case of two-particle correlations.

The results do not change significantly in case of Ψ_{2-3} rotation, results for v_2 and v_3 are in Figs. 36, 37 and 38. Once again, the case of $|y| < 1.5$, the events are fairly different while in the case of $|y| < 0.5$ the difference between event bins is small, proving our previous point.

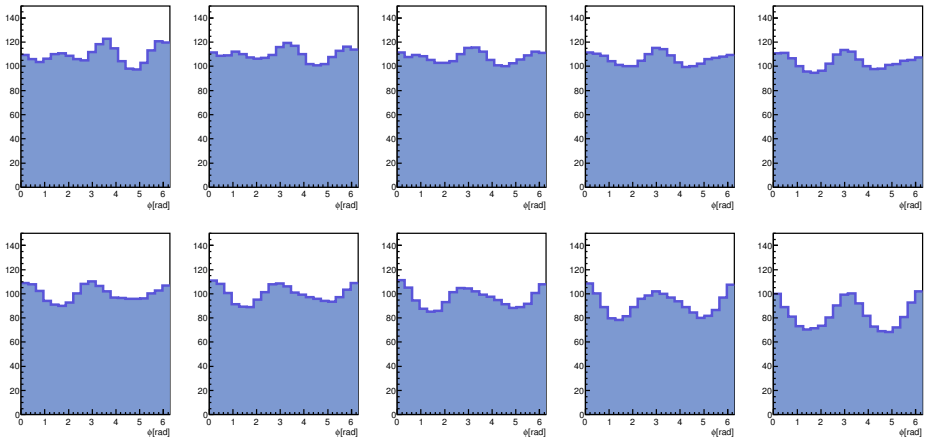

Fig. 30: Average azimuthal angle histograms (central), *after* sorting was used, $|y| < 0.5$.

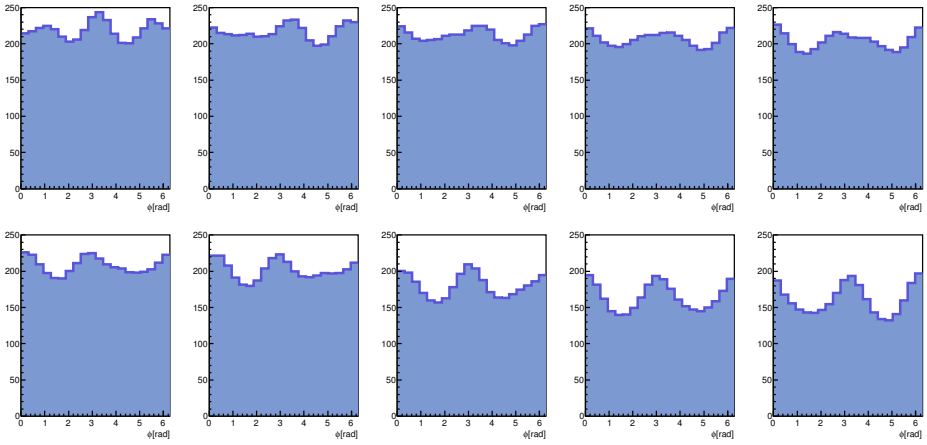

Fig. 31: Average azimuthal angle histograms (central), *after* sorting was used, $|y| < 1$.

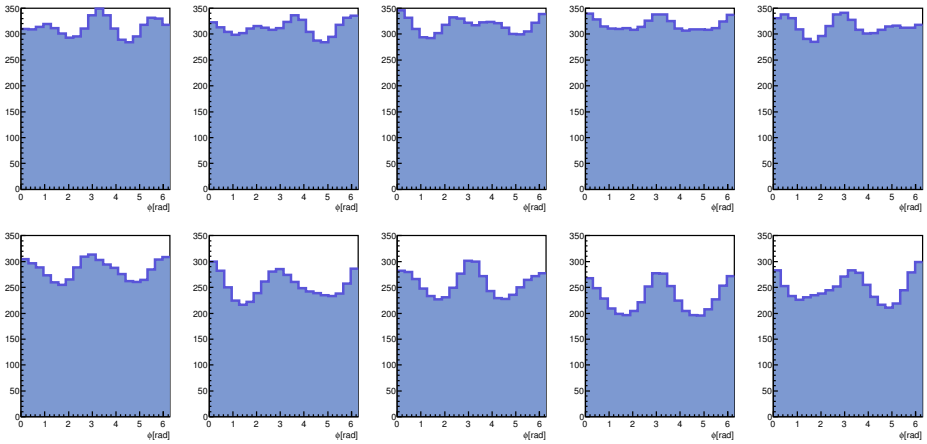

Fig. 32: Average azimuthal angle histograms (central), *after* sorting was used, $|y| < 1.5$.

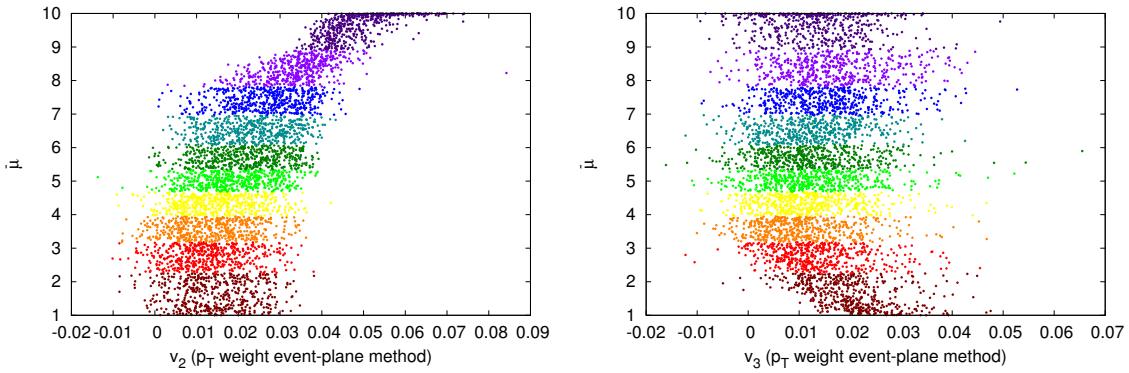

Fig. 33: Final sorting dependence $\bar{\mu}$ on v_2 (left) and v_3 (right) for central collisions. Events were initially rotated according to Ψ_2, $|y| < 0.5$.

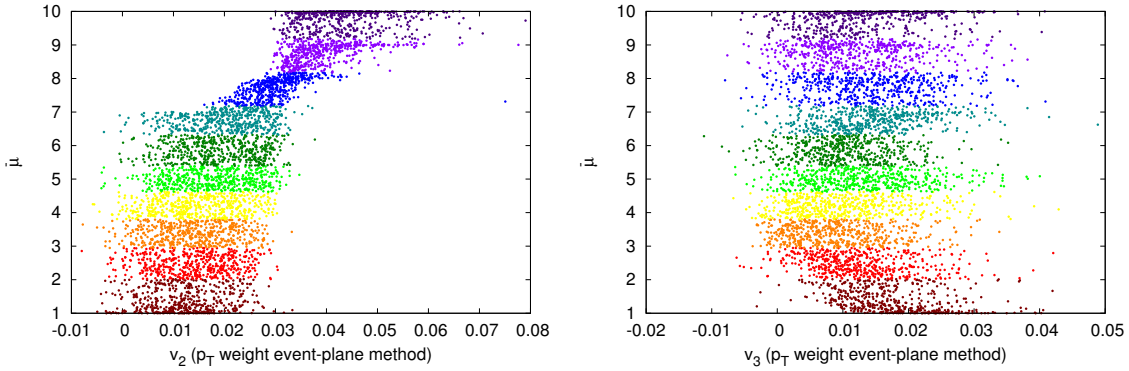

Fig. 34: Final sorting dependence $\bar{\mu}$ on v_2 (left) and v_3 (right) for central collisions. Events were initially rotated according to Ψ_2, $|y| < 1$.

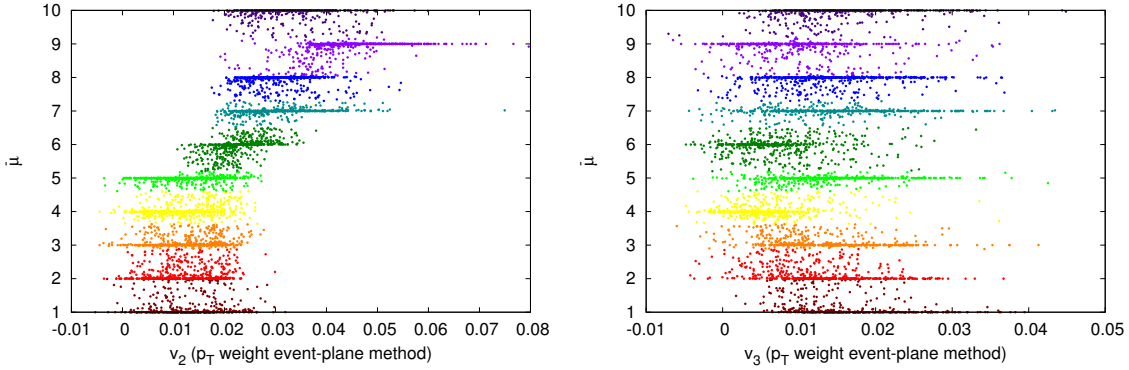

Fig. 35: Final sorting dependence $\bar{\mu}$ on v_2 (left) and v_3 (right) for central collisions. Events were initially rotated according to Ψ_2, $|y| < 1.5$.

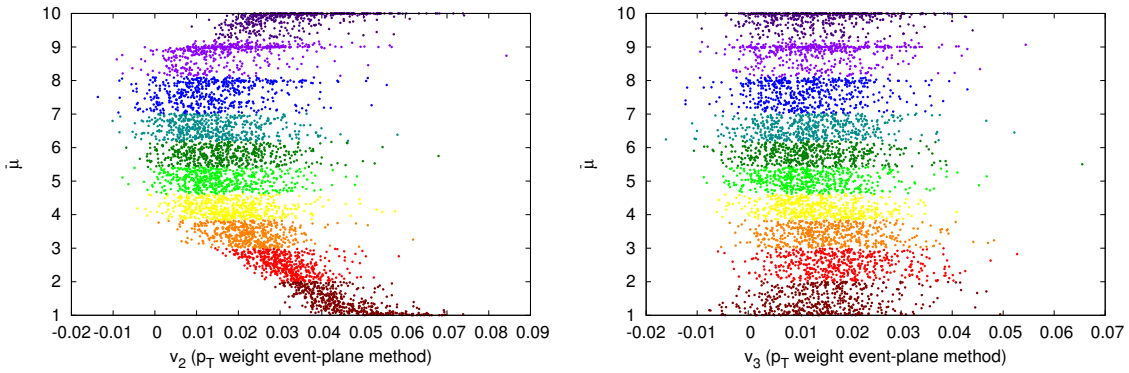

Fig. 36: Final sorting dependence $\bar{\mu}$ on v_2 (left) and v_3 (right) for central collisions. Events were initially rotated according to Ψ_{2-3}, $|y| < 0.5$.

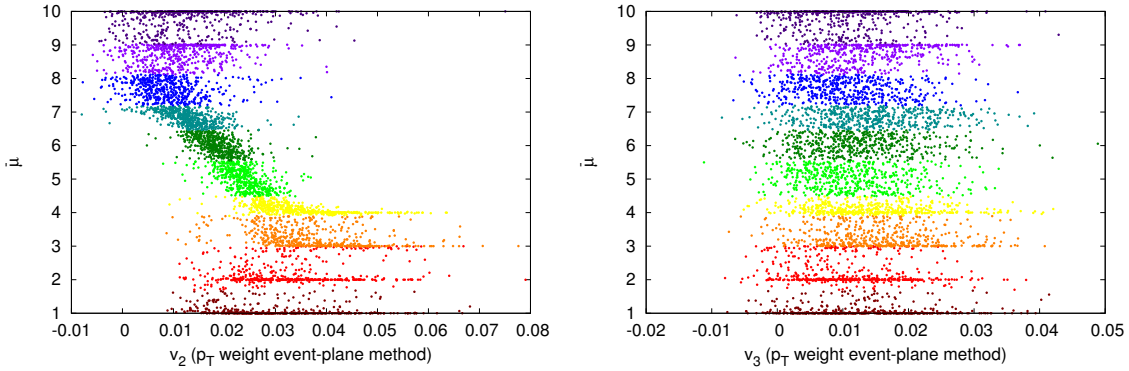

Fig. 37: Final sorting dependence $\bar{\mu}$ on v_2 (left) and v_3 (right) for central collisions. Events were initially rotated according to Ψ_{2-3}, $|y| < 1$.

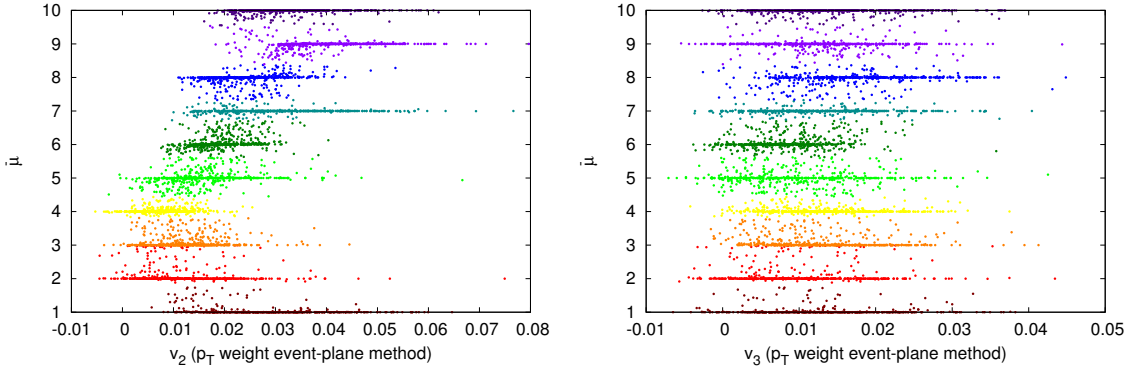

Fig. 38: Final sorting dependence $\bar{\mu}$ on v_2 (left) and v_3 (right) for central collisions. Events were initially rotated according to Ψ_{2-3}, $|y| < 1.5$.

5.5 Correlations of variables

Since the previous results suggest that the shape of the collisions is determined by an interplay of several variables, we tried to determine some variable that would be good for sorting the events.

First, we were interested in the overall correlations among all studied variables, where the sample were all events. For that, we obtained a correlation matrix for each of the central events, $|y| < 1$, rotated according to Ψ_2. This rotation choice is because the difference in variables characterizing the events with $\bar{\mu} < 7$ is not clear (Fig 11). Correlation matrix is a matrix, where each element is a correlation coefficient of two variables, each row and each column represents one variable. The diagonal is always equal to 1: correlation of a variable and itself is always 1. The correlation coefficients are in the Fig. 39. For viewers comfort we removed lower half of the matrix as well as the diagonal.

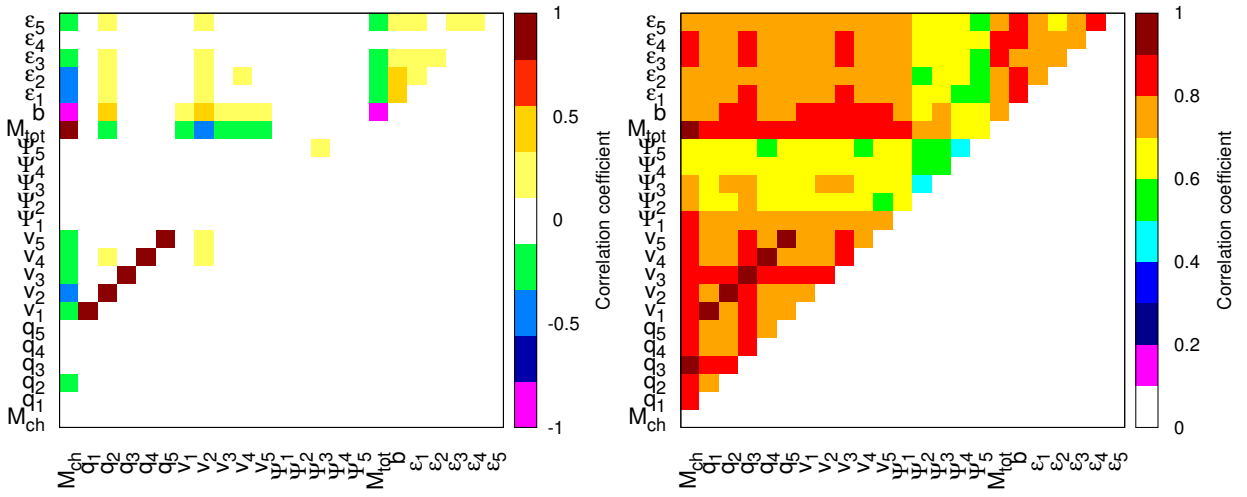

Fig. 39: Multi-dimensional correlation matrix of variables for all events (left) and for one event bin (right). M_{ch} is number of charged particles, M_{tot} is number of all particles. b denotes impact parameter, q_n n$^{\text{th}}$ reduced flow vector, v_n is n$^{\text{th}}$ flow coefficient, Ψ_n is n$^{\text{th}}$ event plane angle, ε_n is n$^{\text{th}}$ partial eccentricity moment.

It is clear from the Fig. 39 that, as we expected, q_n and v_n are strongly correlated in all cases. There is a clear correlation between b, M_{ch} and M_{tot}. Looking at one bin correlations

only, it is clear that all variables are correlated. This is a clear sign of the power of the algorithm: considering the azimuthal shape only, we selected truly similar events. Another expected fact is that the rotations of n^{th} event planes are less correlated with other variables.

For the reasons stated above, we excluded $q_1 \dots q_2$, b, M_{tot}. This also helped significantly reduce (by factor of 10000) the condition number. It is defined as the ratio of the largest and smallest eigenvalue of the correlation matrix. This number describes the difference between the input and output change. If this number is big, small change in input results in huge change in the output. This is best understood using a an example: imagine a system of equations $\mathbb{A}x = b$. If the condition number of the matrix $\mathbb{A}$ is large, small change of x leads to big change in b. If the condition number of the correlation matrix is high, there are two or more variables that are highly correlated. Since we are interested in the variables describing the shape, we want to reduce these correlations and focus on uncorrelated set of variables.

Now, we want to obtain a suitable variable for sorting events. For this purpose, we use so called Principal component analysis (PCA). This method allows us to reduce the number of variables suitable for this analysis. The components have the largest variance possible, therefore they account most for the data variability. PCA can provide us the best *linear* combination of the variables to describe our dataset. Even tough the problem is most likely more complex, linear approximations are usually a good first approximations and higher orders vanish at the limit of small perturbations. The PCA is executed as follows: first, calculate the correlation matrix $\mathbb{C}$. The matrix is symmetric and its dimension is n. Then calculate its eigenvectors b_1, $b_2 \,, \dots \,, b_n$. The eigenvectors are sorted in a way, that b_1 has the largest eigenvalue, b_2 the second largest, ... The eigenvectors are a new base of the n-dimensional space, each vector points in direction of the largest (second largest,...) variance. The vectors b_1, $b_2 \,, \dots \,, b_n$ are used as a new base for the variables.

Looking back at the overall correlation of the events (Fig. 39), we can do the reduction of variables also using PCA. The reduction of parameters is usually done by selecting the largest eigenvalue of the covariance matrix and finding its eigenvector. However, when using different variables with different units, it is better to use correlation matrix since it uses

standardized data. Looking at all rotations (Ψ_2, Ψ_3 and flipped, Ψ_{2-3}), several eigenvalues have small value ~ 0.7 (can be excluded), however, dominance of any eigenvalue is not clear, the highest eigenvalue is ~ 2.5. If we included $q_1, \ldots, q_5$, b and M_{tot}, the eigenvectors in direction of those variables would have small eigenvalues. Hence, our assumption above to exclude them was right.

We calculated the correlation matrix for each event bin. The matrices are in Fig. 40. From that, we obtained the new basis of the space of variables M, $v_1, \ldots, v_5$, $\Psi_1, \ldots, \Psi_5$, $\varepsilon_1, \ldots, \varepsilon_5$. There was always one largest eigenvalue ~ 10 times bigger than the rest of them. The associated vector should define the largest variance in the data. Those eigenvectors are in the Tab. 1. It turns out that the direction of this vector strongly fluctuates from bin to bin and the main direction is usually in the direction of Ψ_5. This suggests there is no apparent linear dependence of the shape on any of the variables mentioned above and that each event bin is very different.

	bin 1	bin 2	bin 3	bin 4	bin 5	bin 6	bin 7	bin 8	bin 9	bin 10
M	0.019	-0.049	-0.157	0.189	-0.201	-0.133	0.098	-0.050	-0.030	-0.063
v_1	-0.045	0.040	-0.017	-0.174	-0.091	0.044	-0.011	0.028	0.073	0.149
v_2	-0.491	0.384	**0.566**	-0.204	-0.353	0.357	0.002	0.161	0.423	**-0.493**
v_3	-0.186	-0.191	0.134	0.116	-0.188	-0.150	-0.048	-0.287	-0.342	0.190
v_4	-0.084	-0.126	0.119	0.391	-0.201	0.210	0.388	0.196	0.198	-0.066
v_5	-0.027	0.148	0.046	-0.280	-0.312	-0.275	0.077	0.204	0.101	0.097
ψ_1	0.277	-0.128	0.405	0.171	-0.096	-0.261	0.155	-0.446	-0.126	0.074
ψ_2	0.063	0.144	0.069	0.085	-0.200	0.016	-0.054	0.119	-0.166	-0.292
ψ_3	-0.063	-0.165	0.197	**0.481**	-0.150	**0.609**	0.402	0.307	0.273	0.118
ψ_4	0.253	**-0.572**	-0.057	-0.270	0.049	-0.023	**0.675**	-0.067	-0.413	-0.064
ψ_5	**-0.506**	-0.430	-0.440	0.194	**0.672**	0.320	0.116	**-0.609**	**-0.483**	-0.392
ε_1	-0.487	-0.315	-0.311	0.416	-0.021	-0.016	0.146	-0.121	-0.172	0.321
ε_2	-0.094	-0.049	-0.003	0.079	0.037	0.251	-0.136	-0.064	-0.027	0.319
ε_3	-0.018	-0.099	-0.221	0.041	0.072	0.002	-0.252	-0.205	0.138	0.347
ε_4	0.012	0.155	0.076	-0.162	-0.243	-0.201	0.089	0.014	-0.114	0.179
ε_5	-0.251	-0.249	-0.254	0.253	0.250	0.253	-0.249	-0.253	0.254	-0.245

Tab. 1: Eigenvectors corresponding to the largest eigenvalue of correlation matrices for central events, Ψ_2 rotation. The bold numbers are the largest contributions to the size of the vector.

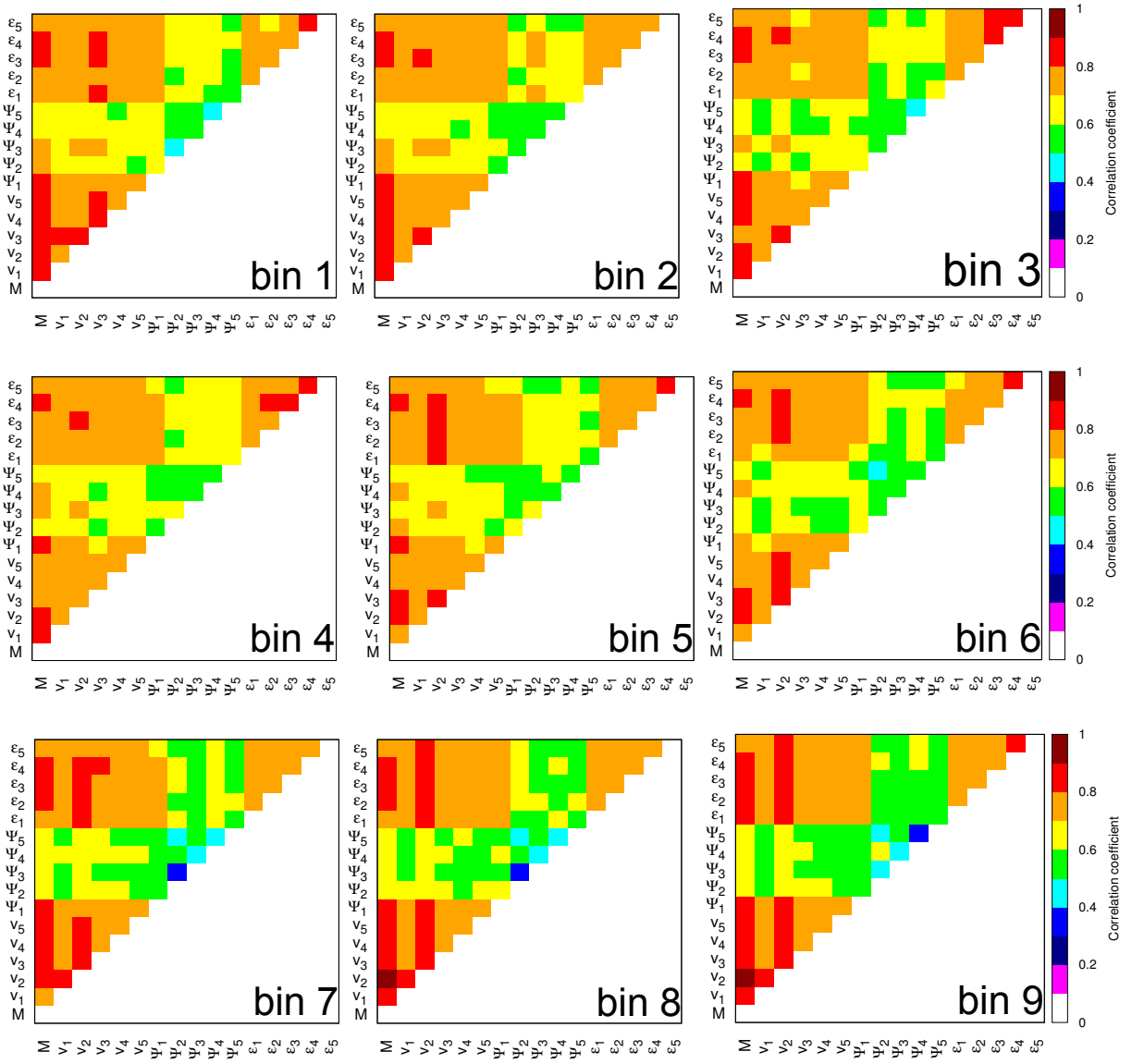

Fig. 40: Multi-dimensional correlation matrix for each event-bin. M is number of charged particles, v_n is n$^{\text{th}}$ flow coefficient, Ψ_n is n$^{\text{th}}$ event plane angle, ε_n is n$^{\text{th}}$ partial eccentricity moment. For viewers comfort we excluded lower part of the matrix, the diagonal and we do not include the last bin.

Conclusions

In this thesis we presented a new study of the event shape. We described the algorithm used, we discussed its possible applications and proposed possible ways of extension of the method. We present our program called ESSTER.

The method was applied on data obtained from AMPT [20]. We presented a study of the data in different centrality and rapidity bins, we discussed different rotations of events and its influence on the results.

The results suggest strong importance of elliptic flow in the event shape analysis. We conclude that v_2 describes the *shape* of an event better than q_2. Nonetheless, the results confirm that the shape is a complicated interplay of more variables. So far, there is no conclusive answer to the question of what variables influence the event shape.

The power of the algorithm is confirmed by calculating the correlation matrices for every event bin. In each bin, all the variables are strongly correlated, proving the fact that our method indeed sorts the events according to their overall similarity. We applied PCA analysis on each bin. The result is that event-bins are very distinct to each other and there is no apparent linear combination of variables determining the shape of events. This issue needs to be investigated in greater detail.

References

[1] N. K. Glendenning, Compact Stars: Nuclear Physics, Particle Physics, and General Relativity, Springer New York (2000).

[2] U. Heinz and M. Jacob, arXiv:nucl-th/0002042v1.

[3] S.A. Voloshin, A.M. Poskanzer and R. Snellings, Ann. Rev. Nucl. Part. Sci. **63** 123-151 (2013).

[4] Z. Fodor and S.D. Katz JHEP **0404** (2004) 050.

[5] P. Braun-Munzinger, Nucl. Phys. A **681**, 119 (2001).

[6] J. Schukraft, A. Timmins and S. Voloshin, Phys. Lett. B **719** (2013) 394.

[7] S.A. Voloshin, A. M. Poskanzer and R. Snellings, arXiv: 0809.2949 [nucl-ex].

[8] R. Hanbury-Brown and R. Q. Twiss, Proc. R. Soc. A **242** (1230) 300-324 (1957).

[9] M. Meissner, U. Uwer and K. Reygers, CERN-THESIS-2014-273 (2014).

[10] Md.R. Haque, L. Zi-Wei and B. Mohanty, Phys. Rev. C **85** 034905 (2012).

[11] V. Bairathi, Md.R. Haque, and B. Mohanty, Phys. Rev. C **91** 054903 (2015).

[12] B. Tomášik, M. Schulc, I. Melo, R. Kopečná, arXiv: 1511.00034 [nucl-th].

[13] NICA whitepaper, Draft v 10.01, e-print: `http://theor0.jinr.ru/twiki-cgi/view/NICA/NICAWhitePaper` [2016-04-26].

[14] G. Aad *et al.* [ATLAS Collaboration], Phys. Rev. C **86** 014907 (2012).

[15] G. Eyyubova [for the ALICE Collaboration], EPJ Web of Conferences **70** 00075 (2014).

[16] R. Kopečná and B. Tomášik, Eur. Phys. J. A (2016) **52**: 115.

[17] S. Lehmann, A.D. Jackson and B. Lautrup, Nature **444** 7122 (2006).

[18] S. Lehmann, A.D. Jackson and B. Lautrup, arXiv: physics/0512238.

[19] R. Kopečná and B.Tomášik, to be published in A. Phys. Pol. B Supp., arXiv: 1603.04997 [nucl-th].

[20] L. Zi-Wei, J. Xu, C.K. Ming L. Bao-An and Z. Bin, Phys. Rev. C **72** 064901 (2005).

[21] AMPT source codes, `http://myweb.ecu.edu/linz/ampt/` [2015-12-31].

[22] D. d'Enterria, Jet Quenching in Relativistic Heavy Ion Physics, Landolt-Börnstein series, Springer-Verlag, **23** 471 (2010).

[23] T.S. Biro, P. Levai and J. Zimanyi, Phys. Lett. B **347** 6 (1995).

[24] B. A. Li and C.M. Ko, Phys. Rev. C **52**, 2037 (1995).

[25] Zi-Wei, A. Phys. Pol. B Supp. **7** 119 (2014).

[26] J. Xu and C.K. Ming, Phys. Rev. C **83** 034904 (2011).

[27] B. Abelev *et al.* [ALICE Collaboration], Phys. Rev. C **88** 044909 (2013).

[28] B. Schenke, P. Tribedy, and R. Venugopalan., Phys. Rev. C **86** 034908 (2012).

[29] ROOT |A Data Analysis Framework, `http://root.cern.ch` [2015-12-30].

[30] LAPACK – Linear Algebra PACKage, `http://www.netlib.org/lapack` [2015-12-30].

[31] W.H. Press, S. A. Teukolsky, W.T. Vetterling and B.P. Flannery, Numerical Recipes 3rd Edition: The Art of Scientific Computing, Cambridge University Press, NY, USA (2007).

[32] A. Bilandzic, R. Snellings and S.A. Voloshin, Phys. Rev. C **83** 044913 (2011).

[33] D. Veberic, e-print arXiv: 1003.1628 [cs.MS].

A ESSTER documentation

Event-**S**hape **S**or**TER** is a Toy Model Monte Carlo generator and Event Shape Sorter. Its main functions were described in Section 3. ESSTER is written in C++, it was implemented using Linux operating system. It also uses ROOT [29], LLAPACK [30] and Numerical Recipes [31] functions.

For comfortable compilation, we include a makefile.

All parameters are stored in `parameters.h`. This header file includes basic constants, Toy Model parameters described in Section 3, three sorting algorithm parameters (number of event-bins (*quantile*), number of azimuthal angle bins (*NoBins*) and the number of iterations when the algorithm gets killed (*MAX_steps*). Moreover, basic cuts values (rapidity y, transverse momentum p_T and multiplicity M) are defined there.

There are 13 source files:

`main.cpp` contains functions used for understanding user commands and connects all the functions from the rest of the source files.

`additional.cpp` Several additional functions are defined there, such as help output for the user, *int*↔*string* conversion or mathematical functions such as factorial. Furthermore, the main file names and paths are specified in `additional.h`.

`ampt.cpp` This source file is used for merging partial files obtained via the AMPT model. It merges and performs basic cuts on the files containing both parton and final hadron function. Moreover, it copies those merged files from the input folder to the folder where the ESSTER analysis takes place.

`analyze.cpp` includes all basic analysis functions. Methods for cumulant method (two-particle, four-particle and four-particle p_T weighted [32]), event plane method (with or without p_T weight [7]) and Event Shape Engineering [6] are performed here.

`bins.cpp` is the main source file for the whole algorithm. Classes for storage of the bins and event info are defined here as well as calculations used for equations (13) - (16). Moreover, sorting algorithms are implemented here. For the first iteration, we use quicksort.

For the rest, insertion method is used. The reason is that first order of events is expected to be random, the performance of quicksort is $\approx O(n \log n)$. After that we assume the events to be approximately sorted. In that case, quicksort $\approx O(n^2)$, while insertion sort $\approx O(n)$. Moreover, the memory requirements of insertion sort is $O(1)$ only, while worst case quicksort is $O(n)$.

`cuts.cpp` contains functions used for event or particle selections, such as type of the analyzed particles or rapidity range.

`eigenvalues.cpp` enables us to obtain a correlation matrix. It is also able to calculate matrix eigenvalues using LLAPACK and perform basic matrix operations.

`generator.cpp` includes several functions taken from [31]. Few random number generators are implemented there. Namely, uniformly distributed from 0 to 1 *double* random number generator, consequently uniform azimuthal angle and multiplicity generators, random *integer* generator and final the normally distributed random number generator.

`list.cpp` defines one-way linked list and its basic operations used for this purpose. Linked lists are used for the analysis of the events.

`my_root.cpp` uses several ROOT methods to create, store and plot histograms.

`toymodel.cpp` is where the toy model functions are implemented. It generates azimuthal angle distribution and p_T distribution motivated by the LHC data [14, 15]. The equation

$$\frac{dN}{d\phi} \propto 1 + \sum_{n=1}^{\infty} 2v_n \cos(n(\phi - \Psi_n))$$

is used for generating azimuthal angles ϕ. The v_n parameters are set for each event depending quadratically on multiplicity M:

$$v_n = aM^2 + bM + c$$

and smeared according to Gaussian, where a, b and c are hard-set coefficients. The values of the coefficients are in Tab. 2. Those values were obtained by fitting ATLAS measurements of v_n in the p_T bin 2-3 MeV and using [15]. The result of the fit is in Fig. 41. Then, the v_n

coefficients are smeared according to Gaussian distribution with $\sigma = 0.025$. This value can be simply modified in the `parameters.h`. Event plane angles Ψ_n are set randomly and do not depend on each other for any event.

n	$a/10^{-8}$	$b/10^{-5}$	c
1	0	0.01667	–0.000680
2	–7.098	20.06	0.07874
3	–2.083	6.658	0.0424
4	–96.38	2.621	0.04897
5	–71.76	2.236	0.01673

Tab. 2: Parameters used for generating multiplicity dependent v_n: $v_n = aM^2 + bM + c$.

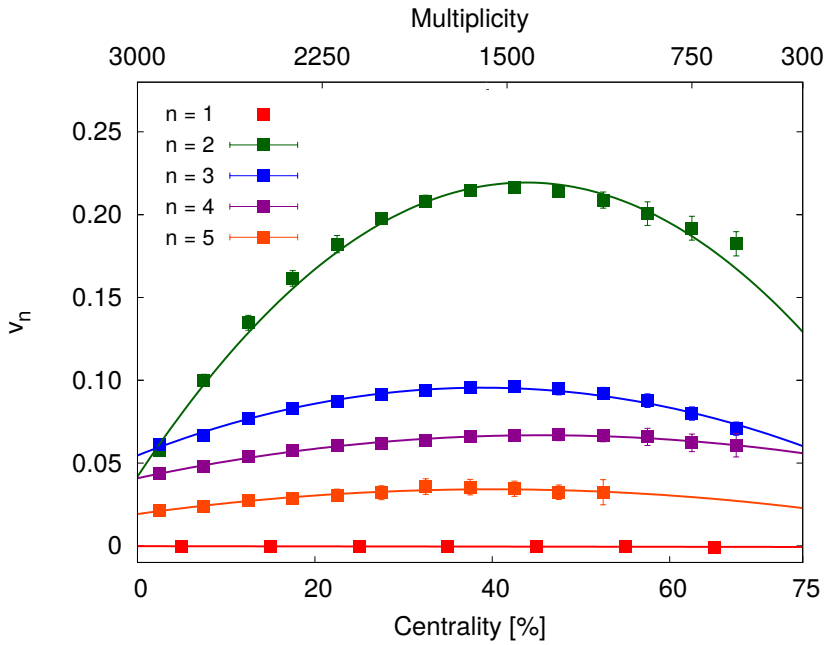

Fig. 41: Flow dependence on centrality and multiplicity. Data points are obtained from [14] and [15]. The data points are fitted with a quadratic function, fit coefficients are in the Tab. 2.

For p_T generation, we use the equation

$$\frac{dN}{dp_T} = C p_T e^{-\frac{p_T}{T}} ,$$

where we set the parameter T as 400 MeV, C is a normalization constant. This is motivated by the LHC data. We generate those values using an iterative calculation of the Lambert function [33].

`zpc_analysis.cpp` includes functions analyzing the parton distributions generated by AMPT. In particular, we calculate the energy density of the fireball and obtain the eccentricity coefficients [28] from the density.

A.1 Program running

For building the program, the user goes to the directory where ESSTER is stored and type

make ./ESSTER

This creates the executable ESSTER.

For running the program, the user is required to provide several specifications. They are listed in the Tab.3.

REQUIRED		
-help		Writes out help report. Does not require additional input.
-ampt/-toy		Specifies the type of generator used. For generating/analyzing ToyModel events, use -toy, for analyzing AMPT events, use -ampt
-central/-mid/-peripheral		Centrality specification.
OPTIONAL		
-merge		Merges files produced by AMPT.
-merge	-zpc	Merges parton files produced by AMPT.
-zpc		Analyses parton file.
-gen NoEvents		Generates *NoEvents* events.
-cml		Analyses generated events via cumulant method.
-cml4		Analyses generated events via four-particle cumulant method.
-cml4+		Analyses generated events via p_T weighted four-particle cumulant method.
-epm		Analyses generated events via event plane method.
-epm+		Analyses generated events via event plane method (with p_T weighing).
-ESE		Analyses generated events via Event Shape Engineering.
-root		
	-psi_0 / -psi_n	Rotates events according to maximum/ n^{th} event plane.
	-y	Makes rapidity y histograms.
	-corr	Makes angle-correlation histograms.
	-mul	Normalizes events according to multiplicity.
-bin		
	-q0/-qn	Initially sorts the events randomly/according to q_n.
	-y	Sorts rapidity y histograms (initial sorting is random).
	-corr	Sorts angle-correlation histograms (initial sorting is random).
	-mul	Sorts multiplicity-normalized histograms as described in 3.2.4.
	-flip	Flips half of the events after sorting and sorts them once more.
-fig		Draws histogram figures in an eps format. Specifications same as -bin.
	-in	Plot every 50th azimuthal angle histogram.
	-art	Plot fancy looking histograms.
-movie		Makes an average histogram figure after every iteration in a png format.
-eig		Outputs correlation and covariance matrices into corresponding folder. Specifications same as -bin.

Tab. 3: Program ESSTER commands.

A.2 Output File organization

The files are organized according to parameters specified in `additional.h`. All files are the same data type specified by *FILE_TYPE*.

The file hierarchy is best explained using an example. One is in the Fig. 42. In the figure, we show an example of a file hierarchy used for mid-central events, rapidity cuts $-0.5 < y < 0.5$ (`y0.5`) and $-1 < y < 1$ (`y1`), p_T cuts $p_T \in (0, 5)\,\mathrm{GeV}$ (`pT0_5`) and no p_T limitations (`pT0_0`). In the `GEN_FOLDER` the information from AMPT or ToyModel is stored, the names of the files are specified in `additional.h` as `GEN, GEN_AMPT, GEN_ZPC, GEN_ADD`. Similarly, results from event analysis is stored in `AN_FOLDER`. In `ROOT_FOLDER`, histograms obtained from ROOT are stored. The results from the algorithm are in `BIN_FOLDER`.

The algorithm used events with the following setting: there were 20 azimuthal angle bins (`bins20`). There are three cases, all initially sorted according to q_2(`init2`): events rotated according to ψ_2 (`psi_2`) without flipping the events (`flip0`) or using normalized events (`norm0`); events rotated according to ψ_3, flipped (`flip1`), not normalized (`norm0`) and finally events rotated according to ψ_3, flipped (`flip1`) normalized (`norm1`).

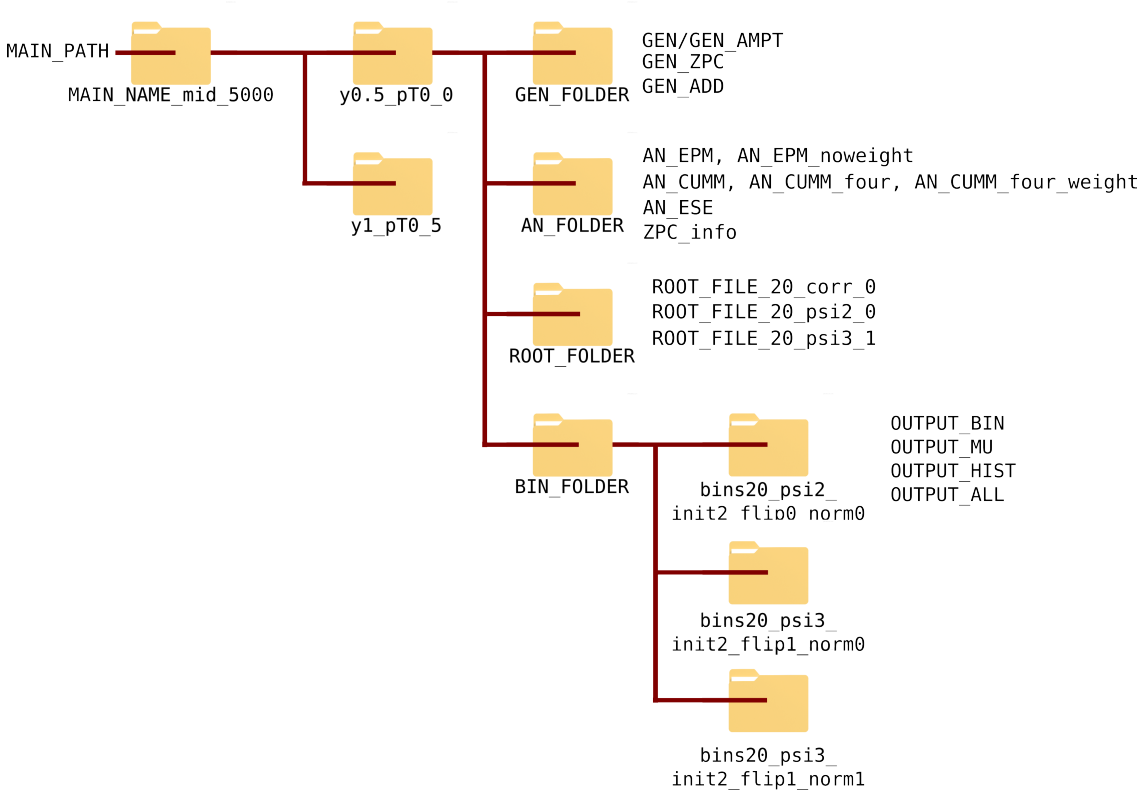

Fig. 42: Folder tree description.

B List of AMPT parameters

760	! EFRM $\sqrt{s_{NN}}$ in GeV if FRAME is CMS)
CMS	! FRAME
A	! PROJ
A	! TARG
208	! IAP (projectile A number)
82	! IZP (projectile Z number)
208	! IAT (target A number)
82	! IZT (target Z number)
500	! NEVNT (total number of events)
0./7.0/10.0	! BMIN (mininum impact parameter in fm)
7.0/10.0/12.0	! BMAX (maximum impact parameter in fm)
4	! ISOFT (D=1): select Default AMPT or String Melting (D=4)
1000	! NTMAX: number of timesteps (D=150)
0.2	! DT: timestep in fm (hadron cascade time= DT*NTMAX) (D=0.2)
2.2	! PARJ(41): parameter a in Lund symmetric splitting function
0.5	! PARJ(42): parameter b in Lund symmetric splitting function
1	! (D=1,yes;0,no) flag for popcorn mechanism(netbaryon stopping)
1.0	! PARJ(5) to control BMBbar vs BBbar in popcorn (D=1.0)
1	! shadowing flag (Default=1,yes; 0,no)
0	! quenching flag (D=0,no; 1,yes), turns off jet quenching.
2.0	! quenching parameter -dE/dx (GeV/fm) in case quenching flag=1
2.0	! p0 cutoff in HIJING for minijet productions (D=2.0)
2.097	! parton screening mass in fm^{-1} (D=2.265d0)
0	! IZPC: (D=0 forward-angle parton scatterings; 100,isotropic)
0.47	! α in parton cascade (D=0.33d0), see parton screening mass
1d6	! dpcoal in GeV
1d6	! drcoal in fm
11	! ihjsed: take HIJING seed from below (D=0)or at runtime(11)
13150909	! random seed for HIJING
8	! random seed for parton cascade
0	! flag for K0s weak decays (D=0,no; 1,yes)
1	! flag for phi decays at end of hadron cascade (D=1,yes; 0,no)
0	! flag for pi0 decays at end of hadron cascade (D=0,no; 1,yes)
1	! optional OSCAR output (D=0,no; 1,yes; 2&3,more parton info)
0	! flag for perturbative deuteron calculation (D=0,no; 1or2,yes)
1	! integer factor for perturbative deuterons(¿=1 & ¡=10000)
1	! choice of cross section assumptions for deuteron reactions
-7.	! Pt in GeV: generate events with ¿=1 minijet above this value
500	! maxmiss (D=1000): maximum number of tries to repeat a HIJING event
3	! flag to turn off initial and final state radiation (D=3)
1	! flag to turn off Kt kick (D=1)
0	! flag to turn on quark pair embedding (D=0,no; 1,yes)
7., 0.	! Initial Px and Py values (GeV) of the embedded quark (u or d)
0., 0.	! Initial x & y values (fm) of the embedded back-to-back q/qbar
1, 5., 0.	! nsembd(D=0), psembd (in GeV),tmaxembd (in radian).
0	! Flag to enable users to modify shadowing (D=0,no; 1,yes)
1.d0	! Factor used to modify nuclear shadowing
0	! Flag for random orientation of reaction plane (D=0,no; 1,yes)

C Published papers related to this thesis

1. R. Kopečná and B. Tomášik, *Event Shape Sorting*, Eur. Phys. J. A (2016) **52**: 115.

2. R. Kopečná and B. Tomášik, *Event shape analysis in ultrarelativistic nuclear collisions*, arXiv: 1603.04997 [nucl-th].
   Proceedings: XI Workshop on Particle Correlations and Femtoscopy, Warsaw 2015.
   Accepted for publishing in A. Phys. Pol. B Supp.

3. B. Tomášik, M. Schulc, I. Melo, R. Kopečná, *Observables of non-equilibrium phase transition*, arXiv: 1511.00034 [nucl-th].
   Contribution to the NICA White Paper.
   Accepted for publishing in Eur. Phys. J. A.

Eur. Phys. J. A (2016) **52**: 115
DOI 10.1140/epja/i2016-16115-1

THE EUROPEAN PHYSICAL JOURNAL A

Regular Article – Experimental Physics

Event shape sorting

Renata Kopečná[1] and Boris Tomášik[1,2,a]

[1] FNSPE, Czech Technical University in Prague, Břehová 7, 11519 Prague, Czech Republic
[2] Univerzita Mateja Bela, Tajovského 40, 97401 Banská Bystrica, Slovakia

Received: 18 September 2015 / Revised: 2 February 2016
Published online: 27 April 2016 – © Società Italiana di Fisica / Springer-Verlag 2016
Communicated by Z.-E. Meziani

Abstract. We propose a novel method for sorting events of multiparticle production according to the azimuthal anisotropy of their momentum distribution. Although the method is quite general, we advocate its use in analysis of ultra-relativistic heavy-ion collisions where a large number of hadrons is produced. The advantage of our method is that it can automatically sort out samples of events with histograms that indicate similar distributions of hadrons. It takes into account the whole measured histograms with all orders of anisotropy instead of a specific observable (*e.g.*, v_2, v_3, q_2). It can be used for more exclusive experimental studies of flow anisotropies which are then more easily compared to theoretical calculations. It may also be useful in the construction of mixed-events background for correlation studies as it allows to select events with similar momentum distribution.

1 Introduction

Hot matter which is created in ultra-relativistic heavy-ion collisions expands very fast in both longitudinal and transverse directions [1–4]. The expansion is always anisotropic. This is true even in most central collisions, where one would expect symmetry in azimuthal angle due to circular shape of the initial overlap region [5]. In non-central collisions, the overlap of the two colliding nuclei has elliptic shape and thus naturally second-order (and higher even orders) anisotropy in the fireball expansion builds up. On top of this —at any centrality— energy deposition in the interactions of the incoming partons fluctuates and this leads to all orders of anisotropy in the transverse expansion of the fireball. Therefore, even within carefully selected centrality class flow anisotropies vary from event to event [5, 6].

Even more degrees of freedom are offered by collisions of deformed nuclei, like uranium. There, the initial anisotropy will also depend on the way the colliding nuclei are oriented.

This makes the comparison of experimental data to theoretical simulations more complicated, because one has to take into account that every event starts with different initial conditions and evolves differently. Simulations are compared to data in order to pin down the properties of the matter which is being modelled. Initial conditions are unknown, however, although recent hydrodynamic results indicate that their fluctuations can be directly mapped onto measured fluctuations of hadron distributions [7, 8].

[a] e-mail: boris.tomasik@cern.ch

Comparison of theory to data must be done with great care so that the spectra of theoretical and experimental fluctuations match each other. Experimentally, events are distributed into centrality classes according to multiplicity. There is a problem with this procedure on the side of theory if very narrow centrality class is demanded, *e.g.* ultra-central collisions corresponding to 0–0.2% centrality. Events with the same multiplicity may evolve from initial states with different impact parameters[1]. Moreover, all those events would differ by the quantum fluctuations in initial energy and momentum deposition [10]. Therefore, events from a class selected according to multiplicity-based centrality may have evolved from different initial conditions and experienced quite different evolution history. It would be useful if there was a more selective method to choose events that are more likely to have

[1] This can be seen, *e.g.*, in fig. 2 of [9], where the procedure that is used by ALICE Collaboration to determine centrality is explained. Within the used Monte Carlo Glauber model if the impact parameter is fixed, then the number of participants may still fluctuate. On the other hand, from the overlap of centrality classes in $N_{\rm part}$ histogram it is clear that fixed $N_{\rm part}$ corresponds to an *interval* of impact parameters. As the experimental multiplicity is determined from multiplicity in a chosen detector, there is yet another source of fluctuation that comes from the uncertainty between multiplicity and $N_{\rm part}$. In summary, if we fix the multiplicity —even in perfectly spherical nuclei like Pb or Au— there is still some freedom for the impact parameter to fluctuate which we estimate of the order 1 fm. Even more fluctuations can be expected in collisions of non-spherical nuclei, like U.

evolved similarly. In addition to this, in collisions of deformed nuclei the multiplicity itself is definitely not a sufficient selection criterion since the same multiplicity may result from events with very different initial *orientations* of the colliding nuclei and thus very different flow patterns. Again, the situation calls for a selection method like the one presented here.

It would thus be advantageous if one could select a collection of events among all measured events (which may or may not belong to the same centrality class) which show very similar distribution of the produced hadrons. For such events one can assume that they also evolved similarly.

The word "similar" when talking about distributions or histograms can be understood in layman's terms so that they have similar shapes when one rotates them appropriately. There is a possibility how to quantify this with the help of the distance measure in the Kolmogorov-Smirnov test, but this will not be used here because it does not automatically provide a way for sorting. We rather use the Bayesian framework where we basically ask the question: how would the events be grouped, based on the shapes of their histograms.

A method aiming for such event selection has been proposed in [11] and is commonly referred to as "Event Shape Engineering". It usually employs the size of the flow vector q_n defined on a selection of hadrons from a given event (usually referred to as subevent) as

$$\boldsymbol{q}_n = \frac{1}{\sqrt{M_s}} \left(\sum_{i=1}^{M_s} \cos(n\phi_i), \sum_{i=1}^{M_s} \sin(n\phi_i) \right), \qquad (1)$$

where M_s is the multiplicity of the subevent and ϕ_i are the azimuthal angles of the individual hadrons from the subevent. Events are then selected based on their values of q_n (in most cases q_2). However, only the subevents *not* used in q_n determination can be used in further studies in order to avoid bias.

It is not clear, moreover, whether selecting events according to the value of q_n provides the best possible selection method aimed at collecting similar events. It actually may not be the case, as we demonstrate below.

In this paper we propose the use of a novel method for comparing, sorting and selecting events according to *similarity* with each other. The method is adopted from [12,13] and was previously used in a different context [14]. Its uniqueness consists in not fixing a single observable which would then be used for sorting of the events. It rather compares complete histograms (*e.g.* azimuthal angle distributions) of individual events and it sorts the events in such a way that events with similar histogram shapes end up close together. After such a sorting has been performed one simply selects similar events just by choosing a group of events which follow each other in the created series.

On the selected groups of events one could measure various observables (v_n's, q_n's, radial flow, temperature, ...) which should fluctuate much less than in the whole measured event sample.

A natural application of the method is in construction of correlation functions. There, one often needs a reference distribution which is constructed via the mixed events technique. If events used in mixing are different, this may introduce unwanted artificial effects into the correlation function. Therefore, the mixed events sample is always constructed with aligned event planes. (For application at intermediate energy nuclear collisions see, *e.g.*, [15,16]).

With the help of the proposed method it would be interesting to perform femtoscopic studies where oscillations of radii in azimuthal angle in both second and third order together at the same time should be visible.

We comment more on the applications in the Outlook section.

In the next section we shall explain the method and in sect. 3 we illustrate its use on Monte Carlo data from a toy model. The method is applied on more realistic Monte Carlo data generated by a transport model in sect. 4. We conclude in sect. 5 and give an Outlook about possible applications of the method and its next development.

2 The method

Suppose that we have a sample consisting of a large number of events. Initially, we can sort and divide those events into N percentiles according to the value of a single observable which can be measured in every event. This can be the value of q_2, v_2, multiplicity or any other observable. Generally, we shall refer to this observable as Q. For the sake of clarity let us explain the method with a particular choice: choose $N = 10$ event bins (deciles) and the observable according to which we sort data is $Q = q_2 = |\boldsymbol{q}_2|$. Let us stress at this point that the method is universal and will not depend on the choice of N and Q.

In each of the event bins we can now produce the histogram of hadron distribution in azimuthal angle summed over all events in the event bin. There is no physics in how the two nuclei are oriented when they collide, and so we have a free choice of how to rotate individual events before adding them to the angle histogram. For the introduction of the method let us align each event according to the second order event plane. Note, however, that the choice of alignment is a sensitive issue which we shall discuss later.

Thus each event is characterized by the bin record of its distribution in azimuthal angle[2] $\{n_i\}$ and belongs to one of the N event bins which we number with μ. (We shall use Latin letters for angle bins and Greek letters for event bins.)

2.1 Basic relations

Imagine that we take a random event from our big sample and ask an unbiased observer, in which event bin he or she thinks that this event belongs. More specifically, we can ask the question in the framework of Bayesian probability:

[2] We denote n_i the number of particles in angle bin i and the whole record of an event is referred to with the help of braces. Thus summation of all angle bin entries gives the event multiplicity $\sum_i n_i = M$.

What is the probability[3] $P(\mu|\{n_i\})$ that an event with bin record $\{n_i\}$ belongs to the event bin μ?

This probability will be evaluated with the help of Bayes' theorem

$$P(A|B) = \frac{P(B|A)P(A)}{P(B)}\,, \tag{2}$$

where $P(A|B)$ is the conditional probability of the event A given event B. The probability of event B can be determined

$$P(B) = \sum_A P(B|A)P(A), \tag{3}$$

where the sum runs over all possible events A. Definitions of symbols $P(B|A)$ and $P(A)$ are analogical.

With the help of Bayes' theorem we can express

$$P(\mu|\{n_i\}) = \frac{P(\{n_i\}|\mu)P(\mu)}{P(\{n_i\})}\,. \tag{4}$$

Here, $P(\{n_i\}|\mu)$ is the probability that if one randomly draws an event from the distribution function given by average histogram of event bin μ, the result will be the bin record $\{n_i\}$. The prior $P(\mu) = 1/N$ takes the value of 0.1 now. The denominator contains the overall probability of drawing the event $\{n_i\}$ from any of the event bins. It can be determined according to eq. (3)

$$P(\{n_i\}) = \sum_{\nu=1}^{N} P(\{n_i\}|\nu)P(\nu). \tag{5}$$

The advantage of using the latter formula comes from the fact that we are able to determine $P(\{n_i\}|\nu)$ for each bin record $\{n_i\}$ and every event bin ν

$$P(\{n_i\}|\nu) = M! \prod_i \frac{P(i|\nu)^{n_i}}{n_i!}\,. \tag{6}$$

Here M is event multiplicity, the product goes over all angle bins i and $P(i|\nu)$ is the conditional probability that random particle falls into angle bin i given that the event to which it belongs stems from event bin ν. It can be determined when we take the number of particles from all events in event bin ν falling into angle bin i. This number is divided by the total number of all particles from events in event bin ν, denoted M_ν

$$P(i|\nu) = \frac{n_{\nu,i}}{M_\nu}\,. \tag{7}$$

When the formula (6) is inserted into (5) and (4) we obtain the practically usable relation from which the large factorials drop out

$$P(\mu|\{n_i\}) = \frac{\prod_i P(i|\mu)^{n_i} P(\mu)}{\sum_\nu \prod_i P(i|\nu)^{n_i} P(\nu)}\,. \tag{8}$$

[3] Obviously, the event must belong to one of the event bins so that the probabilities must be normalised

$$\sum_{\mu=1}^{N} P(\mu|\{n_i\}) = 1.$$

With the help of this conditional probability we can determine for an event with angle bin record $\{n_i\}$ its *mean event bin number*

$$\bar{\mu} = \sum_\mu \mu P(\mu|\{n_i\}). \tag{9}$$

2.2 The algorithm

Now we are able to describe the algorithm which is used for sorting of the events.

1) First, all events are sorted according to the observable Q.
2) Events are divided into N event bins according to current sorting.
3) For each event and all event bins the probability $P(\mu|\{n_i\})$ is determined that the event with record $\{n_i\}$ belongs to event bin μ. The mean event number $\bar{\mu}$ is calculated for each event according to (9).
4) Events are sorted again according to their values of $\bar{\mu}$.
5) Events are divided into N event bins according to current sorting.
6) If the new sorting changed assignment of any events into event bins, the algorithm returns to step 3. Otherwise it converges.

The construction of the algorithm is such that once converged, the events are sorted so that those ending up close to each other are characterized by similar angular histograms. This is the best possible experimental approach to the selection of events that have undergone similar evolution. This is as good working definition of what similar events are as it can be.

In the present formulation the average histograms are more strongly determined by high-multiplicity events. Note, however, that the algorithm is independent of event multiplicity. Of course, if in particular physics analysis certain multiplicity is demanded, one can easily use it for event selection and then use the present method for more refined selection of the events.

The final sorting of events also does not depend on the initial sorting. Hence, this method can also be used for a judgment if the particular observable Q, *e.g.* q_2 or v_2, is a good measure for selecting similar events. If the initial ordering according to Q is correlated with the final ordering, then the observable Q is good for this purpose. This may not always be the case, as we will show later.

Although the final result does not depend on initial ordering, a good initial ordering can lead to faster convergence of the algorithm.

There is a caveat, however, which has been discussed only shortly so far. The algorithm works well for sorting histograms in observables that are not periodic, *e.g.* rapidity. However, the azimuthal angle of particle momentum is a periodic observable, *i.e.* we can always arbitrarily rotate the events. Practically, two angular histograms may be almost identical when they are both aligned properly, but might appear quite different for the proposed algorithm if they are rotated in random directions. Thus the

Table 1. Parameters used for generating multiplicity-dependent v_n.

n	$a_n \times 10^8$	$b_n \times 10^5$	c_n
1	0	0.01667	−0.000680
2	−7.099	20.06	0.07874
3	−2.083	6.658	0.04236
4	−96.38	2.621	0.04897
5	−71.76	2.236	0.01673

way how events are aligned initially plays a crucial role and we observed that it strongly biases the final sorting of the events. At the moment we do not have recommendation for an automatic algorithm which would align the events in the best way. Instead, we tested a few reasonable choices for the initial alignment in our toy model studies. With the simple toy model, quite naturally that initial rotation aligning the second-order event planes ψ_2 will lead to sorting characterized by v_2. Analogically, with aligning the third-order event planes ψ_3, final sorting is given by v_3. In the next section we present results which take into account a combination of both these orderings. That feature was, however, weaker in AMPT-generated events.

3 Illustration of the method

3.1 Elliptic flow

Let us first demonstrate the action of the sorting algorithm on a simple case of events with only first- and second-order anisotropic flow. We generated the azimuthal angles of pions from the distribution

$$P_2(\phi) = \frac{1}{2\pi}\left(1 + 2v_1\cos(\phi - \psi_1) + 2v_2\cos(2(\phi - \psi_2))\right). \tag{10}$$

The parameters v_1 and v_2 depend on the multiplicity of the event M as

$$v_n = a_n M^2 + b_n M + c_n, \tag{11}$$

and parameters a_n, b_n, and c_n for each n can be found in table 1. They have been determined from experimental data as we discuss in sect. 3.2. In addition to eq. (11), flow anisotropy parameters v_n are Gaussian-smeared with a width of 0.25. For each event, the directions of event planes ψ_1 and ψ_2 are random and uncorrelated.

We generated 5000 events with multiplicities between 300 and 3000. Directed flow is practically negligible and the dominant anisotropy is of second order. Thus the most reasonable choice of initial event rotation is the alignment of second-order event planes defined from the generated Monte Carlo data for each event via

$$q_2 e^{2i\psi_2} = \sum_{j=1}^{M} e^{2i\phi_j}. \tag{12}$$

To show the power of the method we first ordered the events fully randomly. The algorithm converged after 65 iterations. In fig. 1 top one can see that the initial ordering indeed has nothing to do with the final ordering of events. In the bottom panel of that figure we show the correlation of final sorting variable $\bar{\mu}$ with the value of v_2 determined in each event via the event-plane method (results from cummulant method are practically identical). One can clearly see that the ordering is given by the elliptic anisotropy of the particle distribution.

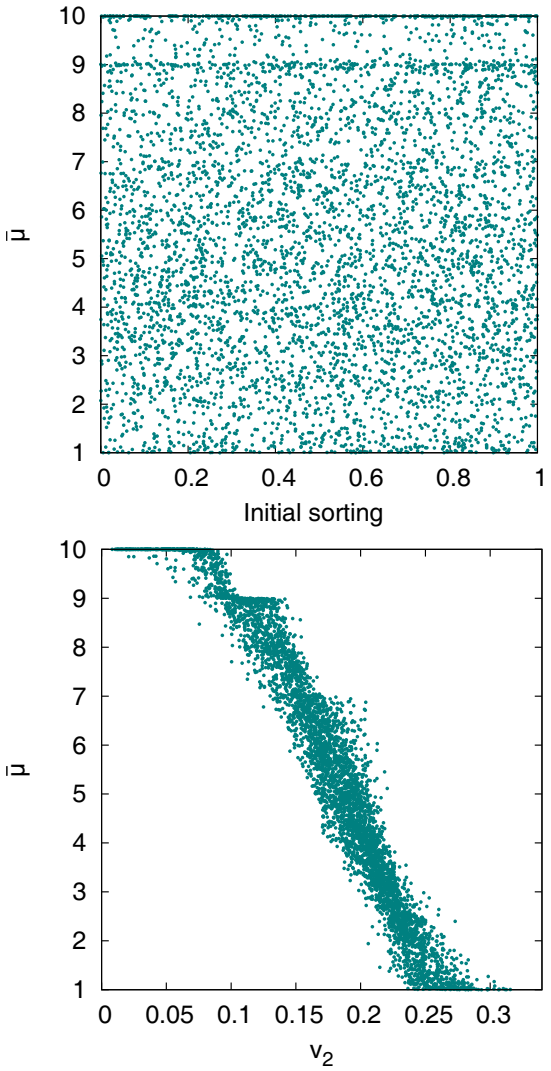

Fig. 1. Top: correlation of the resulting sorting variable $\bar{\mu}$ with the initial ordering. Every dot represents one event. Bottom: correlation of $\bar{\mu}$ with v_2 determined for each event via the event plane method.

Note that when we started the sorting algorithm with initial ordering according to the value of q_2 in each event, the final correlation was just a mirror image of fig. 1 bottom. Small values of v_2 corresponded to small $\bar{\mu}$ and high values of v_2 to high values of $\bar{\mu}$. This illustrates that the algorithm always converges to a sorting of events according to their similarity but the direction how they are ordered along $\bar{\mu}$ may be different.

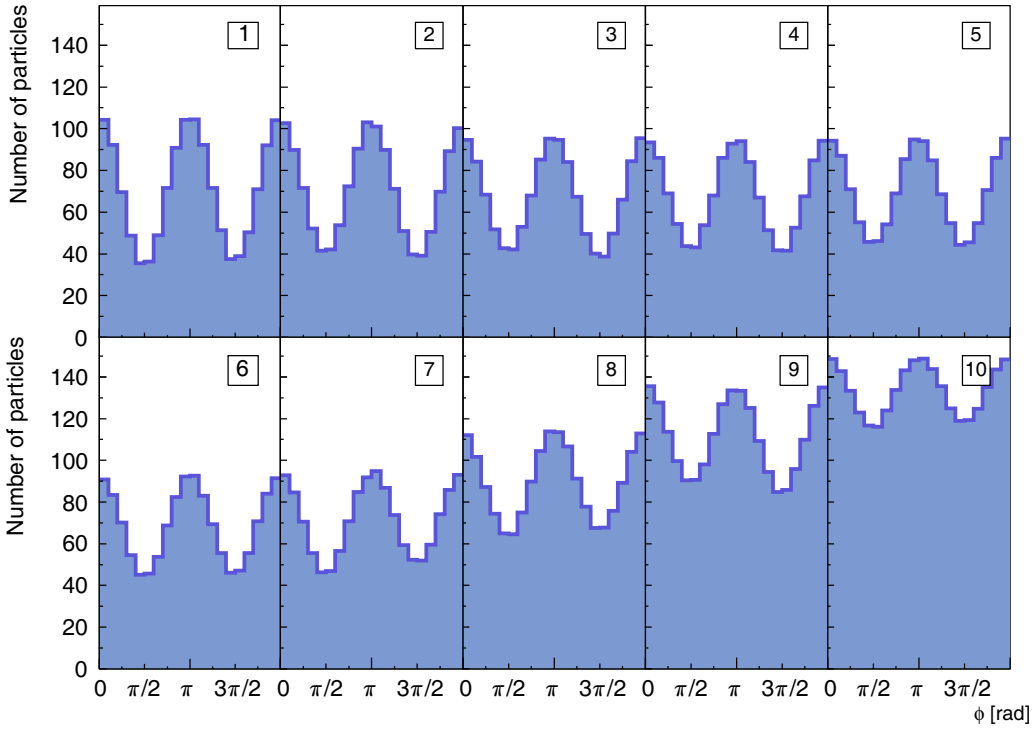

Fig. 2. Average histograms of the azimuthal angles for event bins 1–10, with event bins indicated in the panels. Events with only v_2 and v_1.

There is a congestion of events seen at $\bar{\mu} = 9$ and 10 in the upper panel of fig. 1 and a step in the same place in the lower panel of that figure. This actually shows that the sorting was very clear for these two event bins. The congestion is made out of events for which when evaluating $\bar{\mu}$ according to eq. (9), the sum has one clearly dominant term. The probabilities that the event might belong to other event bins are very small.

For illustration, in fig. 2 we show average histograms of the events in the individual event bins. We see that the relative amplitude of the second-order variation (*i.e.* the amplitude divided by the mean value of the bins) decreases from event bin 1 to event bin 10.

The method is thus able to distinguish different shapes of hadron distributions and sort events according to them. In this simple case, this might not look like a big advantage as we could have sorted the events simply by measuring v_2. Therefore, we proceed with a more complicated example where the algorithm demonstrates its full power.

3.2 Anisotropic flow

We parametrised the dependence of v_n's on multiplicity through a fit to data from ALICE and ATLAS Collaborations [17, 18]. Coefficients v_n for $n = 1$ through 5 are parametrised according to eq. (11) with parameters summarised in table 1.

Then we generated 5000 events with multiplicities between 300 and 3000 pions and angular distributions according to

$$P_5(\phi) = \frac{1}{2\pi}\left(1 + \sum_{n=1}^{5} 2v_n \cos(n(\phi - \psi_n))\right). \qquad (13)$$

The v_n's for every event are set by eq. (11) and then smeared with Gaussian distribution with the width of 0.25. The phases ψ_n are selected from uniform distribution and are not correlated with each other.

Now we have to address the question how to rotate the events so that the comparison of individual events to the event bin histograms yields the most reasonable sorting. There are two symmetries at play here: rotational symmetry and parity symmetry. We can rotate an event around the collision axis, and we can also flip it so that we get its mirror image. We have observed that both these symmetries influence the result.

The two dominant components of flow anisotropy are second and third order. Hence, in our tests we focused on the corresponding event planes. If events are all aligned into the direction of second-order event plane, the algorithm becomes sensitive to the second-order anisotropy and to large extent ignores the third order. Analogically, alignment according to third-order event plane enhances the sensitivity to third-order anisotropy. Thus the resulting sorting is rather sensitive to this choice. Furthermore, in both cases the algorithm distinguishes events which look like mirror images of each other (*i.e.* have opposite parity). This must be taken into account when designing the sorting algorithm.

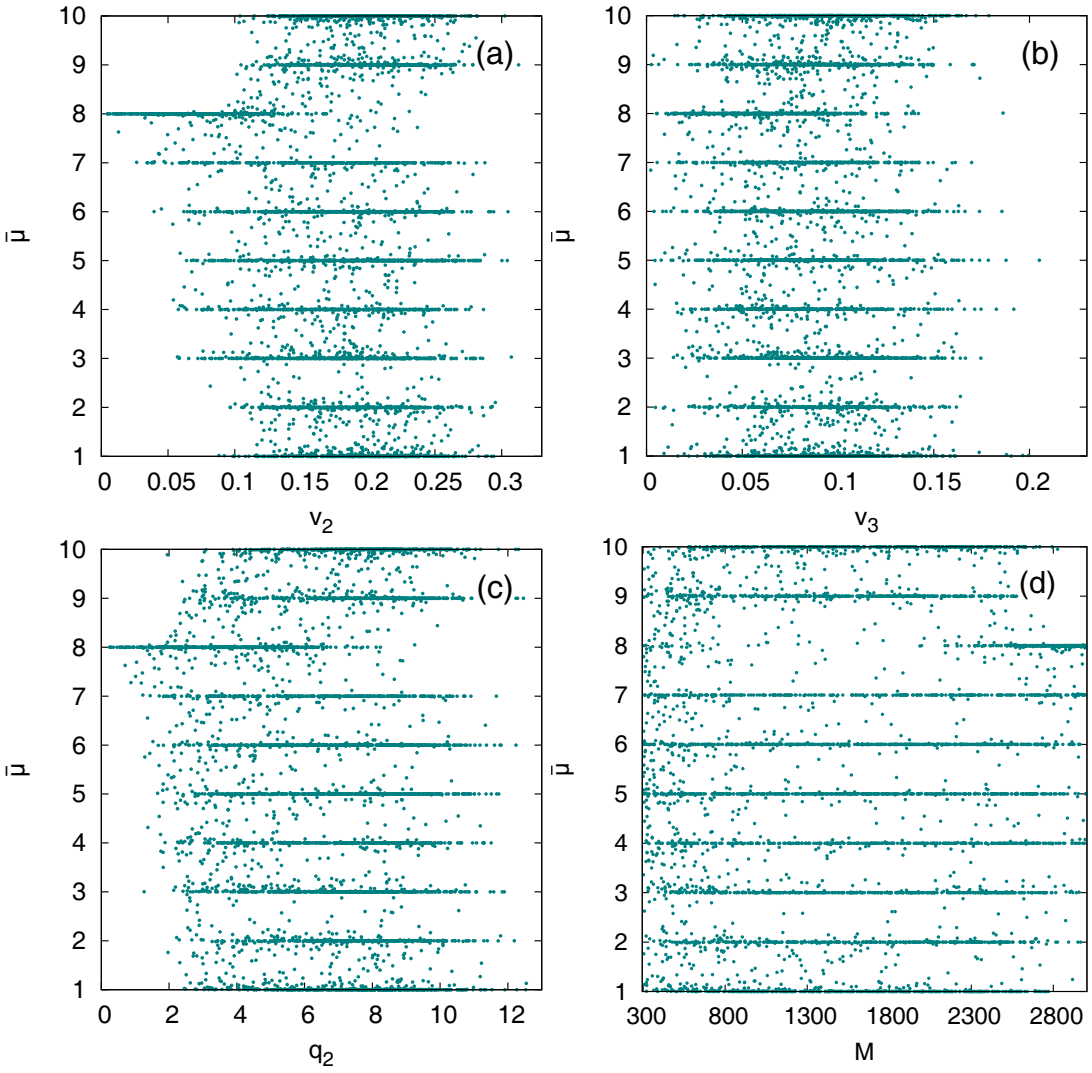

Fig. 3. Correlation of various observables with final sorting variable $\bar{\mu}$. Simulated are events with anisotropies up to 5th order and initial rotation is according to ψ_{2-3}. Correlation with a) v_2, b) v_3, c) q_2, d) event multiplicity.

The shape of hadron distribution is never solely determined by v_2 or by v_3. It rather follows from their combination which is different in every event due to varying phase difference of second and third-order event plane. In order to take into account both these components of anisotropy we rotated all events according to the angle bisector between ψ_2 and ψ_3. We denote its azimuthal angle ψ_{2-3}. Also, in order to take care of the parity symmetry the events were oriented so that ψ_2 is less than $\pi/2$ away from ψ_{2-3} *counterclockwise*.

The initial sorting of the events was random and the algorithm converged after 121 iterations.

From fig. 3 it is clearly seen that in this case sorting of the events is neither determined by q_2, nor by v_2, nor by v_3. Higher-order terms also do not play a big role at all. The event shape is complex and results from an *interplay* of all its simple characteristics. The message of the figure is that q_2 may not be a good variable to select events according to their shape because panel (a) shows that it is not correlated with the overall shape of the event as soon as more flow harmonics are involved. Note that in our toy model there is neither correlation between the flow harmonics nor between the event planes of different order. This may not be so in real events and then the correlation between sorting variable $\bar{\mu}$ and some of the measured quantities may appear. What we show is thus rather an extreme case. It calls, however, for attention: the overall shape of an event and thus the evolution dynamics running in that event cannot be simplified into a single measured variable. There might be a counterargument that variables like *e.g.* q_2 which are used in Event Shape Engineering are proved to be good at event sorting, because events with different values of q_2 show different values of other measured quantities. However, in addition to this, our method

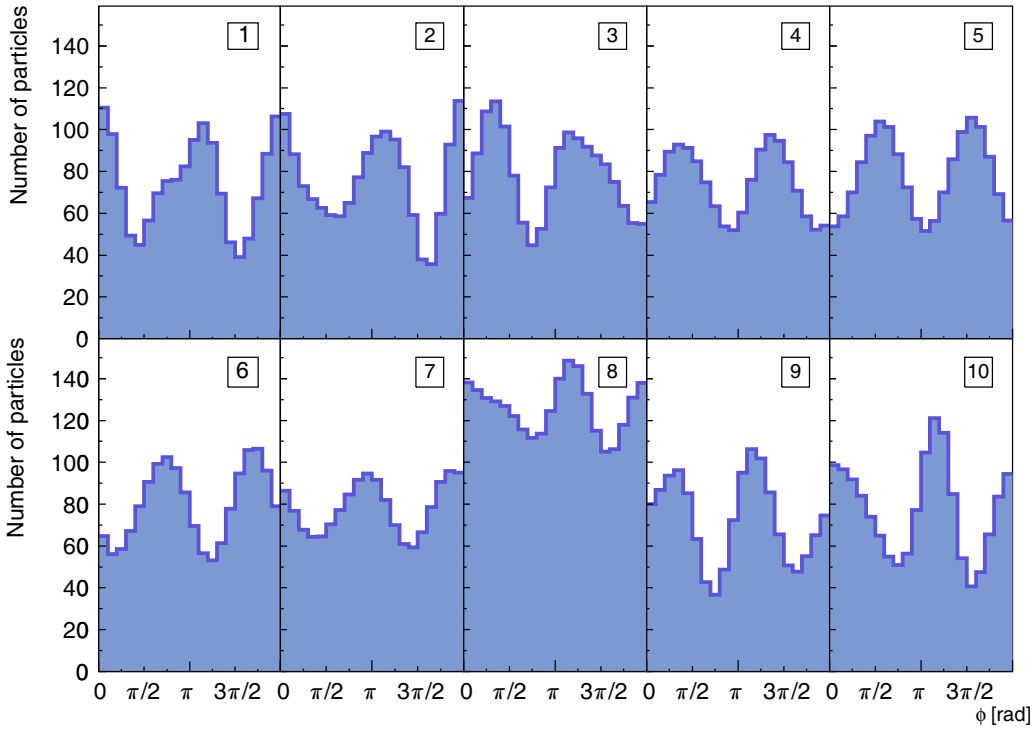

Fig. 4. Average histograms of the azimuthal angles for event bins 1–10, with event bins indicated in the panels. Events with anisotropies up to 5th order.

optimizes the sorting so that events which are placed close to each other share as many event shape characteristics as possible. Figure 3 shows that such a sorting may not be connected with any of the commonly used variables.

In fig. 3 we again observe that the resulting values of $\bar{\mu}$ are grouped around integers. This actually means that the assignment of the events into event bins is very clear, because in determining the value of $\bar{\mu}$ from eq. (9) the probability $P(\mu|\{n_i\})$ is (close to) one for certain μ and (nearly) zero elsewhere. The event then clearly belongs to the event bin μ.

When we tried to start the sorting algorithm with initial ordering according to the value of q_2 it failed to converge within reasonable time (5000 iterations). This happens sometimes when unfavourable initial ordering is used. On the other hand, in other occasions we have checked that also with different initial ordering of events the algorithm converged to identical final sorting. The only difference could arise from the feature that the algorithm does not follow any specific condition in which direction the events should be sorted. Thus different initial orderings may end up in mutually reversed final orderings.

In fig. 4 we show the resulting average angular histograms after the sorting. The events indeed differ by their *shape*, not just only by the value of one of the flow harmonics. Since the second and third-order anisotropies are dominant and due to the initial rotation of the events, higher-order harmonics are washed out by averaging over the event bins and not seen in the figure.

A question may appear to what extent the algorithm would sort the events even if they would be drawn from the same distribution. It would still try to place closer together events with similar histograms, and further apart those events with more different histograms. Then —if in doubt— one can test the hypothesis that events are drawn from the same distribution *e.g.* with the method proposed in [19] or with the help of Kolmogorov-Smirnov test.

4 Application to AMPT events

After we have established and tuned the sorting algorithm, we now use it in a more realistic setting with events generated by the AMPT model [20].

The model was used as commonly distributed with two modifications which are recommended for realistic simulation of Pb + Pb collisions at the LHC collision energy $\sqrt{s_{NN}} = 2.76\,\text{TeV}$: the parton screening mass was re-set to $2.097\,\text{fm}^{-1}$ and the string melting was turned on in order to avoid the underestimation of partonic effects [20].

We have generated 2000 events which correspond to the 0–20% centrality class. On the generated particles we have applied rapidity cut $|y| < 1$ in order to roughly simulate the acceptance of central tracking detectors. For the first rough analysis we have taken all charged hadrons and run the sorting algorithm on them.

The event shapes are dominated by the second-order anisotropy, but it is not the only feature that determines

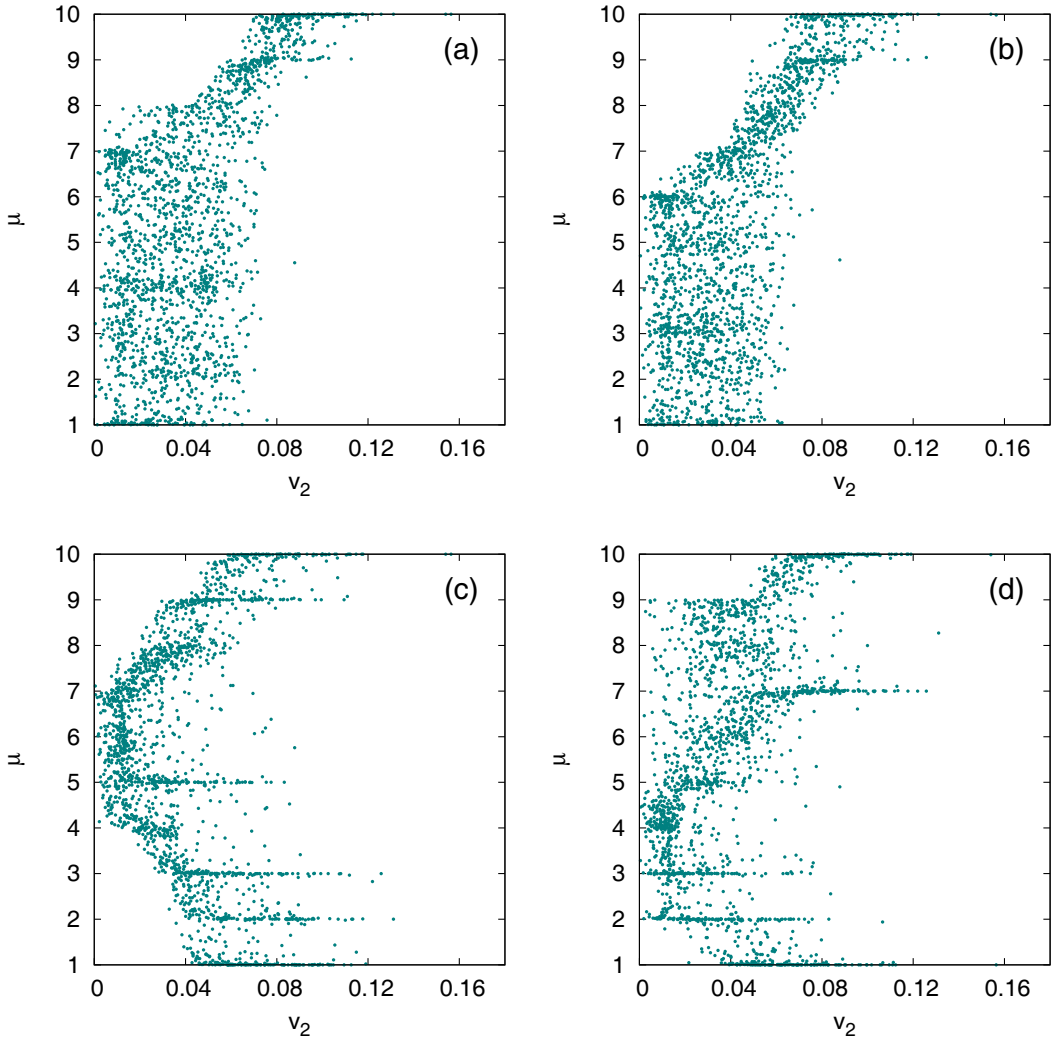

Fig. 5. Correlation of the final sorting variable $\bar{\mu}$ with v_2 of individual events for events generated by AMPT. a) Initial alignment of the events according to ψ_2, b) initial alignment according to ψ_2 and v_2 evaluated with p_t weight, c) initial alignment according to ψ_3, d) initial alignment according to ψ_{2-3}.

the shape of the fireball. When running our sorting algorithm, we have tried three different initial alignments: according to ψ_2, ψ_3 and ψ_{2-3}. In all three cases only v_2 and q_2 of the events show any pattern of correlation with the final sorting. This is shown in fig. 5. Surprisingly, even in the case of ψ_3 initial alignment we have found no correlation of final ordering with v_3. On the other hand, as seen in fig. 5, there is a pattern that shows that also here the sorting of events is strongly influenced by the second-order anisotropy. It will be interesting in the future to see if this dominance of second-order anisotropy survives also in other centrality classes, particularly in more exclusively selected central event.

It is also interesting to see that in realistic simulation, alignment with respect to ψ_2 does not automatically lead to such a clear correlation of v_2 and $\bar{\mu}$ as it was the case with our toy model. This is seen in the upper two panels of fig. 5. Such a correlation exists for the two or three event bins with highest μ's. There, higher μ corresponds to a higher value of v_2. However, for $\bar{\mu}$ below 7 there seems to be no correlation between the ordering of the event and v_2. There is slightly more correlation in case weighted v_2 evaluation, as seen in fig. 5. We would like to understand where the difference between the events shapes comes from, which forces them into different event bins. To this aim, we show in fig. 6 the average histograms in individual event bins after the sorting procedure has converged. In event bins 8, 9, and 10 the gradual growth of v_2 is evident. In the other event bins the histograms show a more complicated structure, where higher-order anisotropies also give an important contribution. We recall, however, that no clear correlation of any higher v_n with the obtained $\bar{\mu}$ is observed.

The next suspected cause of the difference of events is the relative angle between the directions of $\boldsymbol{q}_2$ and $\boldsymbol{q}_3$. We thus studied the correlation between $\bar{\mu}$ and the relative

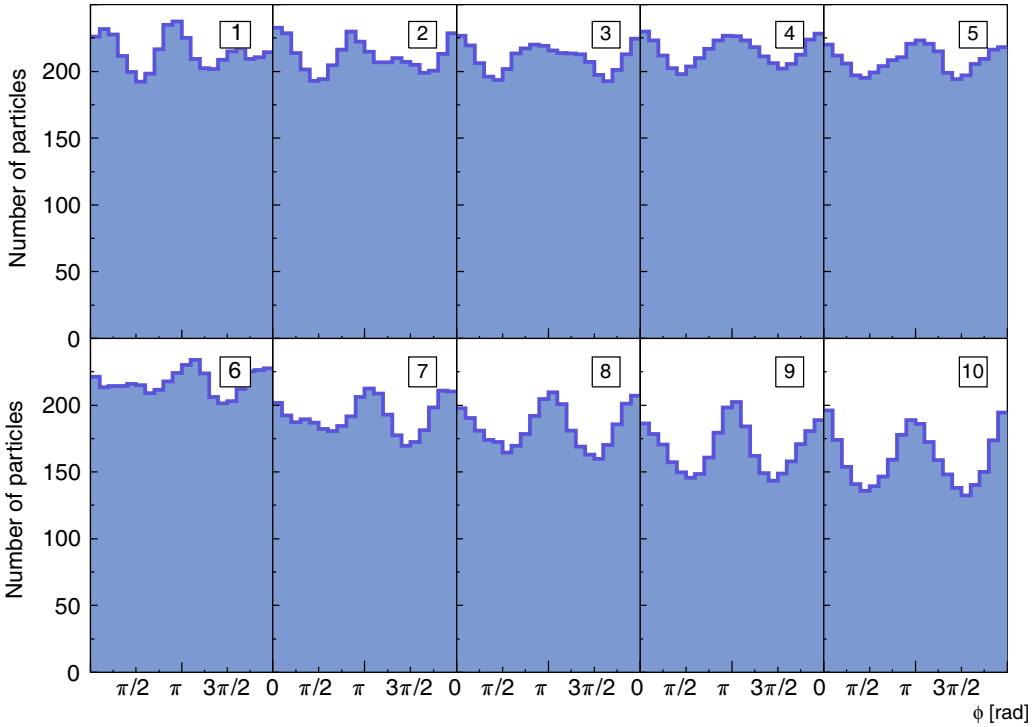

Fig. 6. Average histograms of the azimuthal angles for event bins 1–10, from events generated with AMPT. Initial alignment of events according to ψ_2.

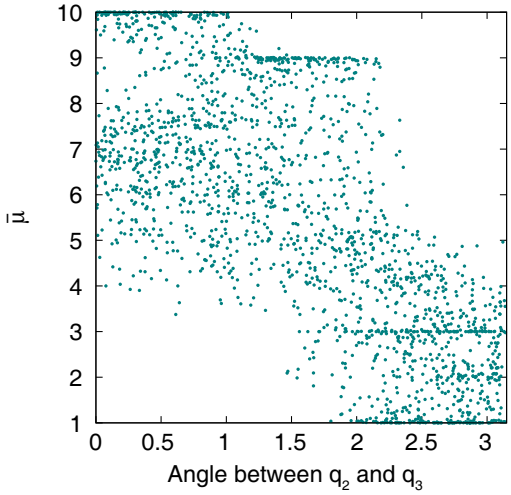

Fig. 7. The correlation of the angle between the flow vectors $\boldsymbol{q}_2$ and $\boldsymbol{q}_3$ and the average bin number of the event $\bar{\mu}$. Events aligned according to ψ_3.

angle. In most cases, no correlation was observed. There is a hint of correlation, though, in case that the events are aligned according to ψ_3. This is shown in fig. 7. Indeed, there seems to be a slight correspondence between the assignment to an event bin and the angle between $\boldsymbol{q}_2$ and $\boldsymbol{q}_3$. The interpretation is at hand, that for the event shape the relative phase is decisive. Unfortunately, this correlation is gone when we align the events differently. Thus, there are hints that the relative angle is important, but the assignment of an event to an event bin appears to be given by more complicated interplay of various individual features.

5 Conclusions and outlook

It is very useful to have a method able to sort events in such a way that it is possible to select those with very similar momentum distribution. One can then assume that they must have undergone similar evolution and this makes it possible to study the dynamics of hot expanding matter more exclusively.

We tested this method on artificial events generated with AMPT. It showed that dividing the events into classes according one selected variable, usually q_2, does not really correspond to selecting event with the same shapes. It still seems that the main role in determining the event shape —at least for the studied centrality class 0–20%— is played by the second-order anisotropy. Nevertheless, other features are important as well. In one case we could identify the difference $\psi_2 - \psi_3$ to co-determine the assignment to event bins, but this observation is not universal for any initial event alignment and any way of evaluation of q_n's.

In addition to the explanation of the method of Event Shape Sorting, we thus gave a first superficial study of realistic events with the proposed method. The study of

event shapes generated by AMPT for various centralities which would include thorough analysis of all features that influence the final shape and their physics interpretation would go beyond the scope of this work and we plan to publish it in a separate paper.

As was mentioned already in the introduction, the presented method allows to select groups of events with similar momentum distributions. If used in data analysis, one can then measure various quantities on such events and study how they are related to the event shape.

The method might even allow to get as close to single-event femtoscopy as possible. First, when doing femtoscopy with a single event one would run into difficulties with the uncorrelated reference distribution which is usually constructed through the event mixing technique. Event shape sorting could provide a selection of events with similar momentum distributions which would make a suitable sample for event mixing. Second, the statistics in a single event would be too small to perform a 3D analysis. However, one could take a sample of events with similar momentum distributions and reasonably expect that they also have the same sizes and undergo the same dynamics. Then, one could analyse the correlation function integrated over the whole selected event sample. The feasibility of such studies will be investigated in the future.

An interesting application appears to be the classification of events from U + U collisions. Due to deformation of the colliding nuclei one expects large fluctuating anisotropies of the transverse flow. Surprisingly, a preliminary study of azimuthally sensitive correlation radii showed no dependence on the value of q_2 [21]. The latter was employed for the selection of events with different final state anisotropy. A short inspection of our fig. 3c would suggest that this is no surprise at all! As soon as there are other harmonic components of the anisotropy, the shape of the events is more complex. The "proper" partition of events into various classes by the type of anisotropy should be done differently. Our algorithm can do such a proper classification.

Let us also comment again on the interesting though perhaps academic question, how the proposed algorithm would proceed if all events were indeed generated from the same underlying probability distribution and the only differences between them would be due to statistical fluctuations. The algorithm would be sensitive to the differences whatever their cause might be. Thus it would sort the events so that typical fluctuations within one event class would be below the normal statistical ones. Such a situation could be detected with the help of standard statistical tests, like *e.g.* the Kolmogorov-Smirnov test. In real data we do not expect this to happen, however.

Also, there are still technical issues which require some discussion and will be addressed in the future. Most important is the ambiguity if initial rotation of the events for which we do not yet have optimised rules. Another is the rather high requirement on CPU time for even moderately large event samples. Note however, that we have not tried any fancy computational optimisation of the algorithm so far, and hence we would expect some room for improvement here.

In fact, we also work on a well optimized routine that can readily be taken and applied directly in data analysis. Integration into standard packages like ROOT or HistFitter [22] will be addressed, as well.

In spite of this, we believe that the Event Shape Sorting is worthwhile to apply in real data analysis and carries potential to gain us better insight into nuclear dynamics in heavy-ion collisions.

Supported in part by APVV-0050-11, VEGA 1/0469/15 (Slovakia) and MŠMT grant LG13031, SGS15/093/OHK4/1T/14 (Czech Republic). We are thankful to Sergei Voloshin, Jürgen Schukraft, Arkady Taranenko, and Burkhard Kämpfer for valuable comments and to Serguei Bityukov for pointing us to ref. [19]. BT thanks the Frankfurt Institute for Advanced Studies for warm hospitality during his stay where a part of this study was completed.

References

1. PHENIX Collaboration (I. Arsene *et al.*), Nucl. Phys. A **757**, 1 (2005).
2. PHOBOS Collaboration (B.B. Back *et al.*), Nucl. Phys. A **757**, 28 (2005).
3. BRAHMS Collaboration (J. Adams *et al.*), Nucl. Phys. A **757**, 102 (2005).
4. STAR Collaboration (K. Adcox *et al.*), Nucl. Phys. A **757**, 184 (2005).
5. CMS Collaboration (S. Chatrchyan *et al.*), JHEP **02**, 88 (2014).
6. ATLAS Collaboration (G. Aad *et al.*), JHEP **11**, 183 (2013).
7. H. Niemi *et al.*, Phys. Rev. C **87**, 054901 (2013).
8. Ch. Gale *et al.*, Phys. Rev. Lett. **110**, 012302 (2013).
9. ALICE Collaboration (B. Abelev *et al.*), Phys. Rev. C **88**, 044909 (2013).
10. C. Shen, Z. Qiu, U. Heinz, arXiv:1502.04636 [nucl-th].
11. J. Schukraft, A. Timmins, S. Voloshin, Phys. Lett. B **719**, 394 (2013).
12. S. Lehmann, A.D. Jackson, B. Lautrup, arXiv:physics/0512238.
13. S. Lehmann, A.D. Jackson, B.E. Lautrup, Scientometrics **76**, 369 (2008) physics/0701311 [physics.soc-ph].
14. S. Lehmann, A.D. Jackson, B. Lautrup, Nature **444**, 1003 (2006).
15. B. Kämpfer *et al.*, Phys. Rev. C **48**, R955 (1993).
16. R. Kotte *et al.*, Phys. Rev. C **51**, 2686 (1995).
17. for the ALICE Collaboration (G. Eyyubova), EPJ Web of Conferences **70**, 00075 (2014).
18. ATLAS Collaboration (G. Aad *et al.*), Phys. Rev. C **86**, 014907 (2012) arXiv:1203.3087 [hep-ex].
19. S. Bityukov, N. Krasnikov, A. Nikitenko, V. Smirnova, Eur. Phys. J. Plus **128**, 143 (2013) arXiv:1309.4649 [physics.data-an].
20. Z.-W. Lin *et al.*, Phys. Rev. C **72**, 064901 (2005).
21. for the STAR Collaboration (J. Campbell), *Poster at the Conference Quark Matter 2014, Darmstadt, Germany, May 19–24, 2014.*
22. M. Baak, G.J. Besjes, D. Côte, A. Koutsman, J. Lorenz, D. Short, Eur. Phys. J. C **75**, 153 (2015) arXiv:1410.1280 [hep-ex].

Event shape analysis in ultrarelativistic nuclear collisions.*

Renata Kopečná[1], Boris Tomášik[1,2]

[1] FNSPE, Czech Technical University in Prague, Břehová 7, 115 19 Praha 1, Czech Republic

[2] Univerzita Mateja Bela, Tajovského 40, 974 01 Banská Bystrica, Slovakia

We present a novel method for sorting events. So far, single variables like flow vector magnitude were used for sorting events. Our approach takes into account the whole azimuthal angle distribution rather than a single variable. This method allows us to determine the good measure of the event shape, providing a multiplicity-independent insight. We discuss the advantages and disadvantages of this approach, the possible usage in femtoscopy, and other more exclusive experimental studies.

PACS numbers: 25.75.-q Relativistic heavy-ion collisions 25.75.Gz Particle correlations and fluctuations 02.50.Ng Distribution theory and Monte Carlo studies

1. Introduction

Initial conditions in heavy ion collisions fluctuate from event to event: there are different impact parameters and different initial energy-density distributions. Hot matter created in those collisions expands very fast in both longitudinal and transverse directions, initial inhomogeneities are translated into all orders of anisotropy of this expansion. The analysis of event shapes can help us identify events with similar initial conditions undergoing similar evolution. We present a novel study of event shapes using the algorithm proposed in [1]. This algorithm studies the *shape* of the distribution rather than a single variable. It compares, sorts and selects events according to *similarity* with each other.

2. The method

The method is thoroughly described in [2]. Here it will be briefly described using a simple example. We generated 5000 events from a toy model.

* Presented at XI Workshop on Particle Correlations and Femtoscopy, Warsaw 2015

It generates azimuthal angles of pions from the distribution

$$P_5(\phi) = \frac{1}{2\pi}\left(1 + \sum_{n=1}^{5} 2v_n \cos(n(\phi - \psi_n))\right). \quad (1)$$

The parameters v_n are quadraticaly multiplicity dependent, details can be found in [2], multiplicity $M \in (300, 3000)$. This choice is motivated by the LHC data [3, 4].

For each event, we made an azimuthal angle histogram with 20 bins. Every event is then described by its record $\{n_i\}$. Since we are studying *angle* distribution, the choice of rotating single events is free. We will address this issue in the next section. The algorithm operates as follows [2]:

1. (Somehow rotate the events)
2. Order events according to a chosen variable
3. Divide the sorted events into quantiles (deciles)
4. For every event calculate the probability that event with record $\{n_i\}$ belongs to event bin μ: $P(\mu|\{n_i\})$
5. For every event calculate mean bin number $\bar{\mu}$ (values 1 - 10): $\bar{\mu} = \sum \mu P(\mu|\{n_i\})$
6. Sort events according to $\bar{\mu}$
7. If the new sorting changed the assignment of any events into event bins, return to (3). Otherwise the algorithm converged.

Events with a similar shape are organized by the algorithm so that they end up close together. There is no specific observable according to which the sorting proceeds. Moreover, the final arrangement of events is independent of the initial sorting.

3. Results

First, we tested the algorithm using events which include only v_1 and v_2. One of the methods used in event shape studies is *Event shape engineering* [5]. This method sorts the events according to a chosen observable, usually $q_2 = |\sum_{j=1}^{n} e^{2i\phi_j}|/M$. We were interested in verifying whether q_2 is truly a good measure for sorting events. As can be seen in Fig. 1, the correlation of $\bar{\mu}$ with v_2 is clearly better than correlation of $\bar{\mu}$ with q_2. This means v_2 is better observable for sorting events than q_2 in this simple case. As mentioned before, the rotation of each event can be arbitrary. Since in this simple case v_2 is clearly dominant, we decided to rotate events in a way that $\psi_2 = 0$.

In order to test more realistic setting, we then generated events with all five orders of Eq. (1). The initial event rotation is not as simple as in

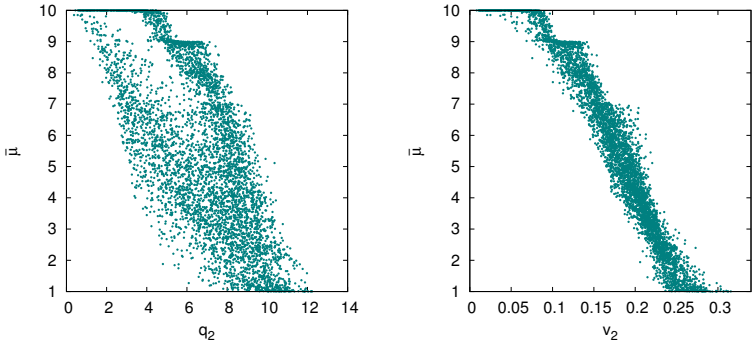

Fig. 1. Left: correlation of $\bar{\mu}$ with q_2 determined for each event. Right: correlation of $\bar{\mu}$ with v_2 determined for each event via the event plane method.

the previous case. Interplay of harmonics comes into play. We rotated the events according to the bisector of ψ_3 and ψ_2. Moreover, we have to take care of the parity symmetry. Hence, the events are oriented so that ψ_2 is less than $\pi/2$ away from ψ_3 counterclockwise. The final event sorting is shown in Fig. 2. It turns out that v_2 is as bad for sorting events as q_2 and the sorting is not even dominated by v_3. Higher harmonics do not play any role at all. This suggests that event shape is determined by an interplay of several observables.

4. Conclusions and outlook

The proposed sorting algorithm provides a novel method to identify events which have evolved similarly. Our results confirm the importance of elliptic and triangular flows for the event shape analysis.

Our approach can be useful in studies including mixed events technique. One could do, e.g., a femtoscopic study of an exclusive group of events. This means that we could get as close as possible to singe-event femtoscopic studies. *Event Shape Sorting* could provide a selection of events with similar momentum distributions which would make a suitable sample for event mixing. In case of statistics in a single event being too small, one could take a sample of events with similar momentum distributions and reasonably expect that they also have the same sizes and undergo the same dynamics. Then, one could analyse the correlation function integrated over the whole selected event sample. The feasibility of such studies will be investigated in the future.

On the technical side, the required computational time is rather high, but since we have not optimised our algorithm yet, we expect the required

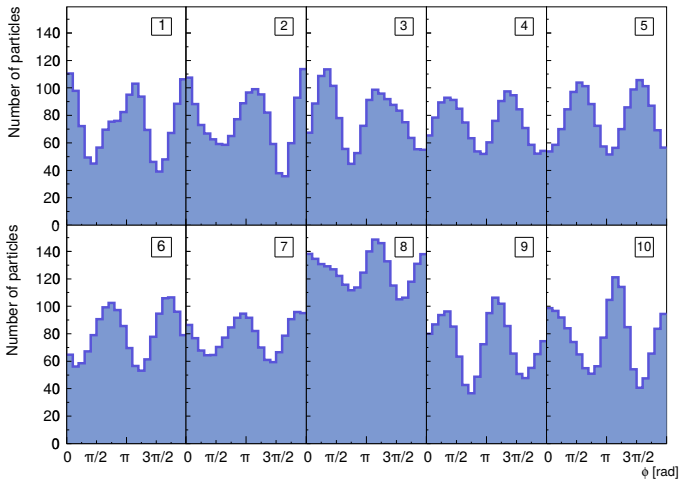

Fig. 2. Average histograms of the azimuthal angles for event bins 1–10, with event bins indicated in the panels.

CPU time to decrease significantly. We will also scrutinise the initial rotation of events.

Furthermore, we are currently studying a set of events obtained by AMPT. This will bring an insight into more realistic events. In spite of these difficulties, we believe that our method is worth applying in real data and that it will bring more detailed understanding of heavy-ion collisions dynamics.

Acknowledgement

Supported in parts by SGS15/093/OHK4/1T/14 (Czech Republic), APVV-0050-11, and VEGA 1/0469/15 (Slovakia)

REFERENCES

[1] S. Lehmann, A.D.Jackson, B. Lautrup: Measures and Mismeasures of Scientific Quality, Arxiv: physics/0512238

[2] R. Kopečná and B. Tomášik, arXiv:1506.06776 [nucl-th].

[3] G. Aad *et al.* [ATLAS Collaboration], Phys. Rev. C **86** 014907 (2012).

[4] G. Eyyubova [for the ALICE Collaboration], EPJ Web of Conferences **70** 00075 (2014).

[5] J. Schukraft, A. Timmins, S. Voloshin, Phys. Lett. B **719** (2013) 394

EPJ manuscript No.
(will be inserted by the editor)

Observables of non-equilibrium phase transition

Boris Tomášik[1,2], Martin Schulc[2], Ivan Melo[1,3], and Renata Kopečná[2]

[1] Univerzita Mateja Bela, FPV, Tajovského 40, 97401 Banská Bystrica, Slovakia
[2] České vysoké učení technické v Praze, FJFI, Břehová 7, 11519 Prague 1, Czech Republic
[3] Žilinská univerzita, Elektrotechnická fakulta, Akademická 1, 01026 Žilina, Slovakia

Abstract. A rapidly expanding fireball which undergoes first-order phase transition will supercool and proceed via spinodal decomposition. Hadrons are produced from the individual fragments as well as the left-over matter filling the space between them. Emission from fragments should be visible in rapidity correlations, particularly of protons. In addition to that, even within narrow centrality classes, rapidity distributions will be fluctuating from one event to another in case of fragmentation. This can be identified with the help of Kolmogorov-Smirnov test. Finally, we present a method which allows to sort events with varying rapidity distributions in such a way, that events with similar rapidity histograms are grouped together.

PACS. 25.75.Dw 21.65.-f

1 Introduction

Experiments at NICA aim to explore the region of the phase diagram where highly compressed and excited matter may undergo a first-order phase transition. It is argued elsewhere in this volume that such a phase transition in a rapidly expanding system may bring it out of equilibrium and end up in its spinodal decomposition. Such a process then generates enhanced fluctuations in spatial distributions of the baryon density and the energy density.

In this paper we focus on observables which could help to identify such processes.

Before we explain various possible observables, we introduce DRAGON: the Monte Carlo tool suited for generation of hadron distributions coming from a fragmented fireball [1]. Then, we report on an idea proposed in [2,3] and further elaborated in [4]: clustering of baryons can be visible in rapidity correlations of protons. Further, we turn our attention to the whole rapidity distributions of produced hadrons and present an idea to search for nonstatistical differences between them with the help of Kolmogorov-Smirnov test [5]. Finally, we propose a novel treatment now being developed which also compares momentum distributions from individual events and sorts events according to their similarity with each other [6].

2 Monte Carlo hadron production from fragments

In order to test the effects of fireball fragmentation into droplets it is useful to have Monte Carlo tool for the generation of artificial events with such features included. One possibility is to construct hydrodynamic models which include such a behaviour in the evolution [7,8,9,10]. They allow to link the resulting effects in fireball evolution with the underlying properties of the hot matter. On the other hand, they offer less freedom for systematic investigation of how the fragmentation is indeed seen in data. Interesting questions of this kind are: what is the minimum size and abundance of fragments that can be seen? What exactly is their influence on spectra, correlations, anisotropies, and femtoscopy? How are these observables influenced by the combination of droplet production and collective expansion?

Such questions can be conveniently explored with the help of Monte Carlo generator that uses a *parametrization* of the phase-space distribution of hadron production. Such a tool has been developed in [1] under the title DRAGON (DRoplet and hAdron Generator fOr Nuclear collisions). All studies presented here have been performed on events generated with its help.

The bedding of the generator is the blast-wave model. The probability to emit a hadron in phase-space is described by the emission function

$$S(x,p)\,d^4x = \frac{g}{(2\pi)^3}\,m_t\cosh(y-\eta)\,\exp\left(-\frac{p_\mu u^\mu}{T}\right) \times \Theta(R-r)\,\exp\left(-\frac{(\eta-\eta_0)^2}{2\Delta\eta^2}\right)\delta(\tau-\tau_0) \times \tau\,d\tau\,d\eta\,r\,dr\,d\phi\,. \quad (1)$$

It is formulated in Milne coordinates $\tau=\sqrt{t^2-z^2}$, $\eta=(1/2)\ln((t+z)/(t-z))$ and polar coordinates r, ϕ in the transverse plane. Emission points are distributed uniformly in transverse direction within the radius R and

freeze-out occurs along the hypersurface given by constant $\tau = \tau_0$. Azimuthal anisotropy has not been used in studies presented here although the model includes such a possibility. There is collective longitudinal and transverse expansion parametrized by the velocity field

$$u^\mu = (\cosh\eta\,\cosh\eta_t, \cos\phi\,\sinh\eta_t, \sin\phi\sinh\eta_t,\, \sinh\eta\cosh\eta_t) \quad (2)$$

$$\eta_t = \eta_t(r) = \sqrt{2}\rho_0\frac{r}{R}\,. \quad (3)$$

The fireball is locally thermalized with the temperature T.

A part of the hadrons, which can be specified in the model, is emitted from the droplets. The droplets stem from the fragmentation of the same hypersurface as assumed in eq. (1). The actual picture is that when the fireball fragments, some free hadrons are born between the produced droplets. The volume of droplets is distributed according to [11]

$$\mathcal{P}_V(V) = \frac{V}{b^2}e^{-V/b}\,. \quad (4)$$

The average volume of droplets is then $2b$. The minimal mass is practically set by the lightest hadron in simulation: usually the pion. The probability to emit hadron from a droplet drops exponentially in droplet proper time τ_d

$$\mathcal{P}_\tau(\tau_d) = \frac{1}{R_d}e^{-\tau_d/R_d}\,, \quad (5)$$

where R_d is the radius of the droplet. Momenta of hadrons from droplets are chosen from the Boltzmann distribution with the same temperature as bulk production. Currently, neither momentum nor charge conservation is taken into account in droplet decays, but an upgrade of the model including these effects is envisaged.

DRAGON also includes production of hadrons from resonance decays. Baryons up to 2 GeV and mesons up to 1.5 GeV of mass are included. Chemical composition is specified by chemical freeze-out temperature and chemical potentials for baryon number and strangeness. (Chemical potential for I_3 should also be introduced but is practically very small and thus neglected in the simulations.)

3 Proton correlations

Hadrons emitted from the same droplet will have similar velocities. This should be seen in their correlations [2,3]. Protons appear best suited for such a study. Their mass is higher than that of most mesons, so their deflection from the velocity of the droplet due to thermal smearing will be less severe. Pions would have better statistics thanks to their high abundance, but their smearing due to thermal motion and resonance decays is too big.

Correlation function can be measured as a function of rapidity difference $\Delta y = y_1 - y_2$ or (better) of the relative rapidity

$$y_{12} = \ln\left[\gamma_{12} + \sqrt{\gamma_{12}^2 - 1}\right] \quad (6)$$

with $\gamma_{12} = p_1 \cdot p_2/m_1m_2$.

The correlation function is conveniently sampled as

$$C_{12}(y_{12}) = \frac{P_2(y_{12})}{P_{2,\mathrm{mixed}}(y_{12})} \quad (7)$$

where $P_2(y_{12})$ is the probability to observe a pair of protons with relative rapidity y_{12}. The reference distribution $P_{2,\mathrm{mixed}}(y_{12})$ in the denominator is obtained via the mixed events technique.

It is instructive to first consider a simple model where the rapidities of droplets follow Gaussian distribution

$$\zeta(y_d) = \frac{1}{\sqrt{2\pi\xi^2}}\exp\left(-\frac{(y_d - y_0)^2}{2\xi^2}\right)\,. \quad (8)$$

Within the droplet i which has rapidity y_i, rapidities of protons are also distributed according to Gaussian

$$\rho_{1,i}(y) = \frac{\nu_i}{\sqrt{2\pi\sigma^2}}\exp\left(-\frac{(y - y_i)^2}{2\sigma^2}\right)\,. \quad (9)$$

This distribution is normalized to the number of protons from droplet i, which is denoted as ν_i.

The resulting correlation function in this simple model is [3,4]

$$C(\Delta y) - 1 = \frac{\xi\langle N_d\rangle\langle\nu(\nu-1)\rangle_M}{\langle N_d(N_d-1)\rangle\langle\nu\rangle_M^2}\sqrt{1+\frac{\sigma^2}{\xi^2}}\,\frac{1}{\sigma}\exp\left(-\frac{\Delta y^2}{4\sigma^2\left(1+\frac{\sigma^2}{\xi^2}\right)}\right) \quad (10)$$

where $\langle N_d\rangle$ is the average number of droplets in one event and $\langle\cdots\rangle_M$ denotes averaging over various droplets. Naturally, the width of the correlation function depends on σ^2, as might have been expected. However, it also depends on the width of the rapidity distribution of droplets: through the factor $(1+\sigma^2/\xi^2)$, growing ξ^2 leads to narrower proton correlation function.

As an illustration relevant for NICA we generated sets of events with the help of DRAGON. On these samples we studied the influence of droplet size and the share of particles from droplets on the resulting correlation functions. It turns out that the relative rapidity y_{12} yields better results, so we have mainly used this observable in our analyses. A more detailed study, though not with specific NICA fireball settings, can be found in [4].

DRAGON was set with Gaussian rapidity distribution with the width of 1. Within the rapidity acceptance window $-1 < y < 1$ there were about 1200 hadrons; this number includes all neutral stable hadrons. Momentum distribution has been set by the temperature of 120 MeV and the transverse velocity gradient $\eta_f = 0.4$. Chemical composition was according to $T_{ch} = 140$ MeV and $\mu_B = 413$ MeV. Recall that resonance decays are included in the model. The same kinetic temperature and chemical composition was assumed for the droplets. Total mass of each droplet is given by its size and the energy density

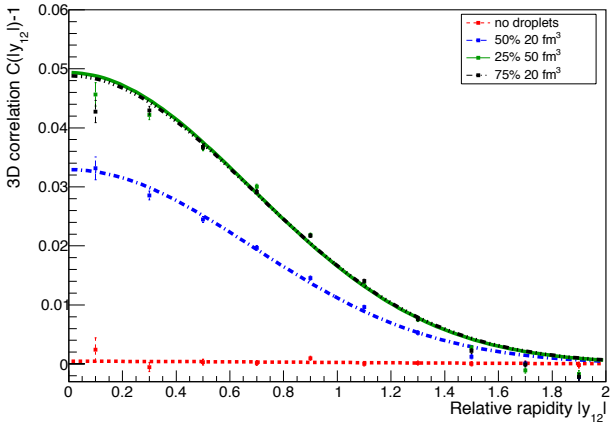

Fig. 1. Proton correlation functions for four different settings of hadron production from droplets.

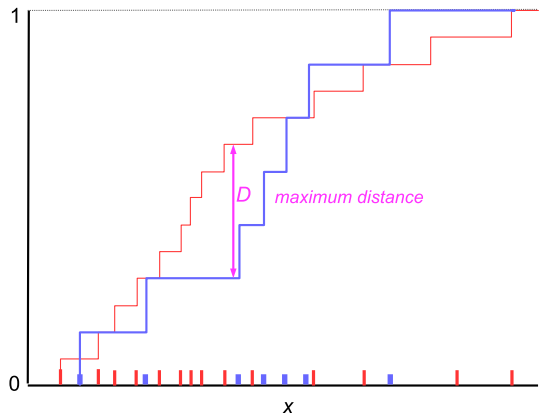

Fig. 2. Definition of the distance between two events. The measured values of variable x are indicated on horizontal axis. Lines of different thickness represent two different events.

0.7 GeV/fm^3. Transverse size of the fireball was set to 10 fm and the lifetime $\tau = 9$ fm/c, but these parameters have no influence on the presented results. Note that we have imposed acceptance cut in rapidity $-1 < y < 1$, so that we do not show results that would not be measurable due to limited acceptance.

In order to see the effect of droplet formation on the correlation function we simulated one data set with no droplets and three sets which differ in droplet settings. We have sets with: $b = 50$ fm^3 and the fraction of 25% of hadrons from droplets, $b = 20$ fm^3 and 50%, $b = 20$ fm^3 and 75%. Recall that the mean droplet volume is $2b$.

The resulting proton correlation functions in y_{12} are plotted in Fig. 1. As expected, without fragmentation the correlation function is flat. The widths of the correlation functions are given by the smearing of the momenta of protons within one droplet, mainly due to temperature.

The level of correlation is expressed in the height of the peak at $y_{12} = 0$. Naturally, this is expected to grow if a larger number of protons is correlated. This can be achieved in two ways: by increasing droplet sizes so that more protons come from each droplet, or by increasing the number of droplets by enhancing the share of particles produced by droplets. By coincidence we thus obtained very similar results for the cases with droplet fractions 25% and 75%, since the latter one assumes smaller droplets.

Note the width scale of the correlation function which is larger than the typical scale of strong interactions. Thus any modification due to final state interactions which have not been included here is expected to be concentrated around the peak of our correlation functions.

4 Comparison of rapidity distributions

The fragmentation of the fireball actually leads to event-by-event fluctuations of rapidity distributions. In each event hadrons are produced from a different underlying rapidity distribution. In [5] it was proposed to use a standard statistical tool for the comparison of hadron rapidity distributions from individual events: the Kolmogorov-Smirnov (KS) test. The KS test has been designed to answer the question, to what extent two empirical distributions seem to correspond to the same underlying probability density.

To apply the test on empirical distributions one first has to define a measure of how much they differ. For the sake of clarity and brevity we shall call empirical distributions *events* and the measure of difference will be their scaled distance, to be defined later. A distance is defined in Fig. 2. Consider measuring the quantity x (this may be e.g. the rapidity) for all particles in two different events. We mark the values of x on the horizontal axis. Then, in the same plot we draw for each event its empirical cumulative distribution function. It is actually a staircase: we start at 0 and in each position where there is measured x we make a step with the height $1/n_i$, where n_i is the multiplicity of the event. The maximum vertical distance D between the two obtained staircases is taken as the measure of difference between the two events. For further work one takes the *scaled distance*

$$d = \sqrt{\frac{n_1 n_2}{n_1 + n_2}} D \tag{11}$$

where n_1, n_2 are the multiplicities of the two events.

Next one defines

$$Q(d) = P(d' > d) \tag{12}$$

i.e. the probability that the scaled distance d' determined for a pair of random events generated from the same underlying distribution will be bigger than d. The formulas for obtaining $Q(d)$ for any d are given in the Appendix of [5]. Thus defined, for large d, the value of Q will be small because there is little chance that two events will be so much different. If all events come from the *same* underlying distribution, then the Q's determined on a large sample of event pairs will be distributed *uniformly*.

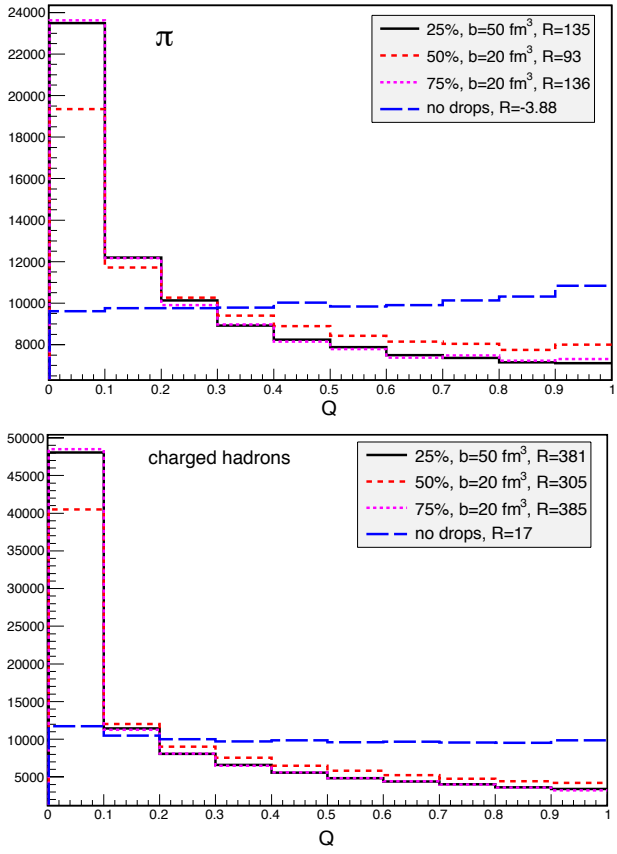

Fig. 3. Q-histograms for samples of 10^4 simulated events. Rapidities of charged pions (top) and all charged hadrons (bottom) are taken into account.

In a sample of events where the shape and dynamical state of the fireballs fluctuate, e.g. due to fragmentation, large scaled distance d will be more frequent. This is then translated into higher abundance of low Q values. Thus non-statistical differences between events will show up as a peak at low Q in the histogram of Q values for large number of event pairs. In order to quantify the significance of the peak above the usual statistical fluctuations we introduce

$$R = \frac{N_0 - \frac{N_{\rm tot}}{B}}{\sigma_0} = \frac{N_0 - \frac{N_{\rm tot}}{B}}{\frac{N_{\rm tot}}{B}} \qquad (13)$$

where N_0 is the number of event pairs in the first Q-bin, $N_{\rm tot}$ is the number of all event pairs and B is the number of Q-bins.

To illustrate the application at NICA, we have used event samples with the same settings as in the previous Section and show in Fig. 3 the Q-histograms for pion rapidity distributions as well as rapidity distributions of all charged hadrons. The signal is very strong and the one for charged hadrons is generally more pronounced than the one for pions. The comparison of different data sets is consistent with results for correlation functions from the previous section. Note that there is basically very weak signal for the case without droplets, which shows that clustering effect due to resonance decays cannot mask the investigated mechanism.

5 Event shape sorting

In presence of fireball fragmentation, rapidity distributions of different events show large variety. This motivates the quest to select among them groups of events which will be similar. Such groups allow to appreciate the range of fluctuations of the momentum distribution. They also may be useful for the construction of mixed events histograms used in correlation functions.

A method for sorting events according to their similarity with each other has been proposed [12,6]. The application in [6] was on azimuthal angle distributions. Here we use it for rapidity distributions. Details can be found in [6]; here we only shortly explain the sorting algorithm.

An event is characterized when all its bin entries n_i are given; i numbers the bins in rapidity. Full bin record will be denoted $\{n_i\}$.

1. Events are initially sorted in a chosen way and divided into N quantiles of the distribution. We use deciles, numbered by Greek letters.
2. For each event, characterized by record $\{n_i\}$, calculate the probability that it belongs to the event bin μ, $P(\mu|\{n_i\})$, using the Bayes' theorem

$$P(\mu|\{n_i\}) = \frac{P(\{n_i\}|\mu)P(\mu)}{P(\{n_i\})}\,. \qquad (14)$$

The probability $P(\{n_i\}|\mu)$ that the event with bin record $\{n_i\}$ belongs to the event bin μ can be expressed as

$$P(\{n_i\}|\mu) = M! \prod_i \frac{P(i|\mu)^{n_i}}{n_i!} \qquad (15)$$

where M is the event multiplicity, the product goes over all (rapidity) bins, and $P(i|\mu)$ is the probability that a particle falls into bin i in an event from event bin μ

$$P(i|\mu) = \frac{n_{\mu,i}}{M_\mu}\,. \qquad (16)$$

(M_μ is the total multiplicity of all events in event bin μ and $n_{i,\mu}$ is the total number of particles in bin i.) Coming back to eq. (14): $P(\mu) = 1/N$ is the prior and

$$P(\{n_i\}) = \sum_{\mu=1}^{N} P(\{n_i\}|\mu)P(\mu)\,. \qquad (17)$$

3. For each event determine

$$\bar{\mu} = \sum_{\mu=1}^{N} P(\mu|\{n_i\})\mu \qquad (18)$$

and re-sort all events according to $\bar{\mu}$. Then divide again into quantiles.

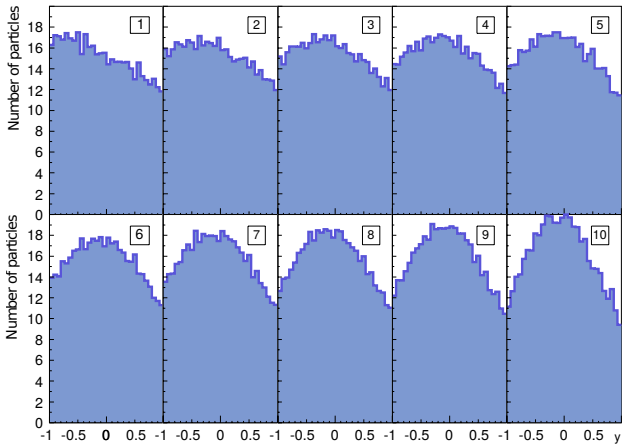

Fig. 4. Average rapidity histograms of the 10 event bins after the sorting algorithm with 5000 events (with rapidity flip - see text) converged. Droplet fraction 25% and $b = 50$ fm^3.

4. If the ordering of events changed, re-iterate from point 2. In a less strict version of the algorithm, the ordering is re-iterated only if the assignment to quantiles has changed.

This iterative algorithm organizes events in such a way, that those which are similar to each other by the shapes of their histograms end up close to each other. It is not specified *a priori*, however, whether there is any specific observable according to which the sorting proceeds. The algorithm itself picks the best ordering automatically. The method actually provides a more sophisticated version of the Event Shape Engineering.

We have tested the algorithm on a set of events generated by DRAGON with the same parameters as in previous two Sections. For illustration, we show in Fig. 4 the average histograms in different event bins after the sorting algorithm. We have chosen the data set with droplet fraction 25% and $b = 50$ fm^3 and the algorithm works with rapidity distributions of pions. As a result of the fluctuations in rapidity distributions, the differences between event bins are large. On one end there are events with almost symmetric distributions, whereas on the other end there are events with strong emphasis on one side.

It should be noted that the simulation setting assumes symmetric Gaussian rapidity distribution and corresponded to symmetric nuclear collisions. Consequently, there is no reason to favour one rapidity direction over the other. The resulting sorting in Fig. 4 is obtained when in the middle of the iteration process one half of the events is flipped over the mid-rapidity.

The difference between event bins is much bigger here than in a sample of events where no droplets are present.

6 Conclusions

We have sketched and explained two kinds of observables that can be used for identification of the fragmentation process: proton correlations in rapidity [3,4] and the Kolmogorov-Smirnov test comparing the event-by-event rapidity distributions [5]. The motivation to look for the fragmentation comes from the fact that a first order phase transition actually should proceed this way.

It should be mentioned that in [13,14] it has been argued that potentially there is a mechanism which may lead to fireball fragmentation even in absence of the first order phase transition. A sharp peak of the *bulk* viscosity as a function of temperature may suddenly cause resistance of the bulk matter against expansion. Driven by the inertia, the fireball could choose to fragment. This possibility puts the uniqueness of the fragmentation process as the signature for the first order phase transition under question. Nevertheless, it is still certainly worthwhile to investigate the consequences of such a process.

A process that could mask the signals of fragmentation is rescattering of hadrons emitted from droplets. It would be interesting to combine the presented methods with models including such a possibility.

Finally, we presented a method which is still being developed and which allows to sort the measured events automatically according to the most pronounced features in their histograms and build groups of similar events [6]. This would allow to study such groups, where event-by-event fluctuations are suppressed, in more detail.

We acknowledge partial support by grants APVV-0050-11, VEGA 1/0469/15 (Slovakia). BT was also supported by grants RVO68407700, LG15001 (Czech Republic). RK acknowledges support from SGS15/093/OHK4/1T/14.

References

1. B. Tomášik, Comput. Phys. Commun. **180** (2009) 1642.
2. S. Pratt, Phys. Rev. C **49** (1994) 2722.
3. J. Randrup, Heavy Ion Physics **22** (2005) 69.
4. M. Schulc and B. Tomášik, Eur. Phys. J. A **45** (2010) 91.
5. I. Melo *et al.*, Phys. Rev. C **80** (2009) 024904.
6. R. Kopečná and B. Tomášik, arXiv:1506.06776 [nucl-th].
7. J. Steinheimer and J. Randrup, Phys. Rev. Lett. **109** (2012) 212301.
8. C. Herold, M. Nahrgang, I. Mishustin and M. Bleicher, Phys. Rev. C **87** (2013) 014907.
9. J. Steinheimer and J. Randrup, Phys. Rev. C **87** (2013) 054903.
10. J. Steinheimer, J. Randrup and V. Koch, Phys. Rev. C **89** (2014) 034901.
11. I.N. Mishustin, in T. Čechák et al. (eds.), Nuclear Science and Safety in Europe, pp. 99–111, Springer, 2006.
12. S. Lehmann, A.D. Jackson, B. Lautrup, Scientometrics **76** (2008) 369.
13. G. Torrieri, B. Tomášik and I. Mishustin, Phys. Rev. C **77** (2008) 034903.
14. K. Rajagopal and N. Tripuraneni, JHEP **1003** (2010) 018.